The Expedition ARKTIS-IX/1 of RV "Polarstern" in 1993

Edited by
Hajo Eicken and Jens Meincke

Ber. Polarforsch. 134 (1994)
ISSN 0176 - 5027

Contents

1. Introduction

The expedition ARKTIS IX/1 was the first winter cruise of *POLARSTERN* in the Nordic Seas. Its aim was to enable meteorologists, oceanographers, chemists, biologists and glaciologists to complete existing data sets from longer-term activities through observations of winter conditions.
During the first part of the cruise (ARK IX/1a, February 26 to March 24, 1993), a drift station was established on an ice floe in Fram Strait for meteorological, oceanographical, chemical, remote-sensing, ice-physics and biological work. In close cooperation with air-plane measurements conducted from Longyearbyen, the boundary layer and the structure of the atmosphere were studied in the marginal ice zone, with a special focus on observations of cold-air outbreaks. These winter measurements within the framework of a long-term research program (Sonderforschungsbereich 318 "Processes relevant to climate") furthermore involved the research vessels *VALDIVIA* (Hamburg) and *PROF. MULTANOVSKY* (Russian Federation). At the ice station, other groups completed detailed studies of the ice and the water column underneath in the vicinity of the ship.
The second part (ARK IX/1b, March 24 to April 17, 1993) focussed on winter surveys of Fram Strait and the Greenland Basin within the framework of the international Greenland Sea Project. A winter Fram Strait section has never been achieved before and was aimed at completing the available information on summertime exchanges of water masses and zooplankton between the Arctic Ocean and the Greenland Sea by corresponding winter data. The winter work in the Greenland Sea was carried out as a repeat of the 1988/89 Greenland Sea Project surveys and was to detect longer term changes in the deep water renewal in the Greenland Basin. In addition it allowed to complete the series of surveys on the seasonal distribution on abundance and activity of dominant zooplankton species and to study winter-ice structures and development, in particular for the Isodden area in the southeastern Greenland Sea.

1.1. Cruise itinerary

1.1.1. Itinerary of ARK IX/1a, February 26 to March 24, 1993 (H. Eicken)

RV *POLARSTERN* left port in Bremerhaven in the late afternoon of February 26, 1993, heading towards Fram Strait with 52 scientists from five countries and 41 crew members on board (see Figures 1.1 and 1.2 for cruise track). Due to unfavourable weather with head-on winds and swell, transit to the research area was at times limited to a speed of 8 knots. On March 4, traces of grease ice and rotten floes were encountered at 73°23´N 3°09´E as part of the "Odden" ice tongue stretching out from the East Greenland current. The first ice bands of the ice edge proper were traversed in the early morning hours of March 5 at 79°33´N 2°53´E. The following two days were spent in bringing the ship further north. After some difficulties in finding open water or new-ice areas, infra-red satellite imagery received on board indicated a system of extended leads at roughly 8°E. Aided by helicopter reconnaissance, the ship entered one of these leads on the morning of March 7 and travelled up to 81°28´N 7°23´E, where further progress was hindered by thick, heavily ridged ice. Based on thickness drilling, a site for the meteorological camp was chosen and the ship put alongside the floe.

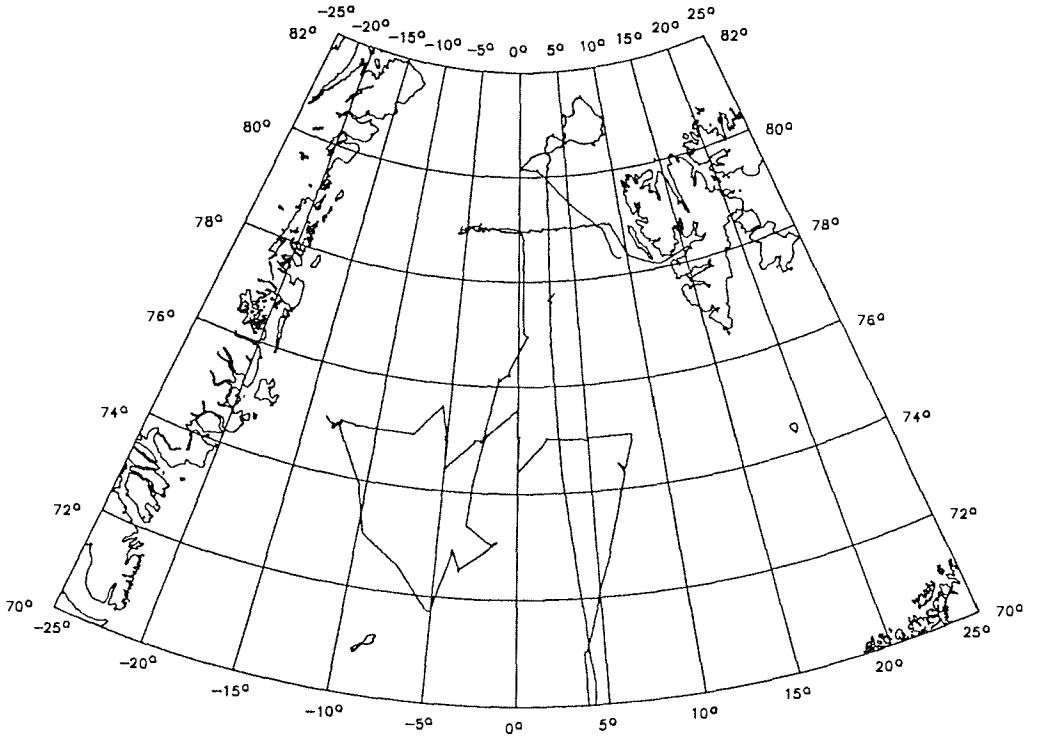

Figure 1.1: Cruise tracks of ARK IX/1 a and b.

During the entire passage, continuous measurements of carbon dioxide partial pressure in surface waters and air had been carried out. Continuous sampling of air for soot carbon and mercury was only hampered by rough weather in the early phase of the cruise. On March 5, 6 and 7, four Argos buoys were deployed by helicopter. At the same time, the aerology program entered its intensive phase with radiosonde ascents every six hours. While sea-ice research on the floe and in an adjacent lead, passive microwave remote sensing and biological sampling in the water column commenced immediately after arrival at the floe, assembly of the meteorological station was hampered by severe icing of the forecastle acquired during the last days of the passage to Fram Strait. Despite persistent joint efforts by crew and scientists over a period of several days, the cranes could not be freed completely of ice.

It became obvious, that due to icing and temperatures persistently below -37 °C, use of the foreward cranes and opening of hatches was out of question within a reasonable amount of time. This prevented the establishment of the meteorological camp as planned, since most of the equipment was stowed in the front cargo hold. On March 10, an alternative program drafted during the previous days came into effect. A 15-m mast and

arrays of sensors mounted on smaller masts and on the ice up to 350 m away from the ship were connected to registration platforms on board *POLARSTERN*. On March 10, first data started coming in, and within the next days the station was fully operative. Sea-ice research and biological sampling progressed mostly as planned, although the low temperatures (average of -33.5 °C for entire drift period, minimum -40.5 °C in the morning hours of March 12) rendered handling of gear and instruments and work on the ice rather difficult. This was also true of helicopter traffic, which had problems coping with the cold below -35 °C, as testified by loss of one turbine and failure of an engine during a flight. Improved heating in the hangar and revised haul-out procedures in combination with rising temperatures during the latter part of the cruise nevertheless allowed for a diverse helicopter program. In total, five buoys were deployed (one recaptured), several video/photography and laser altimeter flights were carried out to characterize ice roughness in the surroundings of the masts, and the sea-ice physics groups conducted work on floes and in leads in the vicinity.

During the main drift station phase a comprehensive data set on the interaction between air, ice and open water could be collected. While radiosonde ascents provided information on the structure of the atmosphere above the planetary boundary layer, the meteorological sites resolved fluxes of energy and momentum at the surface and at height in full detail. Airplane overflights, data collected by the drifting buoys and the analysis of satellite imagery allow for integration of the measurements conducted at the drift station site into a larger-scale context during later analysis. Passive-microwave radiometer measurements supported by studies of the properties of ice and snow will be used to improve evaluation of satellite data. Research done on the sea ice demonstrated how ocean swell becomes increasingly dominant over small-period locally generated waves as one approaches the marginal iced zone, resulting in break-up as wave energy is high enough for the bending strength of floes to be surpassed. Collection of a large data set using a combination of different geophysical techniques to indirectly measure ice thickness will allow for an assessment of the reliability and strengths of different methods. The low brine volumes and high salinities encountered in the upper three-quarters of the ice cover demonstrated to the biologists that life in Arctic (multi-year) sea ice is restricted to the bottommost layers in winter and early spring. Abundant trap catches and underwater video footage suggest though, that even in winter the undersides of ice floes are sites of high biological activity.

Satellite images and helicopter reconnaissance showed that by March 17, the ship had drifted to within 25 km distance from a sharp boundary separating the closed pack ice with floes of kilometer-size from the inner marginal ice zone with floes of few hundred meters diameter at maximum. Ice drift averaged at a speed of 15.1 km/day (0.17 m/s) over the entire drift period from March 7 to March 19 and appeared largely dictated by the wind. Thus, periods of easterly flow caused the ice to shift to the Northwest, veering winds being responsible for the circular drift feature in the ship's track on March 13 and 14 (see Figure 1.2). Due to the proximity of this zone of floe break-up, it was decided to take meteorological instruments that were recording redundantly off the ice on March 18. On the same day at 23:15 UTC, the floe cracked into several fragments, most likely due to an increase in swell. Starting in the early morning hours of March 19, instruments and masts were disassembled, and by the late afternoon all gear was back on board without loss or damage. During the following three days further sea-ice research was carried out in the marginal ice zone along with deep CTD casts and water-sampling. After

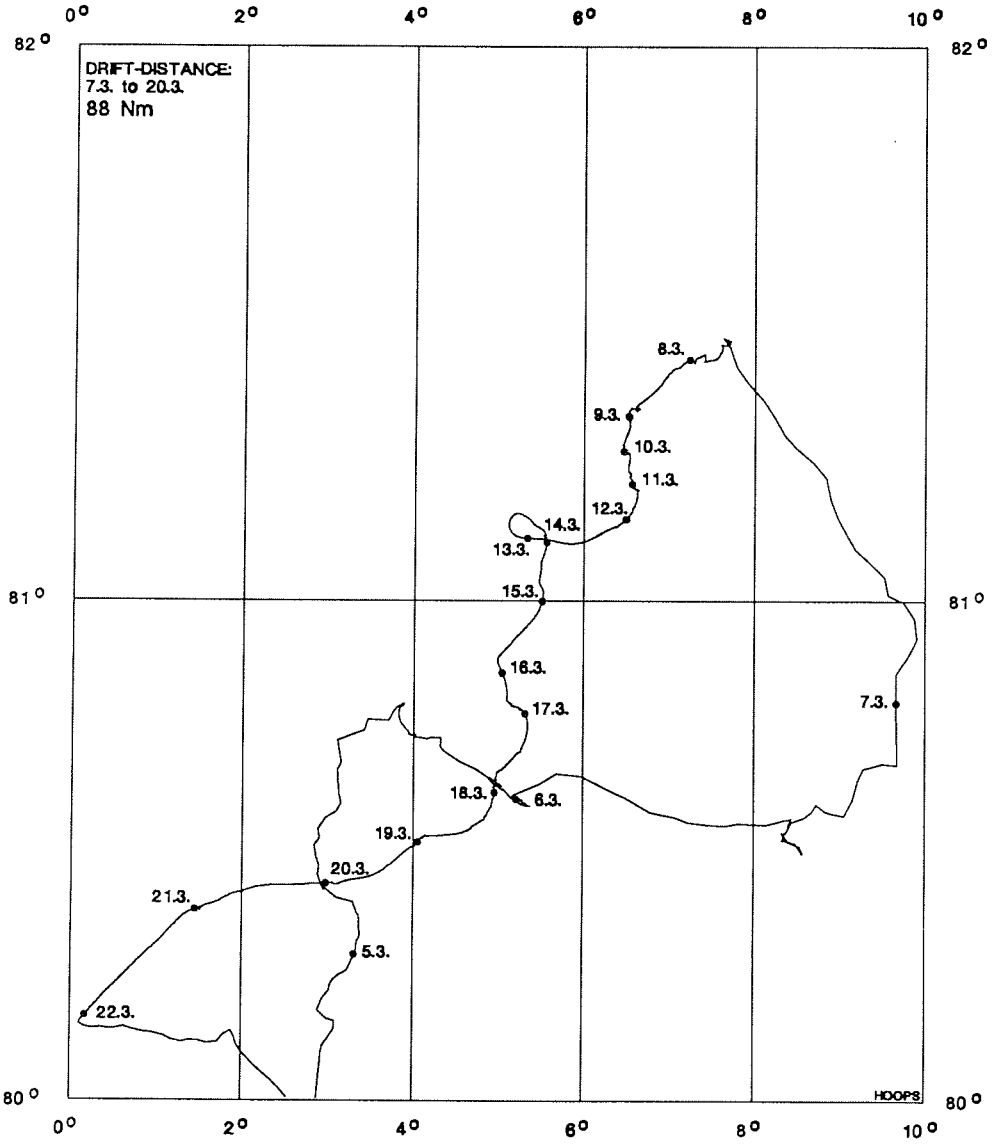

Figure 1.2: Cruise track and drift station track (March 7 to March 19) in Fram Strait during ARK IX/1a.

several attempts at retrieving some of the Argos buoys deployed earlier, one of which was successful, the ship left the marginal ice zone for Longyearbyen in the afternoon of March 22. In the evening of March 23 *POLARSTERN* moored alongside the coal mine pier and with the exchange of personnel ARK IX/1b commenced in the afternoon hours of March 24.

1.1.2. Itinerary of ARK IX/1b, March 24 to April 17, 1993 (J. Meincke)

The vessel left Longyearbyen on March 24, 19.00 for the second part of the cruise leg. The scientific party numbered 53 participants from Canada, Denmark, France, Germany, Great Britain, Russia, Switzerland and USA. The first part of the scientific programme consisted of 18 stations with hydrographical and chemical profiling using the CTD/Rosette and biological sampling using Multinet and Bongonet along 79°N, starting at the shelf edge off Svalbard at 9°E (see Figure 1.3). The East Greenland ice edge was encountered around 2°E, but ice conditions remained relatively light until a huge multiyear floe stopped any further westward progress at 6°W on the Greenland shelf. Additional station work in the ice comprised in situ sampling and remote sensing of individual ice floes on four occasions and recovery of 3 out of 7 moored arrays of current meters and upward looking sonars that had not been recovered in summer '92 because of heavy ice conditions. Weather permitting, the helicopters were used for flight patterns over the East Greenland ice stream with photographic cameras, VIS and IR scanners and a laser altimeter. When the work on 79°N was completed on March 31, the vessel left the ice and moved southward into the Greenland Sea. The basic station pattern there consisted of a N-S section along 2.5°W and an E-W section along 75°N, both spanning the cyclonic circulation in the Greenland Basin (see Figure 1.3).

With favourable wind and ice conditions nearly all sampling could be achieved as planned: A total of 29 full-depth CTD/Rosette profiles was obtained as repeats of the 1988/89 Greenland Sea Project station grid. Three moorings with acoustic sources were deployed around the center of the Greenland Basin, to allow continuous tracking of 6 surface floats released within the Greenland Basin to follow the currents at depths of 300 and 1000 m until June 1993. One long-term mooring over the East Greenland slope at 75°N was recovered as well as three such systems in the central basin. The attempt to recover a further system on the East Greenland shelf failed due to heavy drift ice at the mooring location. Biological sampling using RMT (4x), Multinet (10x), Bongonet (25x) on 19 stations and filtration of phytoplankton from rosette samples resulted in two complete sections across Greenland Sea gyre.

The ice work in the Greenland Basin was faced with rather anomalous conditions. The East Greenland ice edge was right over the shelf edge, representing mean summer conditions. The classical Isodden was not present, instead remnants of it were found as highly variable isolated patches of pancake ice in the eastern part of the basin. They were sampled with in situ work and helicopter-based remote sensing on two occasions during April 3 and April 10.

The station work was terminated on April 13 with re-visiting the Greenland Sea Project in situ intercalibration station in the northern Lofoten Basin, where complete CTD/Rosette profiles were taken for reference purposes within the internationally coordinated effort to establish a high quality hydrographic database for monitoring longer term changes with the Greenland Sea deep water. The route to Bremerhaven could be made in fine weather and *POLARSTERN* arrived at her berth on Saturday, April 17, 13.00.

1.1.3. Acknowledgement

The chief scientists, on behalf of the scientific parties on board during ARK IX/1 a and b would like to take the opportunity to thank captain Greve and his crew for their friendly and professional help. This was not only provided during the routine parts of the cruise, but in particular during the periods with harsh Arctic conditions, when the limits of human and technical capabilities became evident.

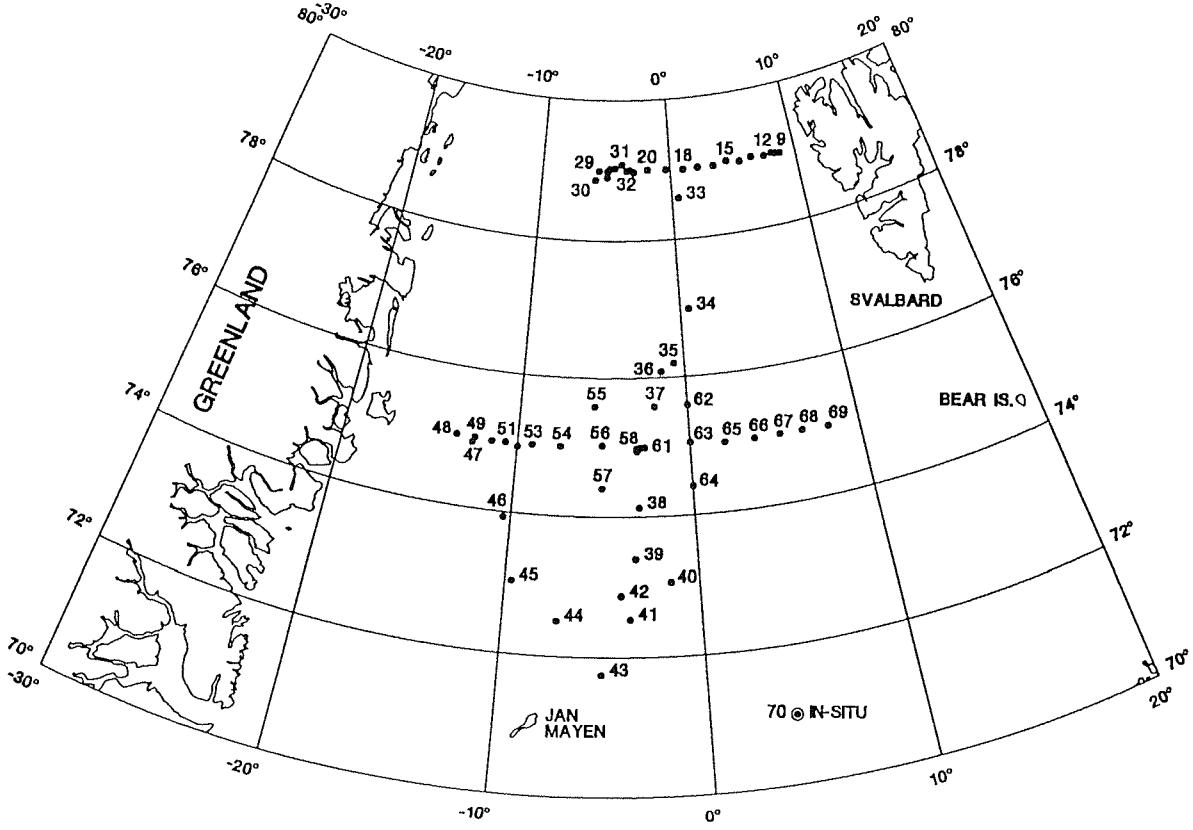

Figure 1.3: Station locations of ARK IX/1b.

1.2. Weather conditions (H. Erdmann)

1.2.1. Weather conditions during leg 1 a, February 26 to March 24, 1993

While leaving Bremerhaven on February 26, 1993 a partial low developed over the Skagerak leeward of Norway as part of a long-stretched coldfront of a cyclone in the Nordic Sea. It moved slowly to the Kattegat and Poland. Southwesterly to southerly winds Bft 4 to 5 prevailed in the German Bay on the evening of February 26. Passing the coldfront in the nighttime of February 27, the wind turned to northwest/north, increasing to force Bft 8 for two hours. Because of mountain effects off southwestern Norway, the wind increased temporarily up to force Bft 9 in the Fischer area. The rough sea, caused by windstress, reached wave heights of about five meters. North of 63°N the wind turned to northeast, decreasing to force Bft 5.

Meanwhile a cell separated from the high west of the British Islands. It moved to the East, crossing the Farøer on its way. The pressure gradient increased in the area of Utsira, with calm weather and good visibility in the ship's vicinity. On March 1, *POLARSTERN* passed through the high pressure axis on her way north. Due to incipient warm air advection, the visibility decreased and several cloudlayers invaded the sky. The wind turned from southeast to southwest and increased during the evening up to force Bft 6 to 7. Meanwhile, a storm depression developed off southeastern Greenland, moving from Jan Mayen to Svalbard within the strong southwesterly stream in the upper air levels. The wind increased to Bft 8 over large parts of the Norwegian Sea. In the night of March 3, the coldfront of the low mentioned above passed *POLARSTERN* at 72°N 4°E with westturning winds up to force Bft 9 and heavy snowgusts. Within a few hours the air temperature decreased from +3 to -11 C. On March 3 winds were around Bft 9 from West to Northwest with waves up to 7 m high. At temperatures of -13 °C seaspray resulted in severe icing of the ship. While the low passed away to the Kara Sea, the wind turned to north, after having passed a significant trough in the Svalbard area. The wind decreased in the evening of March 4 to force Bft 5. Temperatures decreased on the approach to the ice edge.

On March 5, *POLARSTERN* reached Arctic air at 80°N 3°E under the influence of a high-wedge that spread towards the East, coming from northeastern Greenland. Mostly there were good weather conditions with temperatures of -33 °C and good visibility. Winds came from north to northwest. On March 6 cyclogenesis started near Iceland. The developing low moved slowly to the Northeast. *POLARSTERN* remained under the influence of high pressure between the northern Greenland high and a high over northern Scandinavia within a weak northerly airflow. The low reached Svalbard with a core pressure of 975 hPa and moved towards Novaya Zemlya. Meanwhile the wind increased to force Bft 6 coming from the Northeast.

The air temperature was -37 °C (wind chill -65 to -70 °C). With incipient cold-air advection, especially in the upper layers of the troposphere at the back of the low, the inversion near the surface decreased, such that visibility increased and clouds disappeared. During the night of March 10, temperature decreased to -39.4 °C. Until March 11 the visibility was about 10 km. The northerly surface wind ranged below 10 kt. In the night of March 12, air temperature reached the minimum of -40.5 °C.

A "polar-low" genesis over open water southwest of Svalbard produced a massive cloud invasion on March 12. Visibility decreased to <1 km due to the increasing inversion below 300 m height. Winds increased to force Bft 8 to 9

coming from the East. With falling and drifting snow visibility fell below 20 m. The small-scale low passed west of *POLARSTERN* moving northward during the day. At 18:10 UTC the air temperature reached its maximum with -9.7 °C. The wind turned from southeast to south and to southwest, by instantly following of cold air advection in the lower troposphere. The temperature decreased to -30 °C within 4 hours.
A warmfront of a stationary low south of Svalbard affected the working area on March 15 only to a small degree. A weak anticyclone caused northwesterly to northerly winds force Bft 4 and good visibility on March 17. The temperature was -27 °C at the surface and -17 °C at a height of 300 m. On March 18 the pressure gradient increased due to a sharp drop in pressure near Svalbard. The wind increased to force Bft 6 to 7 coming from the North with drifting snow and low visibility.
A "lee-cyclone" developed in the eastern part of the stream, on the western side of Svalbard due to mountain effects. Warm air was advected in its northern part. The surface remained under cold air, building up a strong inversion and causing fog. Sea smoke invaded the ice-covered sea. An anticyclone that had developed over northeastern Greenland began to influence the weather in the working area of *POLARSTERN* . With cloud-free skies and good visibility, temperatures rose from -32 °C.on March 20 to -26 °C on the following day. The wind reached Bft 4 to 5 coming from north to northeast. On the way back to Longyearbyen, *POLARSTERN* encountered a strong anticyclone over the Norwegian Sea with gusty winds from the East and rising temperatures.

1.2.2. Weather conditions during leg 1b, March 25 to April 18, 1993

On the way from Longyearbyen to the working area (79°N 10°E) on March 25, a storm cyclone, that moved from the Norwegian Sea to the Barents Sea, resulted in northerly flow, which increased parallel to the western parts of Svalbard's mountains to force Bft 9. The wind decreased rapidly after a strong pressure rise over Svalbard and turned from west to south. In the frontal zone that moved parallel to the eastern coast of Greenland, several strong, small-scale surface cyclones developed. They moved northeast with warm maritime air advected towards Svalbard. The wind increased to force Bft 9 from the South and on March 26 temperatures rose to 0.5 °C. Due to cold-air advection during the night the air temperature decreased within three hours to -20 °C, while winds veered to northwest. The 10-min-average of the wind velocity showed a maximum of about 46 knots for a short period. The weather remained stable on March 27 with northerly winds force Bft 8, as another cyclone moved rapidly from Jan Mayen to Svalbard. Snowshowers and seasmoke reduced the visibility. A static anticyclone with cold surface air moved from northeastern Greenland to the Southeast and influenced the working area of *POLARSTERN* (79°N 01°W) March 28. The nothwesterly wind decreased to force Bft 2 to 3 and within the ice, weather conditions were good with air temperatures about -24 °C.
At the northern edge of a large-scale stationary storm low near Iceland warm air was advected on March 30 from the North Atlantic to Fram Strait. The cyclone increased the uplift of air in the middle and higher layers of the troposphere. Subsequently snowfall persisted in the area. The surface layer remained under cold air over ice. Along a warmfront that near-parallel to the upper air flow, a warmfront wave developed on March 30 east of the position of *POLARSTERN* . As a consequence, a small-scale low developed, advecting cold air on the back side of a corresponding anticyclone over

northeastern Greenland. The temperature decreased in the working area (79°N 5°30'W) of *POLARSTERN* down to -26 °C while the wind was force Bft 5 from the North. Meanwhile the compact cloud field vanished and the visibility increased. The anticyclone over northeastern Greenland shifted to Svalbard and intensified. The Greenland Sea and Fram Strait were affected by the southeasterly flow on the western side of the anticyclone. While *POLARSTERN* reached the open water area, warm air advection in the surface layer increased so that the temperature increased up to 0 °C on April 1. Because of the weakening processes within the storm low over Iceland, the pressure gradient also decreased over the Greenland Sea. While *POLARSTERN* approached the Greenland Sea, the wind decreased down to Bft 5 coming from southeast. The stratus clouds were located at the surface, such that helicopter flights were sometimes not possible in the Odden area on April 03. On the backside of a weak cold front that shifted slowly from eastern Greenland to the East, the air became dryer and visibility increased. Westerly wind continued with weak force. On April 5 the wind turned to northeast and cold air was advected, in a thin layer at the margin of an anticyclone over Greenland into the Greenland Sea. Temperature decreased to -6 °C. Meanwhile there was good visibility with a relative humidity of about 50 %. While approaching the marginal ice zone of eastern Greenland, the cloud layer thinned and temperature decreased to -11 °C at the surface. In the meantime, the frontal zone reorganized over northern Europe, so that the anticyclone over Greenland moved to the East. The pressure gradient over *POLARSTERN* increased due to a pressure drop over Greenland. After some calm days the wind increased April 7 to force Bft 5 from the South. Occasionally heavy snowshowers developed and after the passage of the cold front the air temperature decreased to -11 °C.

A following anticyclone calmed the weather over the Greenland Sea April 9. During the night of April 10, warm air masses were advected from a low north of Iceland. The southwesterly wind increased during the day to Bft 7 with decreasing visibility and snowfall. The temperature rose to -2 °C. The cyclone then passed the working area with weak variable winds. On April 10 the backside of the low caused cold air advection. Pressure rise calmed the weather. On April 13 *POLARSTERN* headed home between an anticyclone over Scandinavia and low pressure over Iceland, resulting in occasionally strong southeasterly winds.

2. Remote sensing

2.1. Microwave remote sensing: radiometer and ground measurements (K. Flückiger, H. Gmünder)

2.1.1. Motivation

At the present time there are many algorithms and methods to derive sea ice concentrations using different kinds of satellite data. Radiometers working in the microwave range are very suitable for sea ice mapping because the natural microwave radiation of the earth's surface, at specific wavelengths, penetrates almost all cloud and fog cover. Moreover, the contrast between the emissivities of sea ice and open water in the microwave range of the electromagnetic spectrum is very large. Our main objective in participating on this first "Polarstern" winter expedition to the Arctic is to compare summer microwave measurements with winter microwave signatures. With these data we will try to improve existing sea ice concentration retrieval algorithms and, consequently, to improve the accuracy of sea ice distribution maps. In our experiment we measured the brightness temperature with 4 radiometers of the Dicke type at 11 GHz, 21 GHz, 35 GHz and 48 GHz with vertical and horizontal polarisation.

2.1.2. Measurements made during ARK IX/1a

On the first leg of the cruise we measured brightness temperatures of the multiyear ice floe where we stayed several days. The radiometers were mounted on a platform which allowed variation of the nadir angle and switching between polarisations. This platform was fixed to an aluminium frame on skis, 1.5 m above ground. This sledge could be easily moved over the ice surface. On the ice floe we marked 5 fields taking into consideration typical ice topographies:

- a pond with drifting snow
- a flat snow covered surface
- a pressure ridge
- a flat topped mound with a hard snow crust.
- bare ice

Each spot was measured once or twice a day. One measuring cycle consisted of:

- direct surface measurements with nadir angles at 30°, 40°, 50° and 60°, vertical and horizontal polarisation
- sky measurements with a reflector with nadir angles at 120°, 130°, 140° and 150°, vertical and horizontal polarisation
- blackbody measurements for data calibration

Before the first and after the last cycle of the day we made direct sky measurements with nadir at 120° and 180° as well as an additional blackbody measurement for data calibration. In addition to our microwave measurements we dug pits through the snow cover down to the ice surface to take temperature, density and salinity profiles. During the ice station it was very cold - the temperature often dropped below -35 to -40 °C so that electronic equipment sometimes failed. A supplementary measurement in the infra-red range couldn't be done, because the respective IR-radiometer failed at this temperature. The duration of this ice station was too short for our experiment.

2.1.3. Measurements made during ARK IX/1b

During the second leg, we fixed the platform with the radiometers to the railing on the port side of A-deck. The strong winds meant we couldn't use the reflector, therefore we made additional direct sky measurements with nadir angle at 120°

and 180°. It was difficult to measure from the ship down to the ice surface; while moving the ship destoyed the ice surface; during oceanographic work the ship had to keep its position using the bowthrusters which flooded thin ice sheets or pushed away thick ice floes. As nilas and young ice are flexible and didn't break we could measure them from the moving ship. During 3 short ice stations we went on the ice with the 21 GHz/35GHz radiometer mounted onto a tripod. In the Odden we finally could take measurements of pancake ice. On this second part of the cruise we got a good overview of different sea ice types.

2.1.4. General observations

Brightness temperature is calculated from the output voltage of the radiometers, the Dicke temperature and the calibrations. The brightness temperature itself is composed of the sea ice emissivity, the physical temperature of the emitting surface and the portion of reflected sky radiation. A first look at the data shows us the following ideas:

- There is a significant difference between the 5 fields we measured. This may be caused by the melting process in summer.
- There is no significant difference between the emissivities measured on different days, although the brightness temperatures differ a lot. We always had nearly the same weather conditions, so we couldn't investigate dependencies on meteorological parameters. Under a deep snow cover the sea ice conditions will change very slowly.
- The larger the nadir angle the larger the differences between horizontal and vertical polarisations. In places with a deep snow cover fresh snow decreased this tendency, whereas in places with little snow this tendency increased with fresh snow.

The emissivity of a homogenous object with a stable temperature distribution is easy to determine. On the other hand the measured brightness temperature of our icefloe is composed of the radiation of the different layers. The radiation of the lower layers is partially absorbed by the upper layers. The snow cover scatters the radiation to some extent; fresh snow even affects its polarisation. The temperature distribution is dependent on the thermal conductivity and the depth of the different snow and ice layers as well as the variations of the air temperature during the previous few days. To calculate an exact value for the emissivity in different frequencies we should retrieve the portions of radiation of each layer by a model and investigate the likewise weighted temperature to a representative physical temperature. Because we cannot get detailed input for this modelling by satellite data we will have to map the sea ice using brightness temperatures without calculating the emissivities first.

2.2. Microwave remote sensing: radiometer measurements, satellite and airborne observations (R. O. Ramseier, C. Ramplee-Smith, C. Stuart)

2.2.1. Objective

The main objective was to classify and map the extent of thin sea ice types by using a passive microwave radiometer operating at 37 GHz. These measurements and ice thickness observations have also been complemented by concurrent measurements with a helicopter-borne line scan camera, the Special Sensor Microwave/Imager (SSM/I), the ERS-1 Synthetic Aperture Radar (SAR) and hopefully by the ERS-1 scatterometer.

2.2.2. Methodology

In preparation for this experiment, collection of SSM/I data started on January 10, 1993 at two day intervals. The frequency was increased to once a day at the start of the ARK IX/1a experiment. Intensive ship based passive microwave measurement and observation periods occurred from 27 to 31 March, 3 April, 5-6 April and 10 April. Figure 2.1 shows the cruise track with the location of the station. The upper part of the ice edge up to the dashed section corresponds to the ice condition on 27 March. Below the dashed section the ice edge corresponds to the condition of 5 April.The first ice measurements were carried out along latitude 79°N. The second set involved an isolated ice field (73°N 1°W, 3750 km^2 in area) which is part of the "Odden", a promontory usually extending from the East Greenland Current ice pack below 75°N in form of a large tongue as far east as 3° (this year). The third set of measurements were obtained along 75°N in the Greenland ice pack. The final set of observations was carried out along the northern Odden ice field at 75°N along the 0° meridian. Figure 2.2 provides a snap shot of the ice conditions as obtained from the SSM/I on board the ship for the periods involved. The objectives were accomplished without serious equipment problems. Nature was also co-operative by providing significant amounts of uniform thin ice types well within the Greenland Sea ice pack. Particularly gratifying were the measurements of the remains of the "Odden" which consisted primarily of pancake ice ranging in thickness from 20 to 30 cm and from centimetres to decimeters in size.

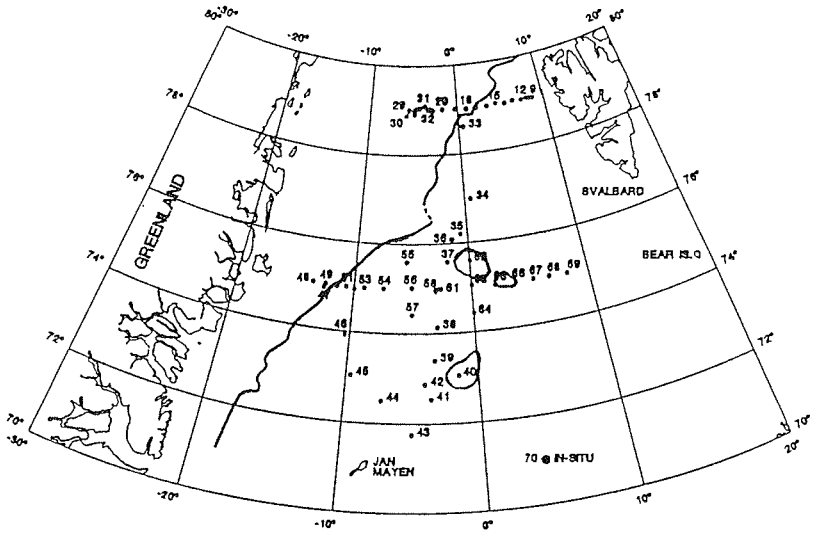

Figure 2.1: Station map for ARK IX/1b. The ice features correspond to the situation at the time encountered. The southern part of the "Odden" was seen on April 3, and the northern part on April 10.

Through out the period of ARK IX/1 SSM/I ice maps were provided to the REFLEX II experiment (Longearbyen aircraft operation) as well as the RV *POLARSTERN* as long as the ship was within the INMARSAT receiving mask. The RV *POLARSTERN* received data either directly from the Microwave Group-Ottawa River, or indirectly through the German Ice Service by sending the SSM/I maps from the Ice Branch R&D office in Stittsville, Ontario to the Bundesamt für Seeschiffahrt und Hydrographie (BSH) in Hamburg, Germany where they were redrawn to a more simplified version for transmission by radio facsimile from Pinneberg. An example of such a map is shown in Figure 2.3a. Although the RV "Polarstern" has a direct receiving capability of NOAA AVHRR data, these data were only useful for planning and navigation on a very few occasions, due to cloud cover and fog preventing the direct observations of sea ice. An example is given by the ice chart published by the U.K Meteorological Office showing the absence of the "Odden" feature in Figure 2.3b as compared to Figure 2.2b.
The helicopter, equipped with the combined LSC and infrared line scanner, was flown on 6 occasions while the ship was in the ice. Four were successful, providing good data. Examples of these data are shown in Figure 2.4.

2.2.3. Results

Passive microwave measurements at 37 GHz. A large data set was acquired with a number of good signatures of all ice types. The analysis of this data will take a significant effort and was not attempted on board. It is anticipated that a good classification of thin ice types will be possible showing the increase in brightness temperatures going from water to the presence of frazil, grease ice, slush, (shuga was observed but not in large enough quantities to obtain a signature), dark and light nilas over the entire thickness range, and grey and grey-white ice. The latter two were often covered with wind blown snow forming crusts and snow. Measurements during a snow fall, again clearly indicated the large increase in brightness temperature and depolarization as observed in 1989 during ARK VI/1.
SSM/I measurements. The SSM/I ice charts were used primarily for planning purposes of ice experiments, the retrieval of moorings, as well as the placement of new moorings. Figure 2.5 provides an analysis of the "Odden" feature during the experiment period. For this purpose, and because the "Odden" was often divided at 74°N into two parts, they are referred to as the northern and southern "Odden" ice fields. A special effort was made to reach the southern isolated ice field as soon as the program permitted it, since the northern field had vanished from the SSM/I ice maps as early as 1 April.
As one can see, the southern ice field disappeared for one day on 5 April. The planning for the retrieval of the moorings AWI 410 and AWI 411 along 75°N was done in a similar way as the planning for the "Odden" as shown in Figure 2.6. The mooring AWI 411 was successfully retrieved in ice free waters within the view of the compact ice edge. AWI 410 mooring was covered with 95% pack ice which provided too much of a risk for a successful recovery.
The location of the Greenland sea ice edge as determined from the SSM/I ice maps and by the Global Positioning System (GPS), which is an integral part of the GBR2 data acquisition and processing system, agreed within ±2 km. At 75°N the ice edge had become very compact as observed visually and on the SSM/I map of 5 April, Figure 2.2c. The "Odden" features provided a very interesting target. It is a fair conclusion to make that without the help of the SSM/I maps, the "Odden" feature would have been missed, since the area was always cloud covered, consequently the features were not visible in the

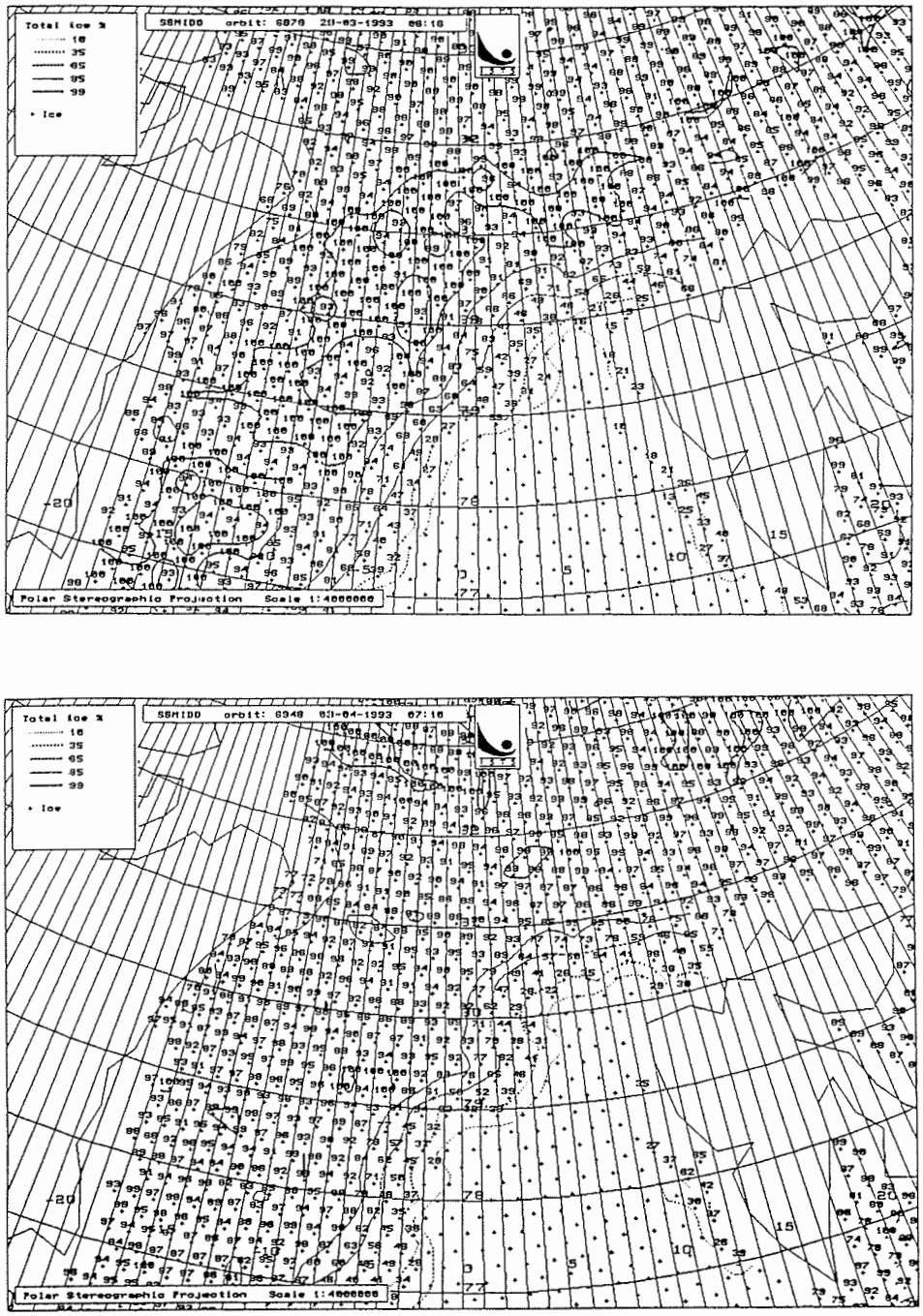

Figure 2.2 a and b: SSM/I ice maps for March 29 (*a*), April 3 (*b*).

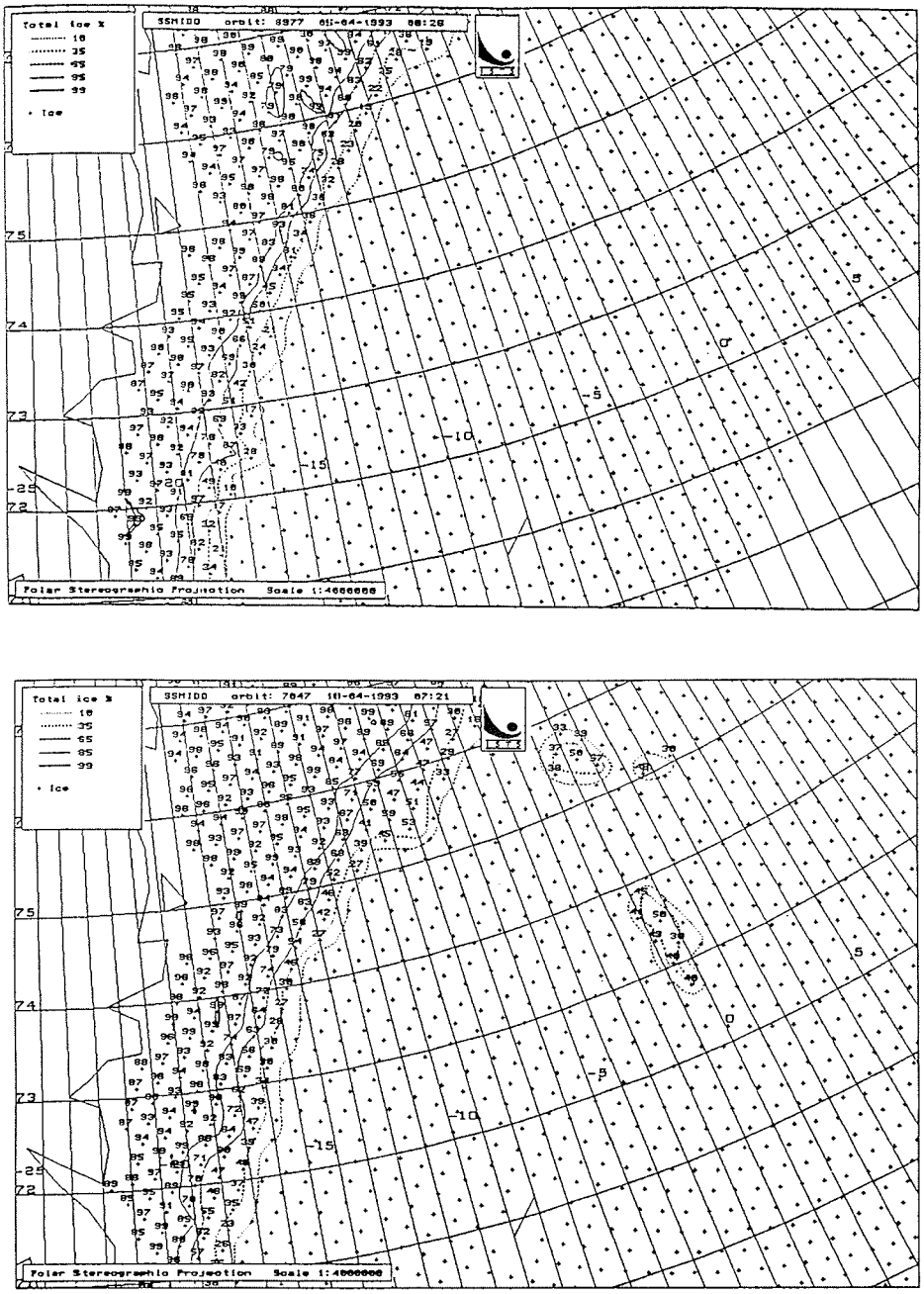

Figure 2.2 c and d: SSM/I ice maps for April 5 (*c*), April 10 (*d*).

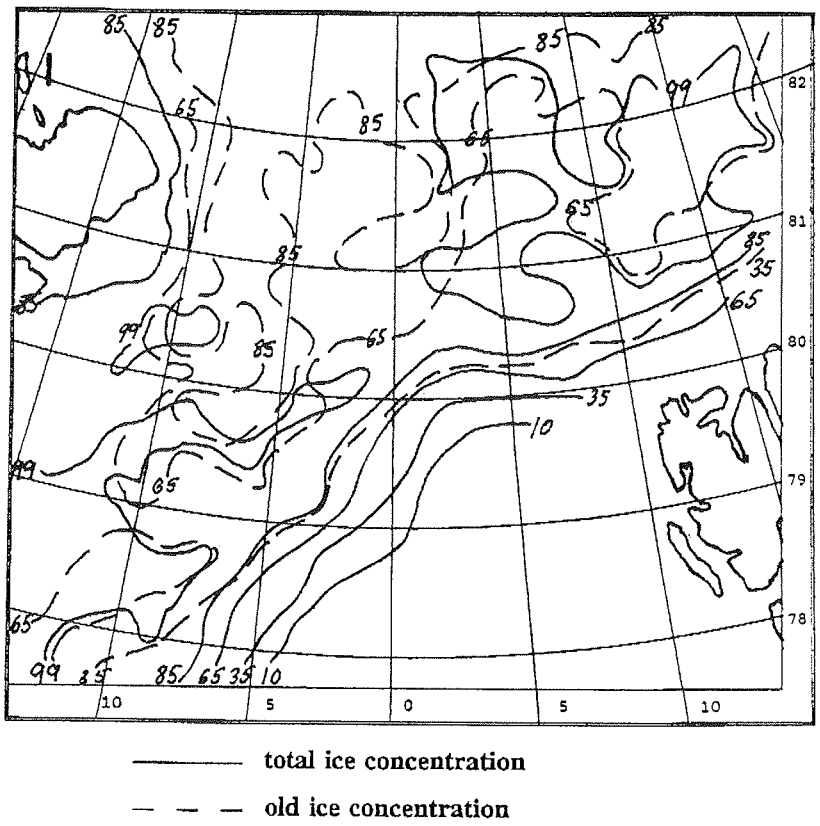

Figure 2.3: Simplified SSM/I ice map as prepared by BSH Marine Weather Service for radio facsimile transmission (total and old ice concentration chart of March 17, 1993, AES SSM/I data of orbit 6708, 07:29 UTC).

NOAA AVHRR images. Figure 2.5 provides an interesting history of the dynamics in ice extent (area) and average ice concentration for the period of ARK IX/1b. Comparing the "Odden" of this year with previous years seems to indicate that its growth and structure at the time of formation in mid January 1993, its subsequent advancements, retreats were very much an indication of the general lack of ice in the Greenland Sea. The persistence of the southern ice field (Figures 2.2b, 2.5b) since 5 March, and the occasional appearance-disappearance of the northern part (Figure 2.5a) are subjects of great interest. Observations during the period spent in the southern ice field (3 April) showed the presence of less than 10 %, of small and old ice floes. The rest of the ice consisted of young and "old" pancake ice. The assumption that the old ice floes took their origin from the east Greenland current and were advected by the Jan Mayen current as far east as 73°N 1°W is quite reasonable. The pancake ice seems to grow and melt in situ. Once the ice fields disappear on the SSM/I ice maps and reappear a day (Figure 2.5b) or seven days later (Figure 2.5a), does not mean that all pancake ice and old ice has disappeared. The

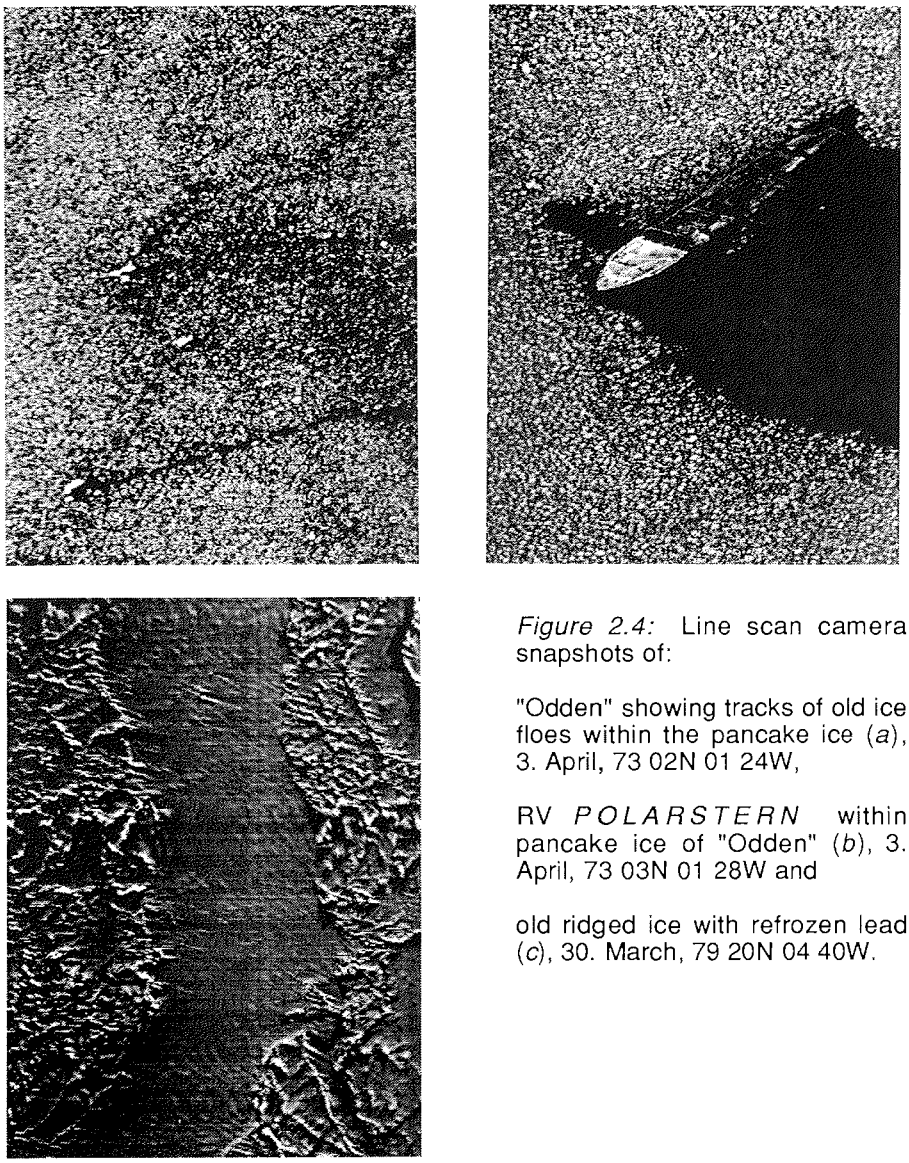

Figure 2.4: Line scan camera snapshots of:

"Odden" showing tracks of old ice floes within the pancake ice (*a*), 3. April, 73 02N 01 24W,

RV *POLARSTERN* within pancake ice of "Odden" (*b*), 3. April, 73 03N 01 28W and

old ridged ice with refrozen lead (*c*), 30. March, 79 20N 04 40W.

threshold of the SSM/I and the algorithm used for determining ice concentration, based on the validation of the sensor, is about 6%. In other words the SSM/I ice maps can not indicate ice concentrations of < 6%. The threshold of old ice fraction is not known but is estimated to be 10% or greater.

As indicated in the objective, the acquisition of ERS-1 SAR data was also part of the experiment. The German Ice Service provided via INMARSAT facsimile the first ERS-1 SAR fast delivery product from April 4th which was received on board the ship on 5 April, a scene depicting small amounts of ice in the area of the northern "Odden" ice field. On the way to the southern ice field, April 2, small pancakes, grease ice and frazil were observed in the vicinity of 75°14'N

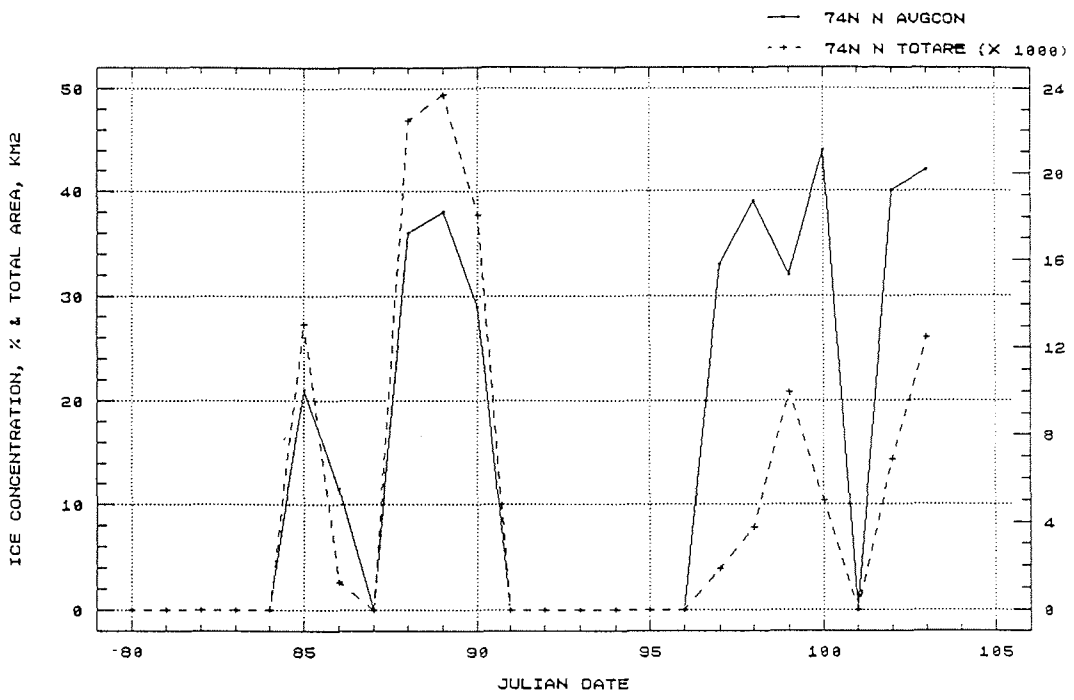

Figure 2.5 (a): Summary of total ice concentration and total area covered by "Odden" during the ARK IX/1b period. "Odden" North.

02°15'W. The last time the northern "Odden" ice field was indicated on the SSM/I ice chart was March 31st. It is safe to assume that the SAR detected this type of ice due to the damping effect the ice has on the waves.

Helicopter measurements. Figure 2.4 shows three examples of ice conditions obtained from the line scan camera mounted at the outboard end of the baggage compartment. Figure 2.4a shows a field of pancake ice with a number of tracks created by small old ice floes. Figure 2.4b depicts the RV *POLARSTERN* in a slightly looser field of pancake ice, some open water and single ice pieces within the open water. Figure 2.4c was taken in Fram Strait with a 100 % ice cover with ridged ice floes and a refrozen lead in the center of the image. These images will be used to determine floe and pancake size distributions.

2.2.4. Conclusions

Based on the data collected by the project as well as by the ship data acquisition system, it will be possible to obtain a much better basis to understand the presence or absence of the "Odden" features. It is also clear that the "Odden" with its old ice floes can provide a significant hazard to the unsuspecting mariner, since the isolated features are seldom reported in the ice charts available to the public.

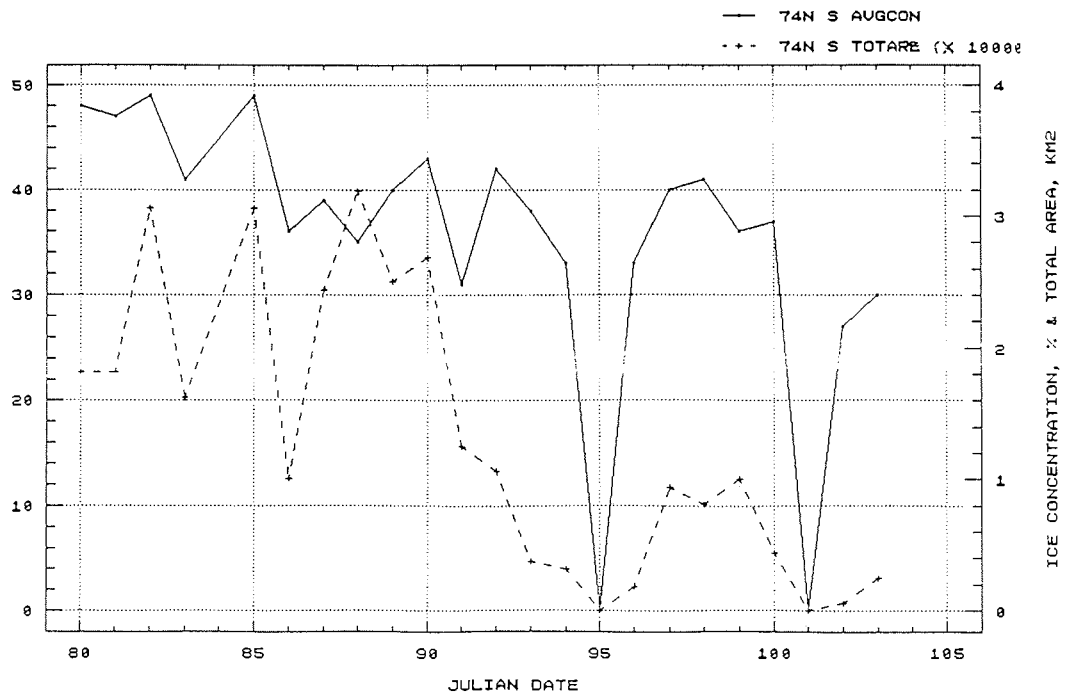

Figure 2.5 (b): Summary of total ice concentration and total area covered by "Odden" during the ARK IX/1b period. "Odden" South.

2.3. Studies of sea ice mass balance in the Greenland Sea (T. Viehoff, C. Oelke)

2.3.1. Objectives

The main objective of this study is to contribute to that part of the European Subpolar Ocean Programme (ESOP) which deals with the seasonal extent and variability of sea ice, the dynamics of sea ice, its mass flux and the exchange of fresh water and heat with the upper ocean on a basin-wide scale. The task of remote sensing techniques in this framework is to monitor the ice extent, concentration, types and velocities. These data are combined with direct measurements of sea ice thickness as well as with ice thickness measurements from airborne Laser systems and moored upward sonars.
The remote sensing programme uses a number of different techniques including the ERS-1 SAR data. The interpretation and validation of worldwide sea ice SAR-imageries is the main task of the Programme for International Polar Ocean Research (PIPOR). This cruise is part of a main validation experiment for interpretation of young ice signatures in the SAR data in the Greenland Sea in general and in the Odden region in particular.

2.3.2. Methods and results

Satellite imagery (visible and infra-red). As part of the ice mass balance studies of the East Greenland Current the remote sensing data were acquired

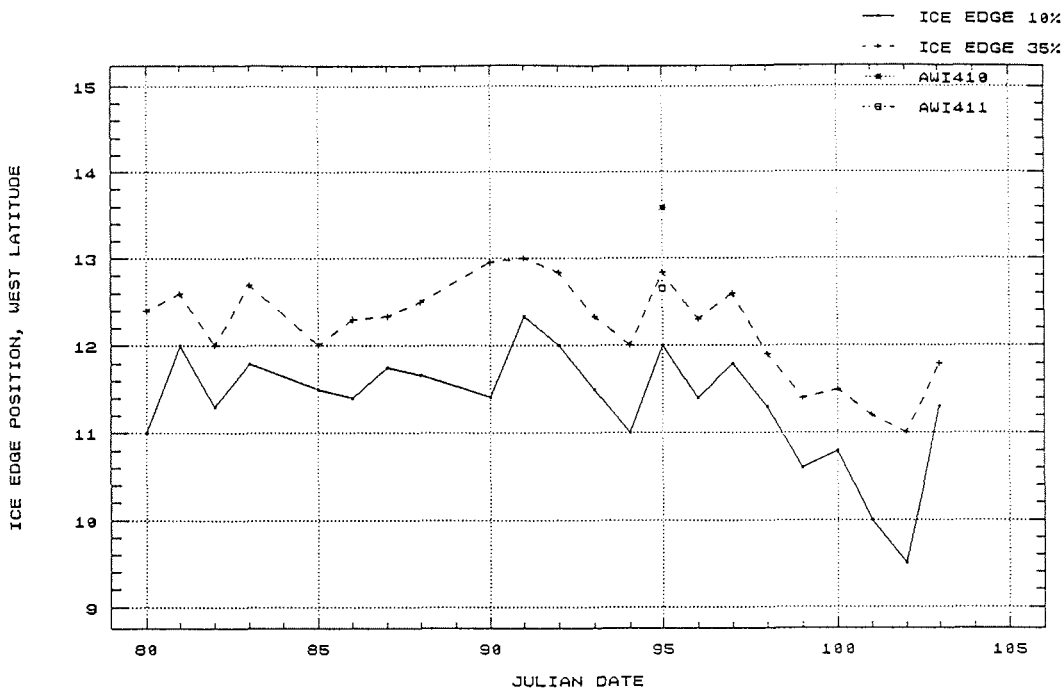

Figure 2.6: Ice edge 10% and 35% contour line positions along 75°N with AWI mooring positions.

for the estimation of the sea ice velocity field. The shipborne High Resolution Picture Transmission (HRPT) receiving station was used to acquire about 180 datasets of of the Advanced Very High Resolution Radiometers (AVHRR) which are flown on the NOAA satellites. This radiometer takes five channels which are located in the visible and in the infrared part of the spectrum. A subset of which 55 datasets of all five channels were calibrated and geometrically navigated to produce maps of the sea ice coverage in the Arctic basin and in the Greenland Sea between 85°N and 67°N (Figure 2.7).
The data will be used for a detailed analysis of sea ice motion und late winter conditions. This sea ice velocity study will be carry on for the next three year to collect a respresentive dataset of the variations in sea ice motion in the East Greenland Current.
Additionally the HRPT receiving station was used for a near real time ice support for the ship as well as for the planning of the scientific programme. Besides this the information from the Data Collection System (DCS) included in the HRPT data stream could be extracted and the decoded values of position, pressure and air temperature of a number of ARGOS bouys and automatic stations were used by the ships met office for forcast purposes.
The programming of the receiving station and the data handling was modified in a way that operational usage of the station for ice support is now possible.
For the calibration of the AVHRR-based sea ice concentration algorithm radiometric surface measurements were done using an infrared radiometer

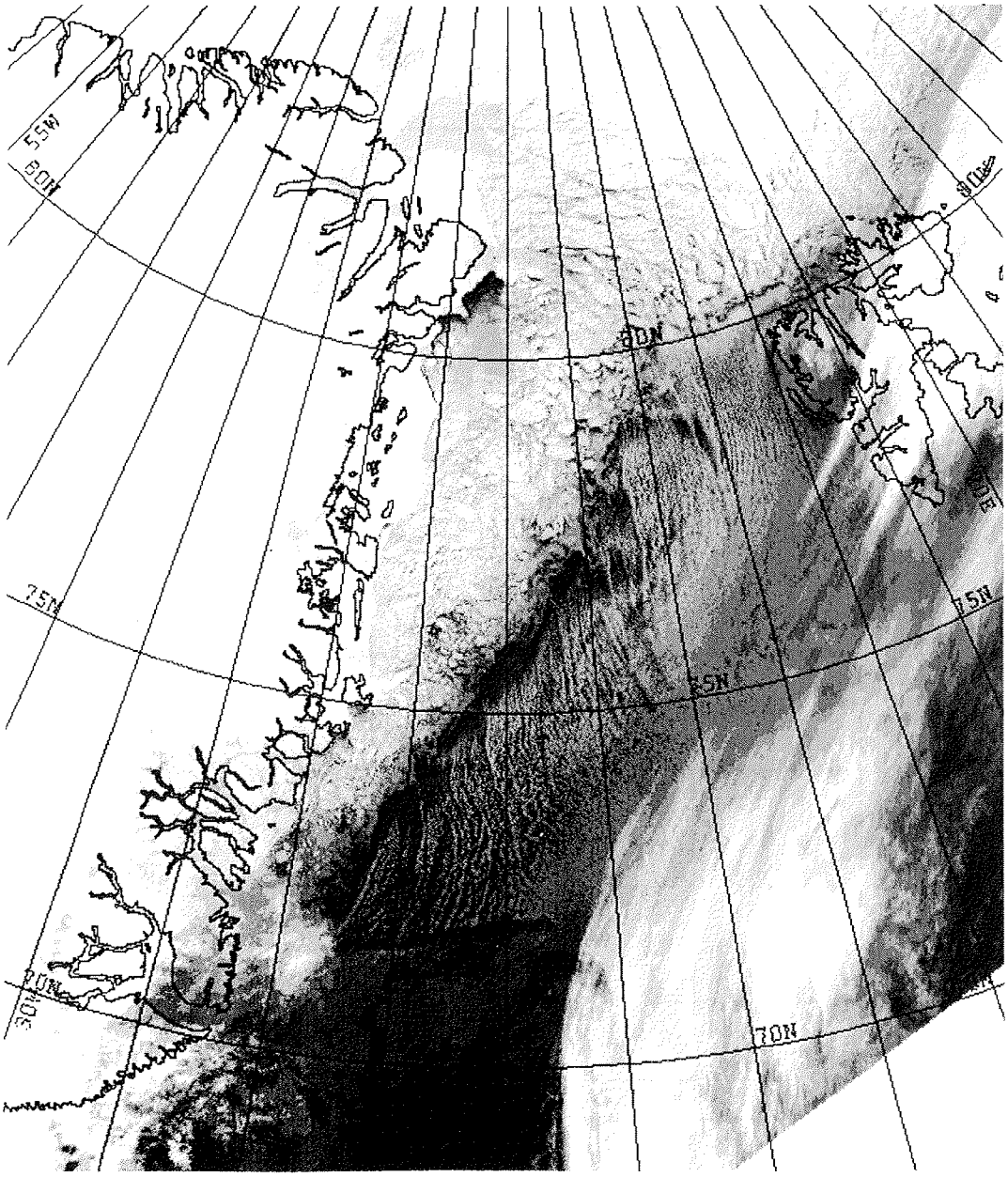

Figure 2.7: NOAA AVHRR infrared image from March 27 showing the ice edge along the East Greenland Current and Fram Strait during an off-ice wind situation. Low ice concentration is indicated in the North-East-Water polynya region off the Greenland coast at 81°N.

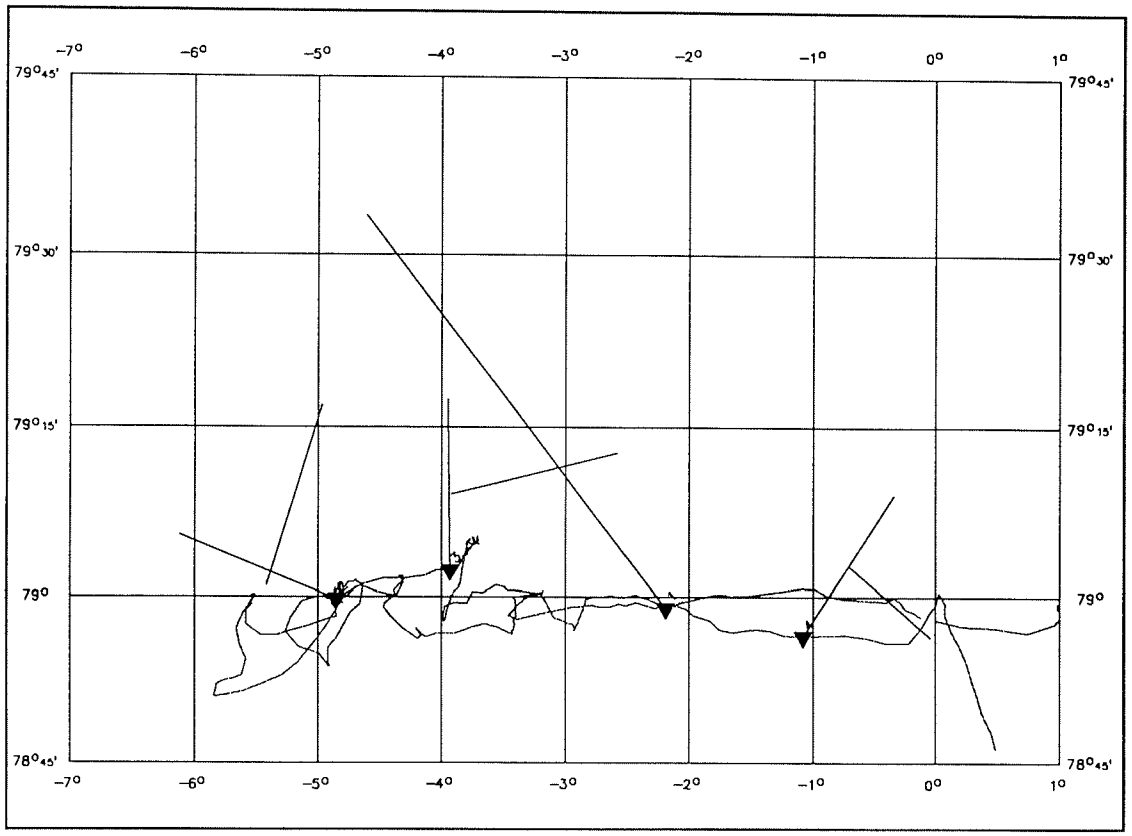

Figure 2.8 a: Flight pattern of the Laser profilometer flights and *POLARSTERN* cruise track along the Fram Strait section

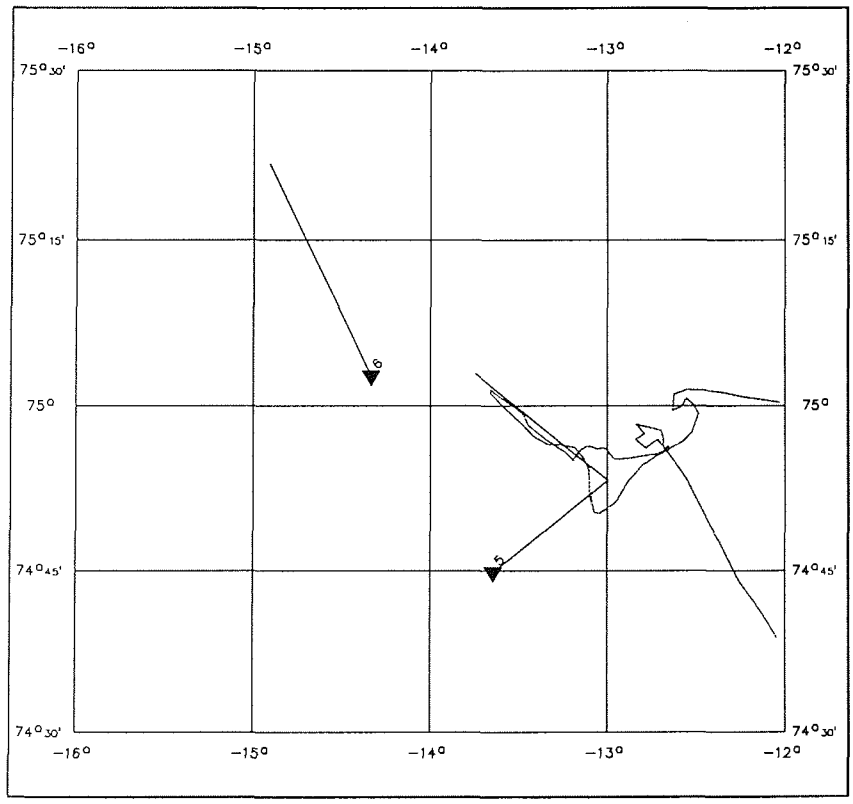

Figure 2.8 b: Flight pattern of the Laser profilometer flights and *POLARSTERN* cruise track along the 75°N section

mounted on the rear at A-Deck. The spectral range of the instrument is from 10 to 14 µm. Data were collected during the operation in ice covered areas only. Besides the comparison with the AVHRR data the IR data will be used for validation studies of an atmospheric radiative transfer model of microwave radiation. This model calculation will be done using also the microwave emissivity data from the swiss group and radiosonde profiles which were taken four times per day during operation in the ice. The aim of this project is the investigation of the atmospheric influence to the SSMI mircowave data used for sea ice concentration analysis.
The sea ice observations of all ice groups onboard the ship will be compared with the data from the Synthetic Aperture Radar (SAR) flown onboard the ERS-1 satellite. Therefore a detailed planning of the SAR acquisistion times was carried out in close cooperation with ESA prior to the cruise. This task was taken over by the PIPOR Coordinating Office located at AWI. During the period of February 20 to March 31 nearly all passes covering the Fram Strait area up to 83°N could be planned and acquired. For the period April 1 to April 20 the area 78°N from 72°N and from 5°E to 20°W was covered by ERS-1 overpasses. Additional to these offline processed data an averaged number of 3 scenes per day were processed by ESA as Fast Delivery Products. Some of

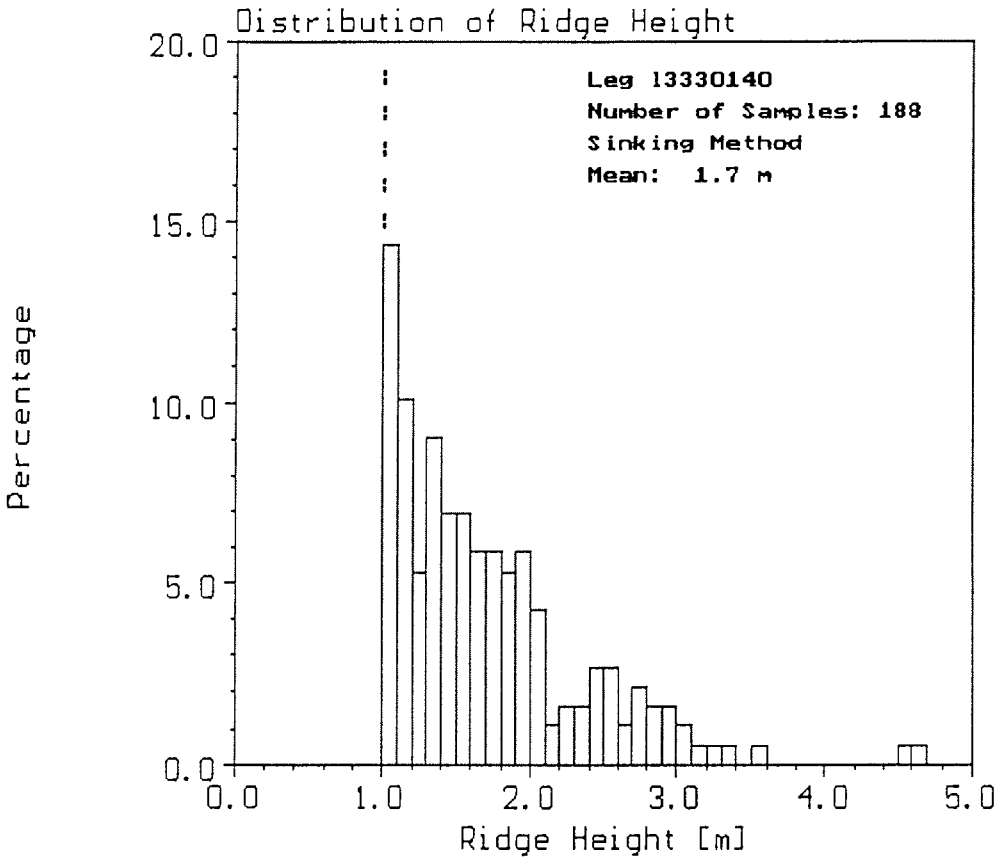

Figure 2.9: Example of the ridge height distribution for the flight 2 (March 30, 1993)

these data were transmitted to the ship via BSH, Hamburg and AWI within 24 hours after data acquisition. These near real time data turned out to be useful for the planning of the scientific programme especially in the Odden area. A detailed analysis of the data with respect to surface roughness, floe size distribution and ice type classification has to be done as soon as the offline data are available.

Airborne laser altimetry. A helicopterborne Laser Altimeter system was used to measure the surface roughness of the sea ice cover and to estimate the surface elevation (free-board) of the floes. The results of the freeboard investigation should be used for interpreting the data from moored Upward Looking Sonars (ULS) located in the same area. Therefore 5 flights were carried out at the transects in the ice at 79°N (3 flights) and at 75°N (2 flights). All together 9 profiles with lengths between 10 nm and 19 nm (134.1 nm in total) could be measured (Figure 2.8). The mean horizontal resolution of the profiles was about 15 cm with a vertical resolution of about 0.2 cm.

The data along both transects will be used for a statistical analysis of the ridge heights, mean ridge slopes and the distribution of the ridge spacing. In

combination with freebord calculations an estimation of mean ice thickness as measured by the moored ULS will be done.
In addition the surface roughness data will be used for the interpretation of the radar backscatter signal as measured by the ERS-1 SAR. During the experiment one direct SAR underflight (March 30) and three underflights with time lags of less the one day (February 29, March 30 and April 6) could be carried out. For one of these underflights the data from the optical LineScan Camera can be used for estimating the two dimensional distribution of the ridges.
A first analysis of the data from the 79°N section indicates that the ridge activity in the inner part of the ice cover (about 30 nm from the edge) seems to be nearly constant. The mean ridge height was about 1.7 m and the mean ridge widths was between 3 and 8 m . The height distribution shows an exponential distribution of the ridge heights between 0.5 m and 4 m (Figure 2.9). The mean ridge spacing was about 140 m with a maximum between 10-20 m. The distribution of ridge slopes shows a maximum at about 20° with a second maximum at about 50°.
At the 75°N section the different sea ice regimes could be measured. The diffuse outer ice edge was characterised by fields of MY broken floes with diameters of 10-50 m and relatively high freebord of about 1 m. At about 30 nm from the ice edge the influence of the swell disappeared and the mean floe size increased to more than 2-5 km. The ridge activity seems to be nearly constant in both regimes.

3. Boundary-layer meteorology

3.1. General remarks (H. Jeske)

Within the frame-work of the first part of the expedition ARK IX/1 from February 26 to March 24, 1993 two research-campaigns were coordinated simultaneously, namely ARKTIS '93, mainly produced by the "Sonderforschungsbereich 318 of Hamburg University (Processes Relevant to Climate)", and REFLEX II, mainly carried out by the Alfred Wegener Institute for Polar- and Marine Research, Bremerhaven. The main aim of the campaign ARKTIS '93 was the investigation of cold air outbreaks from the inner Arctic ice cover, especially west of Svalbard. These outbreaks are of immense importance for climatological processes. They are responsible for deep convection in the ocean and formation of new ice and for intensive convection in the atmosphere, coupled with cloud formation of organized structures. The convective pattern along a down-stream trajectory depends on the initial and boundary conditions in the pack ice and on the large-scale weather conditions. The main topic of the campaign REFLEX II was the determination of the budgets of momentum and energy (eddy fluxes of sensible and latent heat, short- and longwave radiation) at the boundary between atmosphere and ice or broken ice or water and its influence on cloud and haze formation. For both campaigns four research aircrafts were in operation from Longyearbyen airport at Svalbard.
The position of the ice-strengthened research vessel *POLARSTERN* was about 100 km within the pack ice (mean position: 81°N 5°E) in order to get the relevant meteorological parameters for the initial and boundary conditions and - together with other research vessels (*VALDIVIA* from Hamburg University (mean position: 73.5°N 10°E), *PROF. MULTANOVSKY* (mean position: 75°N 5°W) from the Arctic and Antarctic Research Institute of St. Petersburg, Russia) and weather stations at Svalbard, Bear Island, Norway, Jan Mayen, and Greenland (east coast) - to obtain the large-scale weather conditions (divergence, advection, geostrophic wind, baroclinicity). This network was supported by six ice drift buoys installed in the measuring area (see Section 3.4).

3.2. Ship-based measurements (H. Jeske)

The RV *POLARSTERN* operated between March 4 and March 23 within the measuring area of interest, from March 7 to March 20 moored to an ice floe (see Section 3.3). On board *POLARSTERN* aerological soundings with a frequency of four per day (00, 06, 12, 18 UTC) were performed, meteorological surface parameters (pressure, temperature, humidity, wind velocity, -direction, water temperature, short- and longwave radiation) were continuously monitored (from the automatic weather station on board), and hourly synoptical observations (cloud cover, cloud type, cloud height, visibility and other special weather phenomena) were carried out. All the data were transmitted to the synoptic network of weather services in order to use the data for global or regional weather forecast models.
The weather situations are described in detail in Section 1.2 by the meteorologist of the weather station on board of RV *POLARSTERN* . Some statistics of surface parameters during the cruise are included.
As a general overview of the weather conditions during the measuring period the time series of pressure, temperature, wind velocity and wind direction are

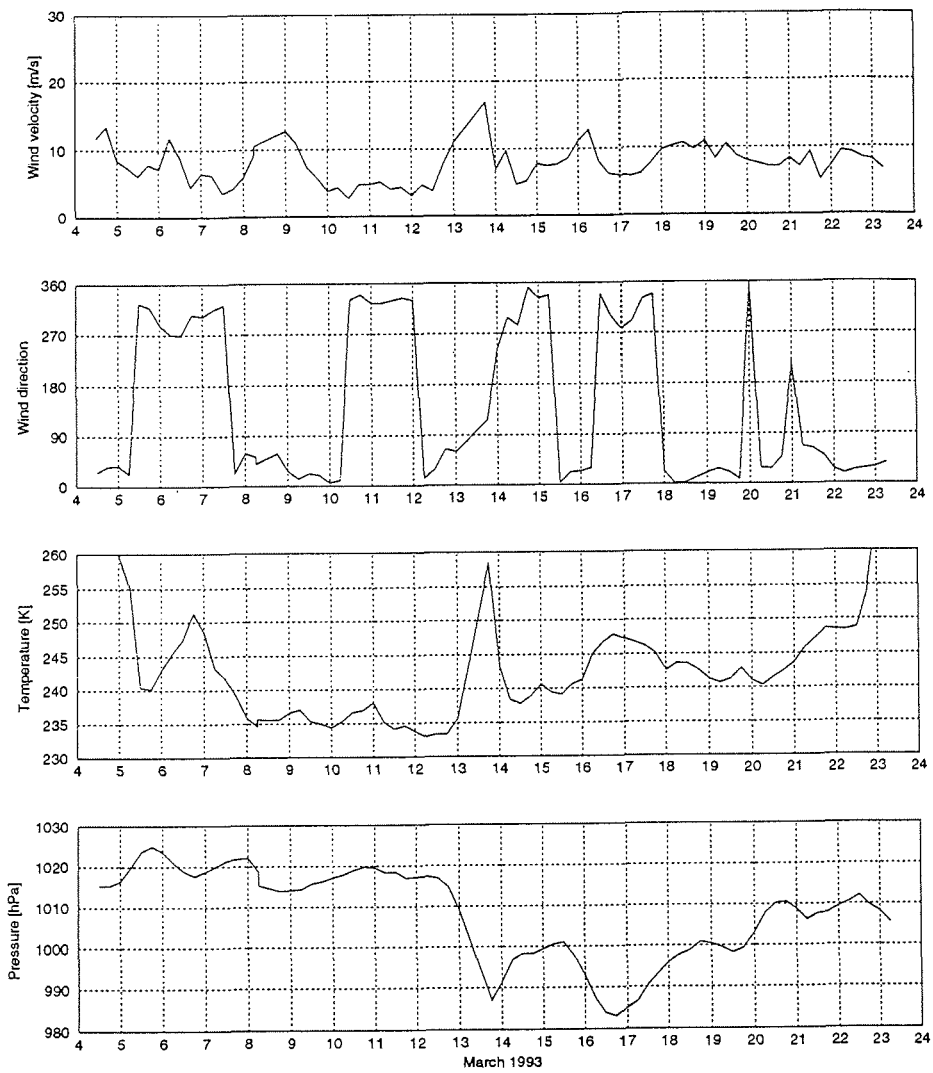

Figure 3.1: Time series of wind speed, wind direction, temperature, and surface pressure at RV *POLARSTERN* from March 4 to 23, 1993.

plotted in Figure 3.1. Four situations with definite cold air outbreaks from the north were observed, namely from March 4 to March 5, March 9 to March 11, March 18 to March 20 and March 23 to March 25. Figure 3.2 represents a typical satellite picture of such a situation. As another very interesting meteorological phenomenon the development and passage of a Polar Low near *POLARSTERN* at March 13 and March 14 is mentioned (Figure 3.1). The temperature increased from -37 °C to -9 °C, the wind velocity increased to 36 knots with changing its direction from 20° to 360° (right-handed).
The aerological soundings were performed with a Vaisala MicroCora system with Omega windfinding. The radiosondes of the type RS80-15 were started

with 350 g balloons with ascent rates between 250 and 350 m/min. The maximum heights reached were between 15 and 28 km. As an overview of the aerological data Figure 3.3 shows the height of the tropopause as a function of time. Examples of the vertical structure of temperature, dew point, wind velocity and -direction are given in Figure 3.4 (situation of cold air outbreaks) and Figure 3.5 (Polar Low situation).

3.3. Central ice station (A. Grelle, H. Lohse, G. Peters)

3.3.1. General conditions and major events

On March 8 the search of a suitable place for the ice station ended at the northeastern end of a lead at 81°28'N 7°37'E at about 60 miles distance from the ice margin. The ship was moored to a large ice-field at the northwestern side of the lead because only on this side the ice was solid enough to carry heavy equipment.

Despite of extreme exertions of crew and scientists to remove the ice cover from the foredeck the crane could not be put into operation. Therefore none of the major instruments stowed in the forecastle could be unloaded. Consequently the core of the measuring program - remote sensing of wind and temperature in the lower 1000 m of the atmosphere - had to be dropped. Only small portable equipment could be set to operation on the ice.

One fortunate exception was the 15-m mast, which was stowed on the quarter deck and which could be mounted without difficulties using the aft crane of the ship. As the mast was erected at the floe edge, single sided stay poles rather than guy wires had been used to stabilize the mast. This position of the mast was selected in order to study the boundary layer for different upwind surface conditions (dependent on wind direction): open water, thin ice and multi-year ice. The possibility of quick dismounting and recovery of the instruments was an additional reason to select this position. The mast was equipped with 10 Pt-100 temperature sensors, 5 sonics, 1 fast temperature sensor (2.5-µm wire) and 1 fast Lyman-alpha humidity sensor. An additional sonic was mounted on a boom over the open water at 1.4 m height. The installation work was made more difficult by extremely low temperatures (down to -40 °C), which prevailed during the first days. This explains, why the measurements could not start before March 11. Eventually measuring systems had been deployed at 12 places in up to 300 m distance from the ship.

Due to the frozen bow-crane power supply and data recording units for the instruments had to remain on the ship. Therefore the distance between sensors and ship was limited by the available cable length which was not quite satisfying in all cases. As far as wind, air-temperature and humidity measurements are concerned the ship's disturbance was acceptable because the sensors were never in lee of the ship. But the radiation sensors were sometimes disturbed by the ship's shadow. It should be possible to identify disturbances as redundant sensors for up- and downwelling long wave and short wave radiation, air-, skin-, snow-, and ice-temperature, wind, momentum-flux and sensible and latent heat-flux, installed at different sites, offer ample possibilities for cross checks and validation of results.

The site surface conditions and the locations of the measuring systems listed in Table 3.1 are shown in Figure 3.6. The surface structure in the farther environment has been surveyed by a helicopter-borne laser altimeter. The flight legs are indicated in Figure 3.7.

One additional difficulty was caused by the ship-based operation: All data lines suffered from a high noise level. This interference prevented control and

data recording for some of the systems. In these cases provisional local data logging had to be installed. In other cases the measured data showed some susceptibility to these interferences. This was definitely the case for the temperatures measured at the 15-m mast. But the disturbances could be reduced to an acceptable level by shielding the data cables and averaging over 3000 samples (5 min). There was some indication that not all of the interference was caused by the ship, but that part of the trouble was due to electrostatic discharges between communicating systems, if they were operated with floating potentials (no galvanic connection). Due to the adverse weather conditions and to the lack of time this effect could not really be traced down. But it seems that electrostatic charging - especially in case of snow drift - has to be considered at these low temperatures. Most sensors were subject to considerable rime cover and had to be cleaned or exchanged in short intervals. One exception was the sonic type USAT which contained a sensor-head-heating.

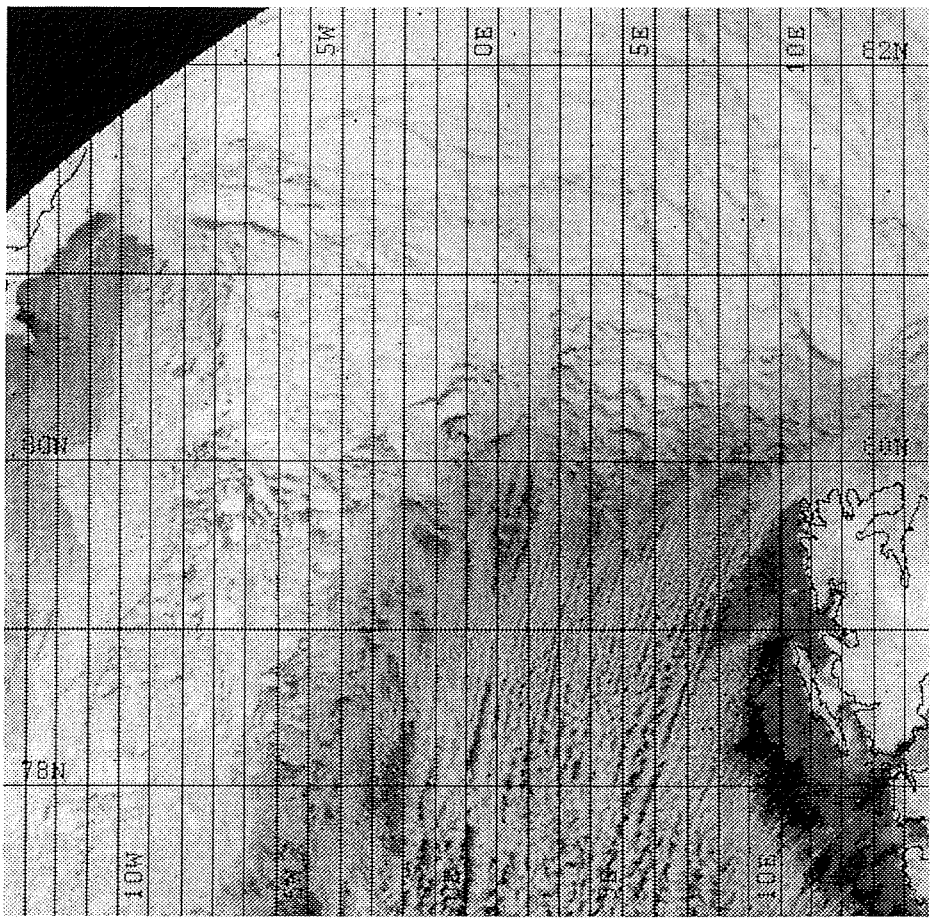

Figure 3.2: Satellite picture of a "cold air outbreak", NOAA-9, Channel 4, March 4, 1993.

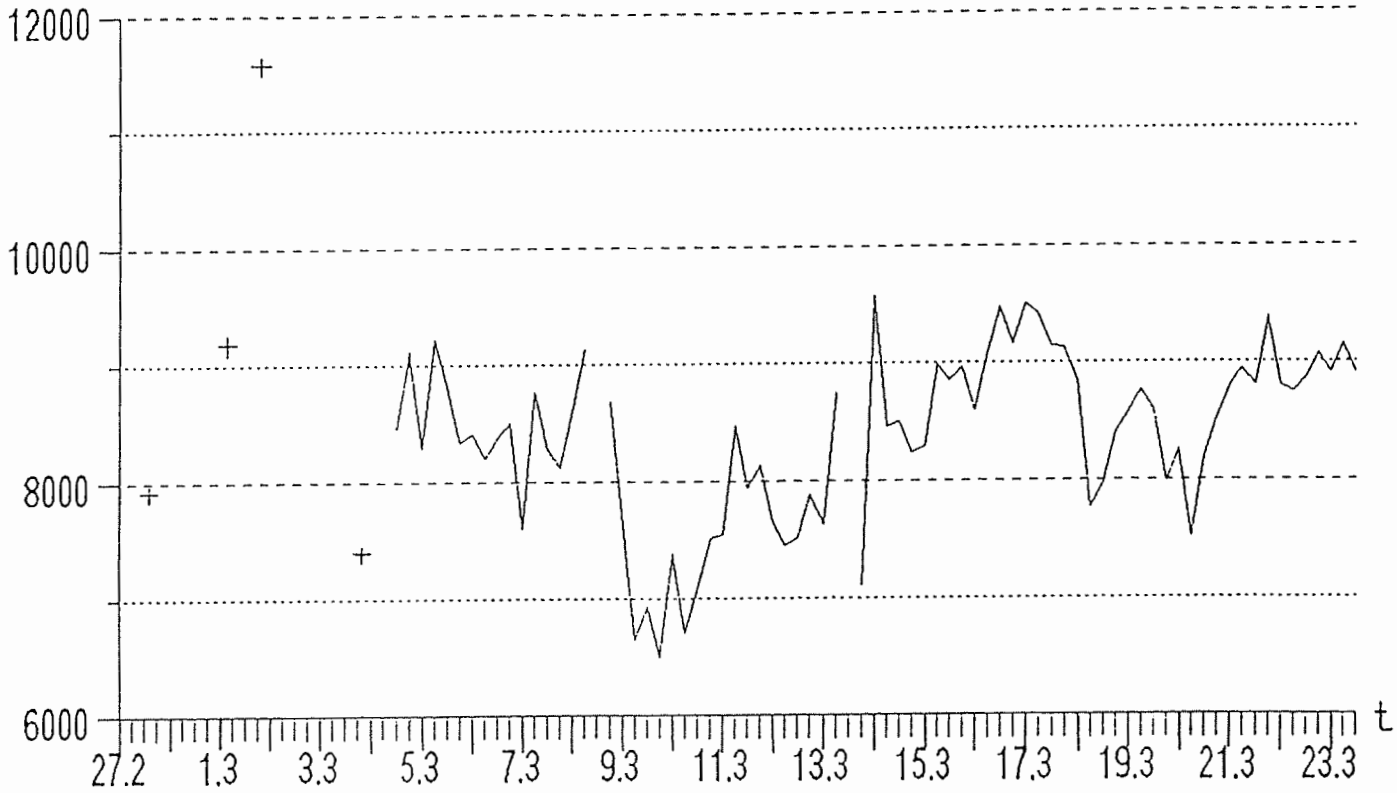

Figure 3.3: The height of the tropopause (gpm) as a function of time.

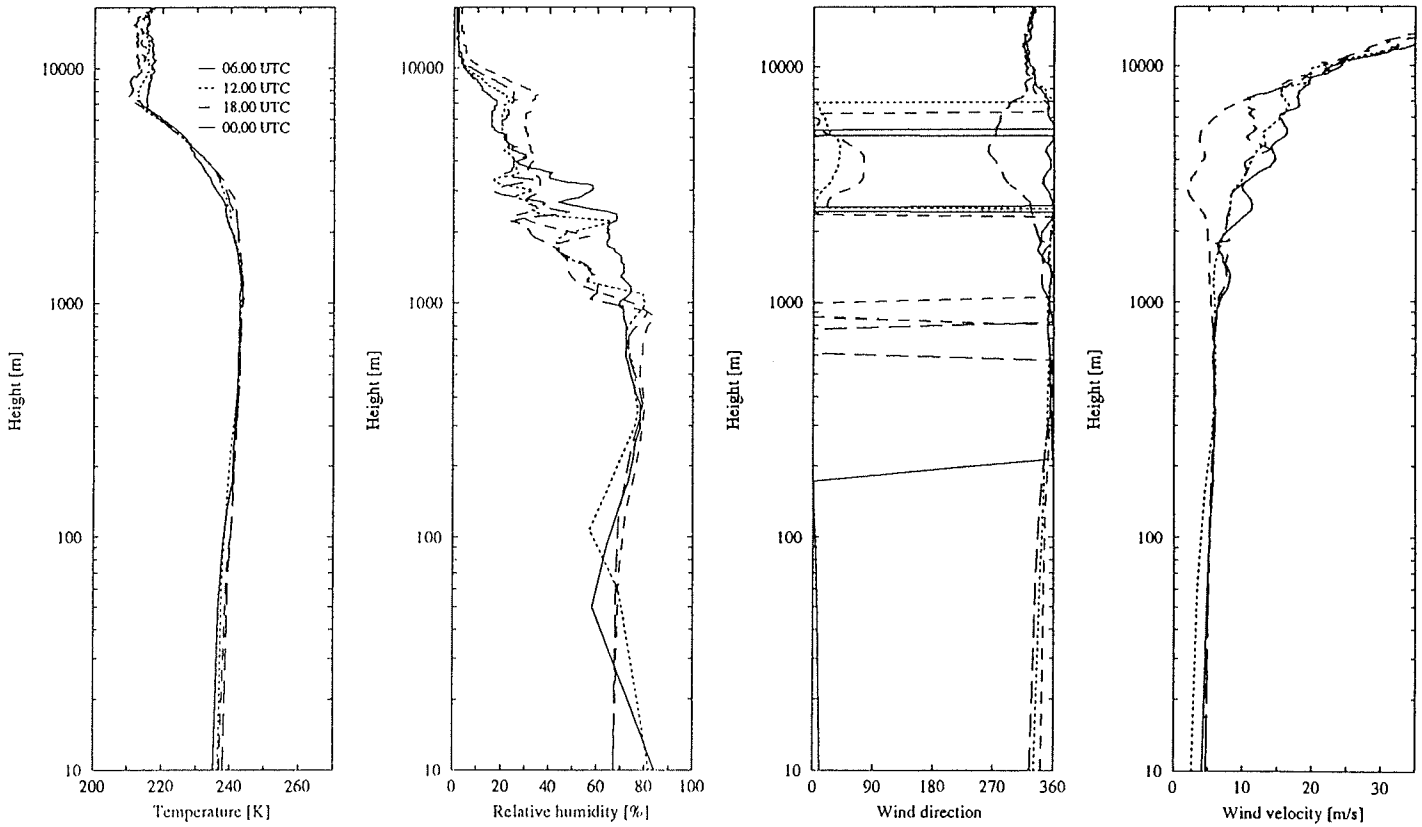

Figure 3.4: Radiosoundings: Vertical profiles of temperature, relative humidity, wind speed, wind direction, March 10 at 06, 12, 18 UTC and March 11 at 00 UTC.

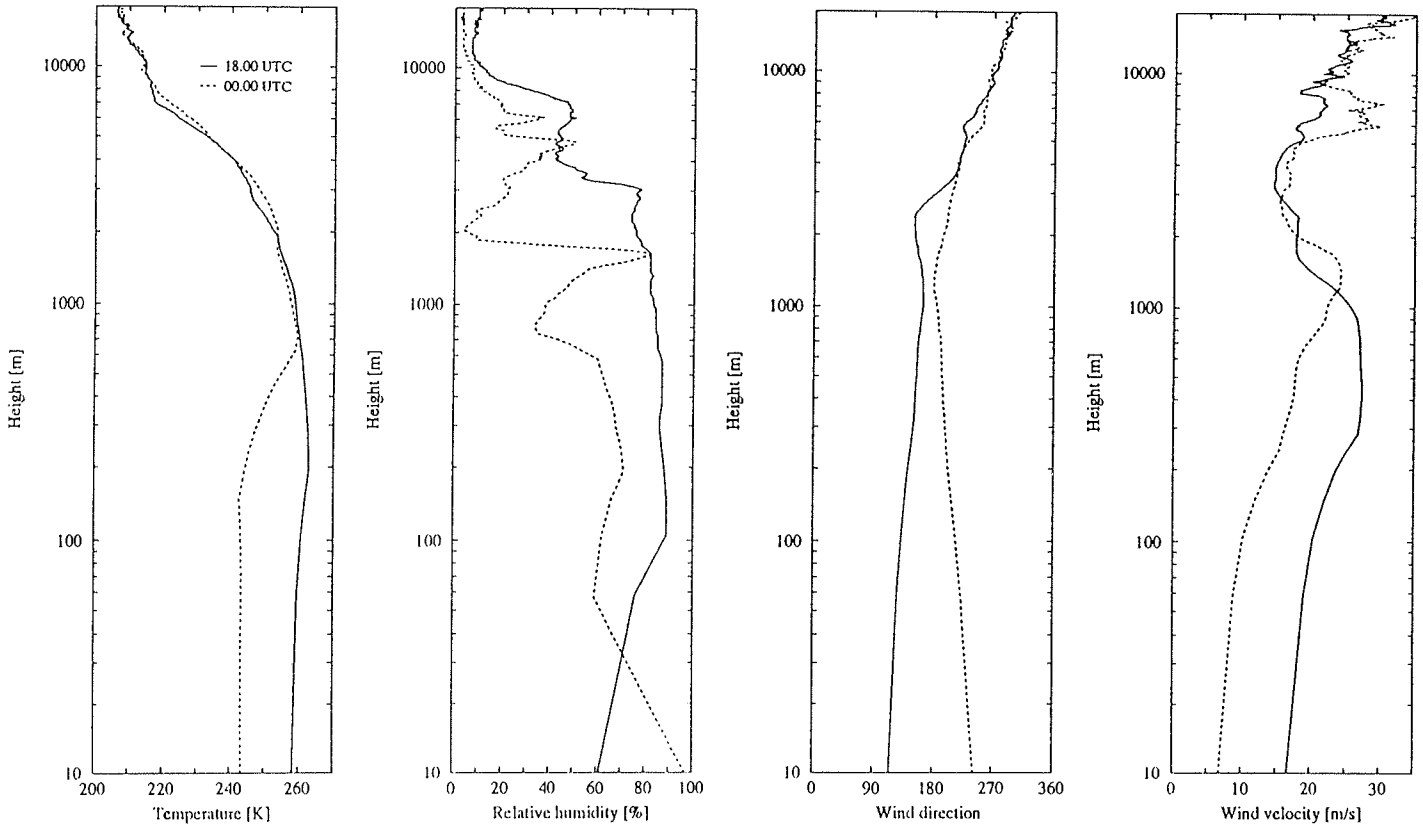

Figure 3.5: Radiosoundings: Vertical profiles of temperature, relative humidity, wind speed, wind direction. March 13 at 18 UTC and March 14 at 00 UTC (during and near the end of the Polar Low situation).

Table 3.1: Timetable of measurements

Site No.	System	Sensor or Subsystem	March 11	12	13	14	15	16	17	18	19
			Operation time in quarters of a day								
1	15 m Mast	10xPt100a	2	4	4	4	4	4	4	4	
		USAT1	1	4	1	4	4	4	4	4	1
		USAT2	1	4	1	4	4	4	4	4	1
		USAT3	0	0	0	0	2	4	4	4	1
		USAT4	0	0	1	4	4	4	4	4	1
	GKSS-Turb.	Kaijo-Denki-1	0	1	4	4	4	4	4	4	1
		Lyman-alpha-1	0	1	4	4	4	4	4	4	
		Fast-Temp-1	0	0	0	0	2	4	4	4	
1a	Boom	Kaijo-Denki	1	4	4	4	4	4	4	4	
2	CR10	CR10	0	0	0	0	0	0	3	4	
3	Argos 2	Argos 2	0	0	0	0	2	4	4	4	
4	Minerva	Minerva	2	4	4	4	4	4	4	4	
5	SLU	Solent	2	4	4	4	4	4	4	4	
		LI-COR	2	4	4	4	4	4	4	4	
		Fast-Temp	2	4	4	4	4	4	4	4	
6	GKSS-Turb.	Kaijo-Denki-2	0	3	4	4	4	4	4	4	
		Lyman-alpha-2	0	3	4	4	4	4	4	4	
		Fast-Temp-2	0	0	0	0	2	4	4	4	
7	CR7	CR7	0	0	0	0	2	4	4	4	
7a	Snow-Ice GKSS	10xPt100s	0	0	0	0	2	4	4	4	
8	Szintil-lometer	Szintil-lometer	0	0	0	0	0	0	0	0	
9	Radiation Garden	Radiation Garden	0	0	0	0	2	4	4	4	
10	Argos 1	Argos 1	4	4	4	4	4	4	4	4	
11	KT19	KT19	0	0	0	0	1	4	4	4	
12	Snow-Ice HH	20xPt100s	0	0	0	1	4	4	4	4	
13	Snowdrift	Snowdrift	0	0	0	0	0	0	0	0	
14	Ceilometer	Ceilometer	4	4	4	4	4	4	4	4	

On March 17, 11:00 UTC (Falcon) and 13:00 (Polar 2) aircraft intercomparisons took place.

The measuring campaign was terminated by a sudden break of the ice field into small floes during the night of March 18/19 at the final position 80°29'N 4°02' E. Now all measuring systems were scattered over many disconnected ice floes and the drift of the ship caused the immediate break of most of the cables. Only the connection to the 15-m mast could be maintained for three more hours thanks to the fast start of the ships engines. The last data - turbulent fluxes of momentum and heat - were received at 02:40 UTC. All instruments including the 15-m mast could be recovered during the next day without any damage.

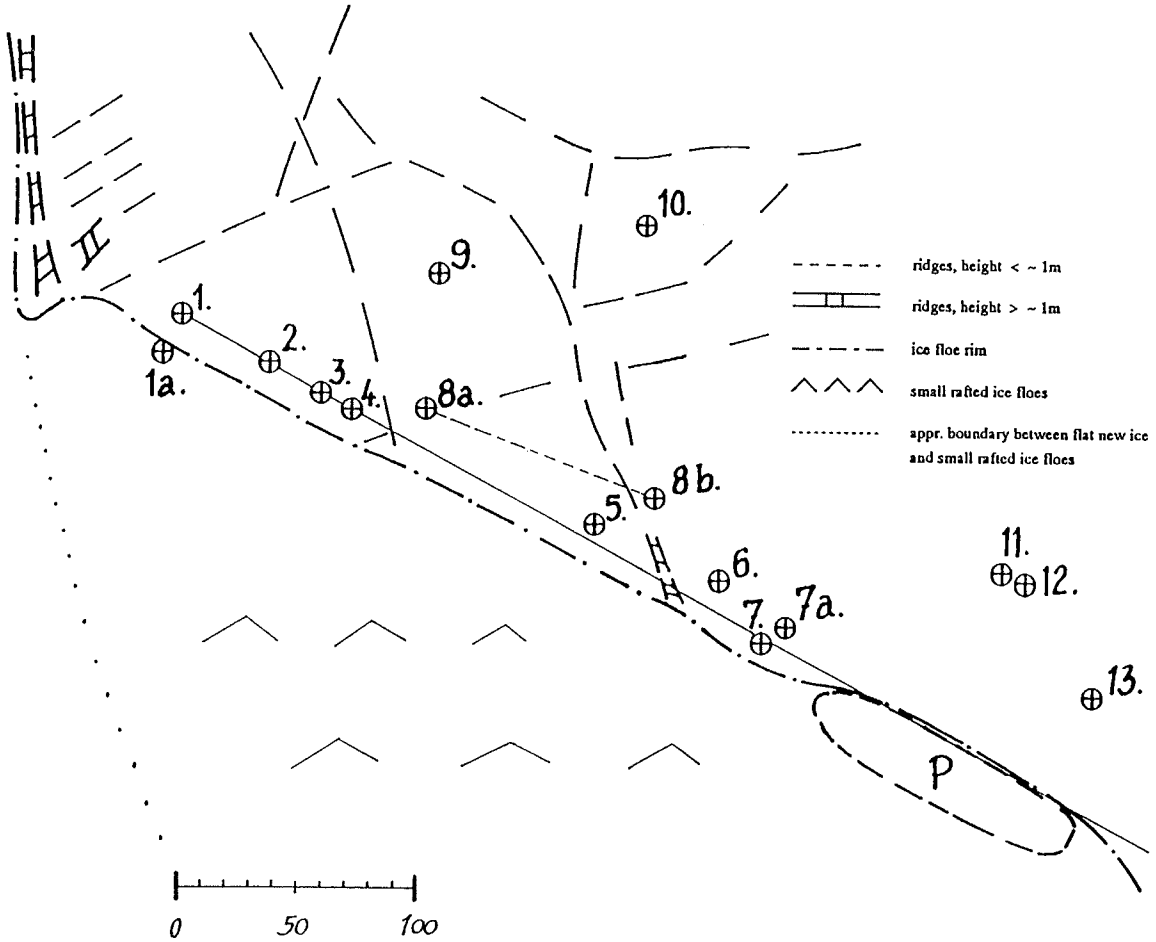

Figure 3.6: Meteorological experiment site. The numbers correspond to the measuring systems listed in Table 3.1.

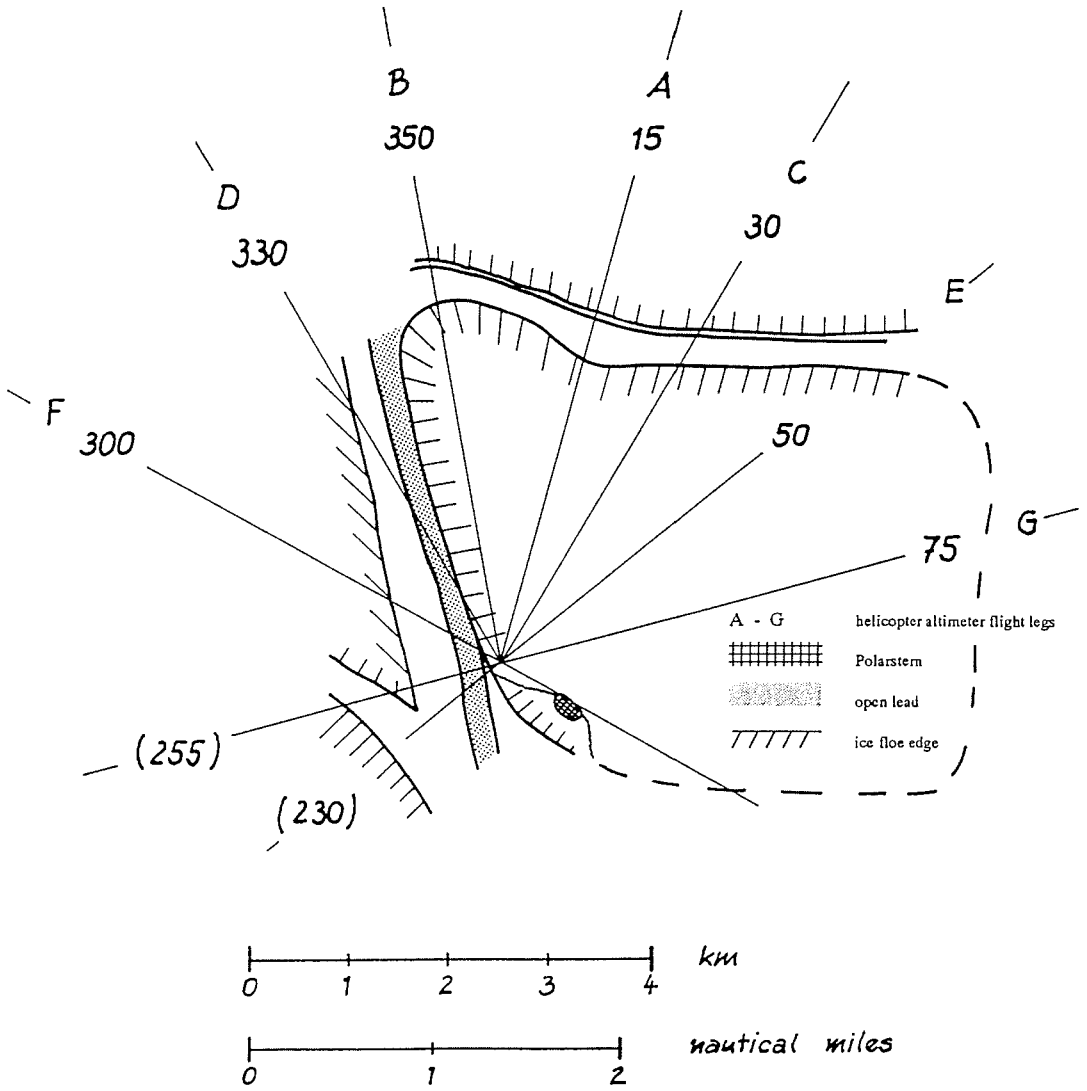

Figure 3.7: Farther environment of the measuring site, March 18, 1993, 12:00 UTC.

3.3.2. Description of subsystems and sensors

(1) Pt100a (MPI)
Ventilated and radiation shielded Pt100 sensors for air temperature
Measuring heights: 15, 10, 8, 7, 6, 5, 4, 3, 2, 1 m

(2) USAT (MIH, AWI, GKSS)
3-dimensonal sonic anemometer thermometer
Measuring heights: 15.6, 10.0, 7.0, 3.65 m
Sampling rate: 20 Hz
Measuring path length: 40 cm,
Measured parameters: three wind components, temperature, second moments and cross-covariances
Special features: sensor-head heating, improved operation in case of snow due to automatic rejection of corrupted samples (only USAT1)

(3) Kaijo Denki (MPI, GKSS)
3-dimensonal sonic anemometer thermometer
Measuring heights: 4.15, 3.65, 1.45 m
Sampling rate: 20 Hz
Measuring path length: 20 cm
Measured parameters: three wind components, temperature, second moments and cross-covariances
Special features: correction of instantaneous values by a two dimen sional calibration table based on wind tunnel measurements (only GKSS-systems)

(4) Lyman-alpha (GKSS)
Fast optical (UV) water vapor sensor
Measuring heights: 3.90, 3.40 m
Sampling rate: 20 Hz (each sample based on 25 measurements)
Measuring path length 0.7 - 1.0 cm

(5) Fast Temperature (GKSS)
2.5-µm platinum wire
Measuring height: 4.15 m, 3.65 m

(6) CR10 (GKSS)
GKSS measuring system
PTA 427: pressure
HFT: flux plate + 4 x temperature for soil heat flux
SKS 1100: downwelling short wave radiation
PAR: photosynthetic active radiation
THRDS5: downwelling and upwelling total radiation
Humicap: humidity and temperature (measuring height 1.52 m)
3x Pt100: Snow temperature (measuring height rel. to snow surface -2, -5, -10 cm)

(7) Argos 1 (AWI)
Automatic measuring buoy with data transmission via Argos satellite system
Position, pressure, humidity, temperature
Measuring height: 2 m

(8) Argos 2 (MPI)
As Argos 2 but with additional sensors for wind speed and wind direction

(9) Minerva (MPI)
MPI measuring system
Pressure, 3-dimensional magnetometer, temperature, (sometimes) humidity
Measuring height: 1.35 m

(10) Solent (SLU)
3-dimensonal sonic anemometer thermometer
Measuring height: 3 m
Sampling rate: 10 Hz
Measuring path length: 14.5 cm
Measured parameters: three wind components, temperature, second moments and cross-covariances,
Special features: continuous storage of raw data, wind tunnel calibration of flow distortion

(11) Fast Temperature (SLU)
25-µm platinum wire
Sampling rate: 10 Hz
Measuring height: 3 m
Special features: continuous storage of raw data

(12) LI-COR (SLU)
LI-6262 gas analyzer with modified air pump
Sensitive to water vapor and CO_2
Measuring height: 3 m
Sampling rate: 10 Hz
Special features: the air to be analyzed is sucked through a 4 mm tubing with 7 l/min from the Solent sonic measuring volume providing minimum flow distortion; continuous storage of raw data

(13) CR7 (GKSS)
GKSS measuring system as CR10 plus wind direction and ice temperature profile
10xPt100 with 5 cm vertical spacing

(14) Radiation Garden (MPI)
Pyranometer Kipp & Zonen: upwelling and downwelling short wave
Pyrgeometer Eppley: upwelling and downwelling long wave, housing temperature
Schulze-Lange: upwelling and downwelling total radiation

(15) KT19 (MPI)
Skin radiation temperature
Sampling rate 0.1 Hz

(16) Air-snow-ice-water-temperature (MPI)
14 Pt-100 sensors mounted in a 100 mm diameter plastic tube
Measuring heights relative to upper ice surface: +0.9, +0.6, +0.3, 0.0, -0.3, -0.6, -0.9, -1.2, -1.5, -1.8, -2.1, -2.4, -2.7, -3.0 m

Remark: the ice core drilled for the installation is stored at the AWI with id. no. R9107302
6 Pt-100 sensors without mounting
Measuring heights relative to upper ice surface: +0.00, +0.09, +0.18, +0.26, +0.34, +0.42 m (= snow surface at 15 March)

3.3.3. Preliminary results of surface-layer flux measurements (M. Claussen)

During the period of Monday 15th till Thursday 18th of March, many instruments worked properly allowing a preliminary, nevertheless comprehensive diagnosis of surface-layer momentum and energy fluxes.
The most prominant feature found in the data is the dominant influence of atmospheric radiation on the surface-layer dynamics. Two distinct cases have been identified in which clouds appeared or disappeared leading to a sudden increase or decrease in atmospheric radiation of some 60 W/m^2. As a consequence the skin temperature of snow increased or decreased by up to 4 K, respectively. This change in skin temperature in turn triggered a change in sensible heat flux. For cloudless sky, the surface layer was generally stably stratified with a downward heat flux of approximately -10 W/m^2. When clouds appeared, stratification changed sign, and the heat flux was directed upward with maxima of roughly 25 W/m^2. (The fast temperature sensors generally yield smaller amplitudes of heat fluxes than the ultra sonic sensors.) This change in stratification is also recognized in variations of momentum flux. Furthermore, the sudden increase or decrease of skin temperature gave rise to a temperature wave into the snow. The influence of atmospheric radiation on surface-layer momentum and energy fluxes is seen in all turbulence sensors at all heights.
Estimates indicate that, due to the winterly conditions experienced during the drift phase of RV *POLARSTERN* , the sensible heat flux over open water should have reached 1000 W/m^2 and the latent heat flux, 250 W/m^2 approximately. Often, strong sea smoke was observed at larger distances from the experiment site (and on Thursday, March 18 also in its vicinity). Unfortunately, during the period of intensive measurements, the leads were frozen. Hence no internal boundary layers of temperature or humidity could be identified in the data. Moreover, when leads opened (during Thursday, March 18) the wind came across the 3 km wide ice floe.
The ice floe was covered with pressure ridges varying in height and spatial density. The western rim of the ice floe was heavily rafted with ridges up to 3-4 m high, while the central part of the ice floe was rather flat with few, small ridges. Roughness lengths have been computed from the uppermost and lowest ultrasonic anemometer at the 15-m mast, mounted at 15.7 m and 3.7 m, respectively. First results (see Figure 3.8) indicate that roughness lengths vary with wind direction being strongest or smallest when the wind was directed from the west rim (between 270 and 330°) or the central part of the ice floe (between 330 and 30°), respectively. Estimates of roughness lengths agree in their magnitude with data reported in literature for rough, rafted ice and flat snow fields. Rather small values of roughness lengths are computed from the uppermost sensor for directions between 350 and 30° during the 16th of March. It turns out that snowfall was reported for these wind directions which would lend support to the theory of drag reduction over surfaces with sand or snow drift. The data from the lowest sensor for the same period are to be taken

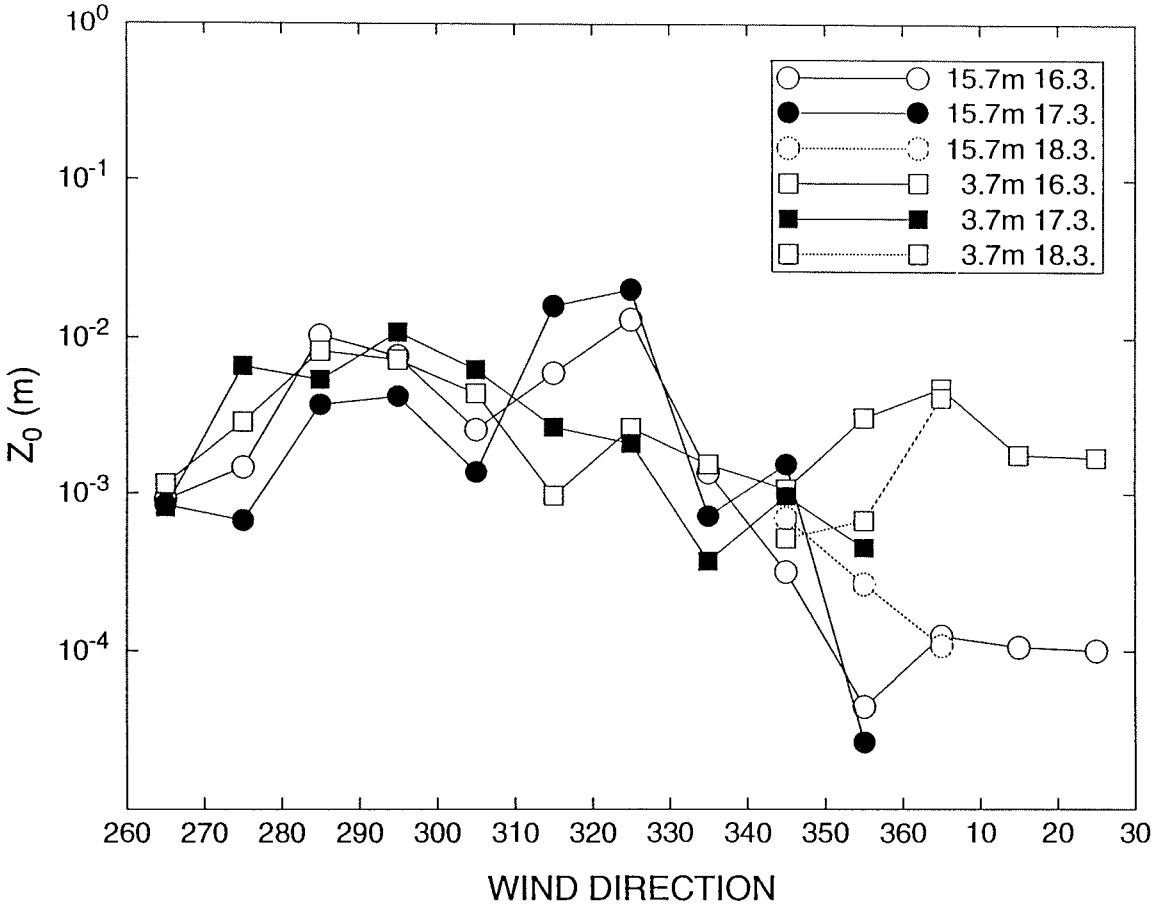

Figure 3.8: Roughness length as function of wind direction computed from the uppermost (15.7 m) and lowest (3.7 m) ultrasonic sensor at the 15-m mast. Roughness lengths are averaged for each 10° interval (e.g. for the interval between 260 and 270°, and so on).

with care because this sensor could not eliminate data failures due to drifting snow flakes.
Altimeter data from the laser mounted to the helicopter have no yet been examined. A first look at the recordings revealed, however, quite often an echo failure, presumably due to malfunctions of the laser at low temperatures.

3.4. Surface buoy network (H. Hoeber/MIH)

To support the central ice station, a network of automatic meteorological buoys was established in the ice surrounding *POLARSTERN* 's position. These buoys measure surface atmospheric pressure, air and ice temperature, and the wind vector, and report their data using the satellite-based Argos system. The system supplies the stations' positions employing a Doppler frequency shift method using the satellite transmission link.
The purpose of the network was mainly to improve the meteorological surface network in this otherwise data sparse region. To this end, the data were sent - via the Argos system - to the Global Telecommunications System of the WMO and, thus, were included in the daily analyses of the weather services. They will be part of the mesoscale analyses of the Norwegian Weather Service using the HIRLAM model, which will be made available for further investigations, in particular, of divergence/convergence in the atmospheric flow field of the boundary layer in the area. In addition, they will be used for an analysis of ice kinematics and their relation to the atmospheric forcing.

Table 3.2: Drifting surface buoy network during Arktis '93

Stat. ID	Inst.	Deployment Time	Deployment Position		Recovery/Loss Time	Recovery/Loss Position	
3312	AWI	10.3./14z	81.279N	6.575E	19.3./08z	80.541N	4.096E
3330	MIH	6.3./16z	80.402N	1.063E	21.3./21z	76.364N	9.651W
3331	MIH	6.3./16z	80.589N	6.590E	24.3./16z	75.824N	11.772W
3332	MIH	7.3./15z	81.497N	11.019E			
3333	MIH	7.3./17z	81.461N	3.041E	22.3./09z	79.984N	1.452W
3334	MIH	12.3./12z	81.947N	6.554E			
3335	MIH	15.3./18z	80.963N	5.439E	19.3./12z	80.525N	3.970E

Table 3.2 provides the details of the deployment and the performance of the network; Figure 3.9 shows the network on March 12, when six stations (including the central ice camp which is not plotted) were first available, and on March 21, when station 3330 was lost. During the deployment of station 3334 in the north, the helicopter experienced engine trouble due to the extremely low temperature, which made it advisable to refrain from further long distance flights. The scheduled network could, thus, not be established; only one more buoy at the central ice station was deployed, in addition.
We observe that large horizontal differences of ice drift speed exist in the area of the campaign. While stations 3330 and 3331 were well within the East Greenland Current (EGC) setting south-wards at a speed of 0.5 to 0.8 m/s, the rest of the stations remained in the north-eastern branch of the ice stream

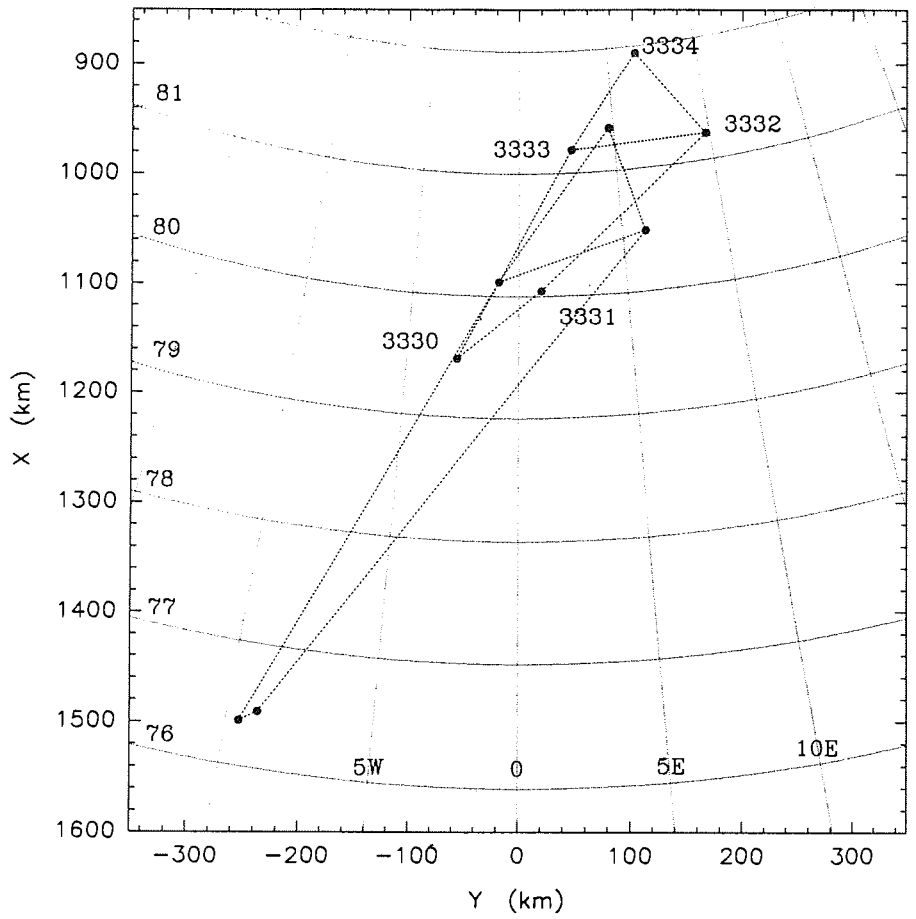

Figure 3.9: Surface buoy network on March 12, 1993
(when the five stations were first available) and on March 21, 1993 (when station 3330 was lost). Numbers are Argos ID-codes of the stations, and are plotted close to the position on March 12. Central ice camp is approximately half way between 3332 and 3333.

which originates north of Franz-Josef-Land and Spitsbergen and has to merge with the EGC branch before being accelerated southwards. Consequently, divergence of drift velocity prevailed, implying frequent opening of the ice cover and - most likely at those low temperatures - formation of new ice.
Figure 3.10 shows, as an example, the data series of station 3331 from March 6 to March 24. Temperatures range from -37 to -3 °C, depending largely on wind direction: with off-ice wind, the temperatures fell below -30 °C, while on-ice wind blowing from the relatively warm water of the West-Spitsbergen Current let the temperatures rise close to the freezing point of sea water. This is nicely illustrated by the temperature trace of March 13, when a small polar low travelling along the ice edge from south to north with a core pressure of

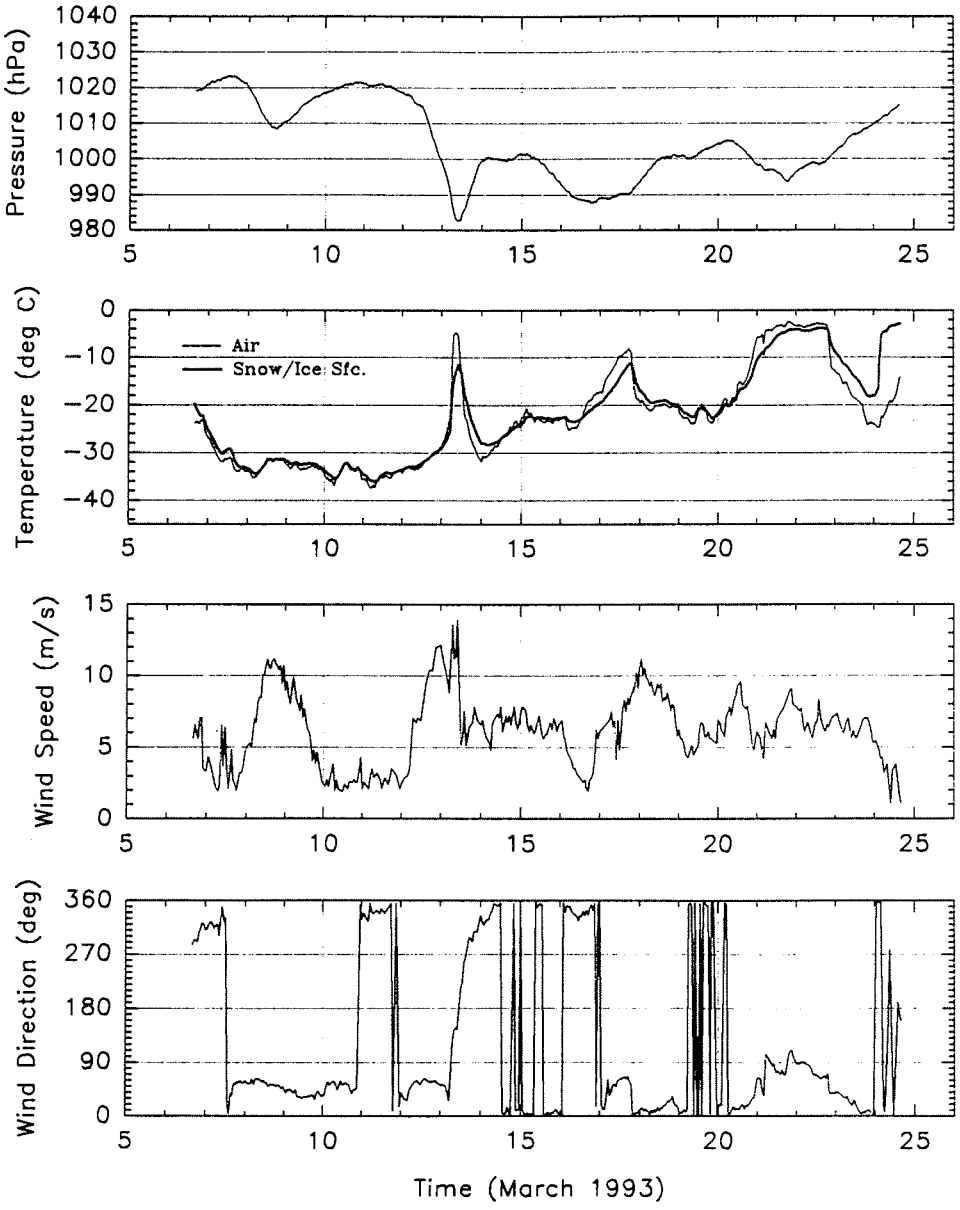

Figure 3.10: Time series of surface pressure, air and ice temperature, wind speed, and wind direction from March 6 to 24, 1993 at station 3331.

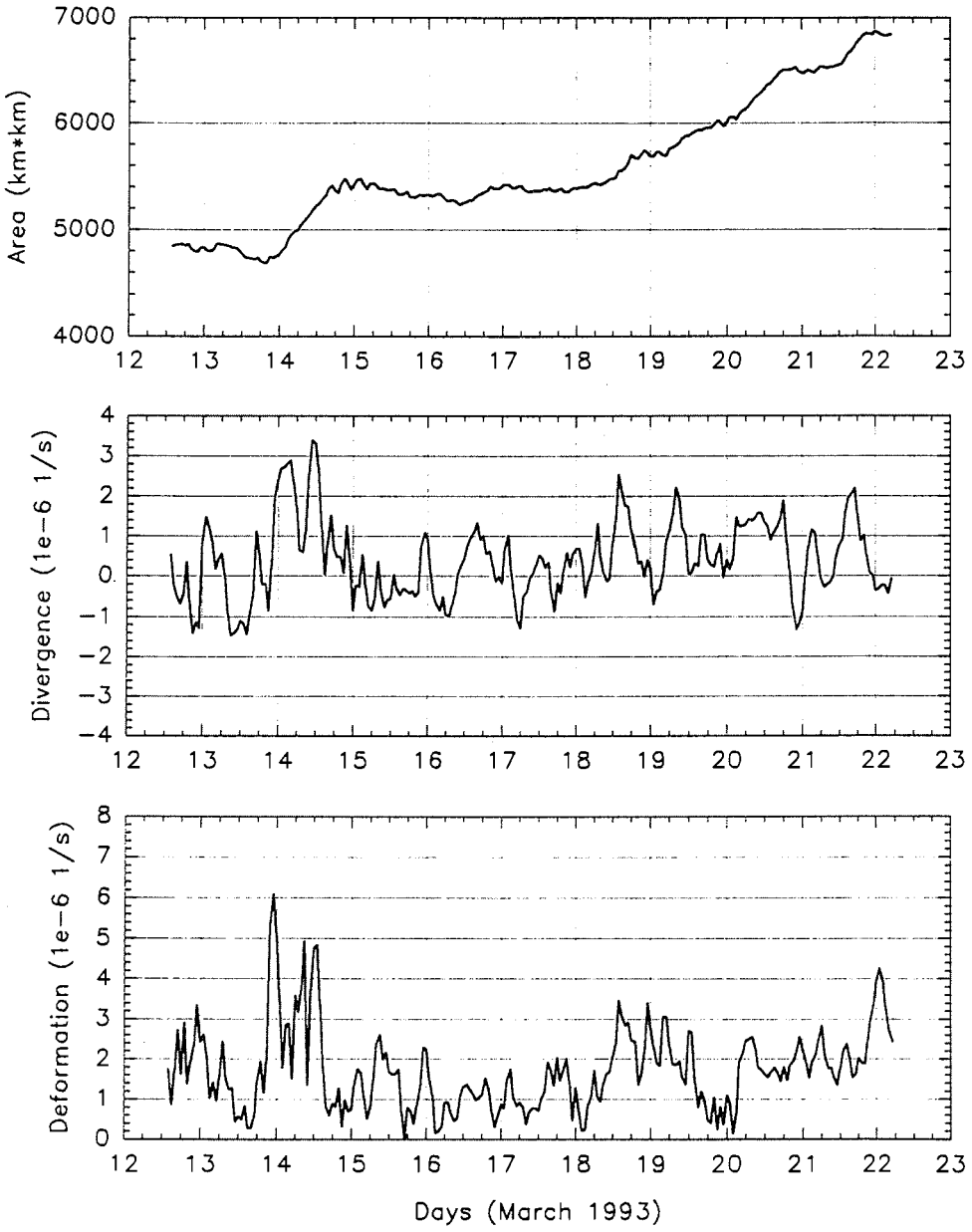

Figure 3.11: Kinematics of ice drift in the northern triangle formed by stations 3332, 3334, and 3333 (see Figure 3.9). Triangle area (above), divergence (middle) and deformation (below) from March 12 to 22, 1993.

983 hPa caused the wind direction to make a 360° turn, let the wind speed rise to above 13 m/s (measured at 2 m height), and raised air and ice surface temperatures considerably.
The polar low event is reflected in the kinematics of ice drift. Using the triangle of stations north of *POLARSTERN* (3332-3334-3333) the area of the triangle, the divergence, and the deformation were computed. From Figure 3.11 we observe a stepwise increase of the triangle area, which is equivalent to divergence of 3×10^{-6} s^{-1}, after the passage of the polar low. Deformation reaches a maximum. A second marked change of the triangle area occurs at noon of March 18 with divergence as high as 2.5×10^{-6} s^{-1}; this might have preconditioned the ice field for the break-up occuring on the evening of March 18. The stepwise occurrence of divergence is a characteristic behaviour of the ice plate, but cannot easily be predicted.

3.5. New applications of remote sensing data (L. Kornblueh)

The surface energy fluxes are describing various short- and long-term climate-relevant processes. Dominating factors for the development of different states of balance of the surface energy budget are the daily variations of duration of sunshine, the amount of sea-ice in proportion to the ocean, and the interaction of the surface with clouds via radiation and turbulent fluxes of humidity and heat, rain, and snow. A solution for not routinely possible measurements may be the simulation with a numerical model using the data which were produced every day by the NOAA-N satellites. This data will be used with an adjoint version of a numerical model to get the surface energy fluxes by a consistent state of the atmosphere and the boundary conditions.
For the simulation, a huge amount of different system components must be taken into consideration. Because of the resolution of the satellite data and the homogeneity of the topography of the Arctic a one-dimensional formulation of the model as first step seems to be justified. Testing the procedure, this has the advantage to be not very time consuming. The major model components are:

- the dynamical model,
- a turbulence model for the boundary layer and for the free atmosphere (different assumptions on the parametrisations must be made),
- a microphysical cloud model including the thermodynamic processes, including all processes which are important for the simulation scale,
- a radiative transfer model interacting with all other model components,
- the possibility to calculate the radiance in separate wavelength areas, and using a geometrical structure close to the model grid,
- a soil model, where soil means on one hand sea-ice and on the other the ocean water, because of the large area which has to be simulated, it is important to make a difference in the calculation of the occuring fluxes of the area covered by sea-ice or ocean.

For the verification of such a model many boundary-layer data measured during this cruise can be used. All components for the surface energy budget are measured directly or can be calculated. These are:

- the sensible heat flux with various Sonics,
- the latent heat flux with Lyman-alpha sensors,
- the shortwave and longwave down- and upward-fluxes,
- the vertical temperature distribution in the sea-ice, snow-cover and underlying sea-water.

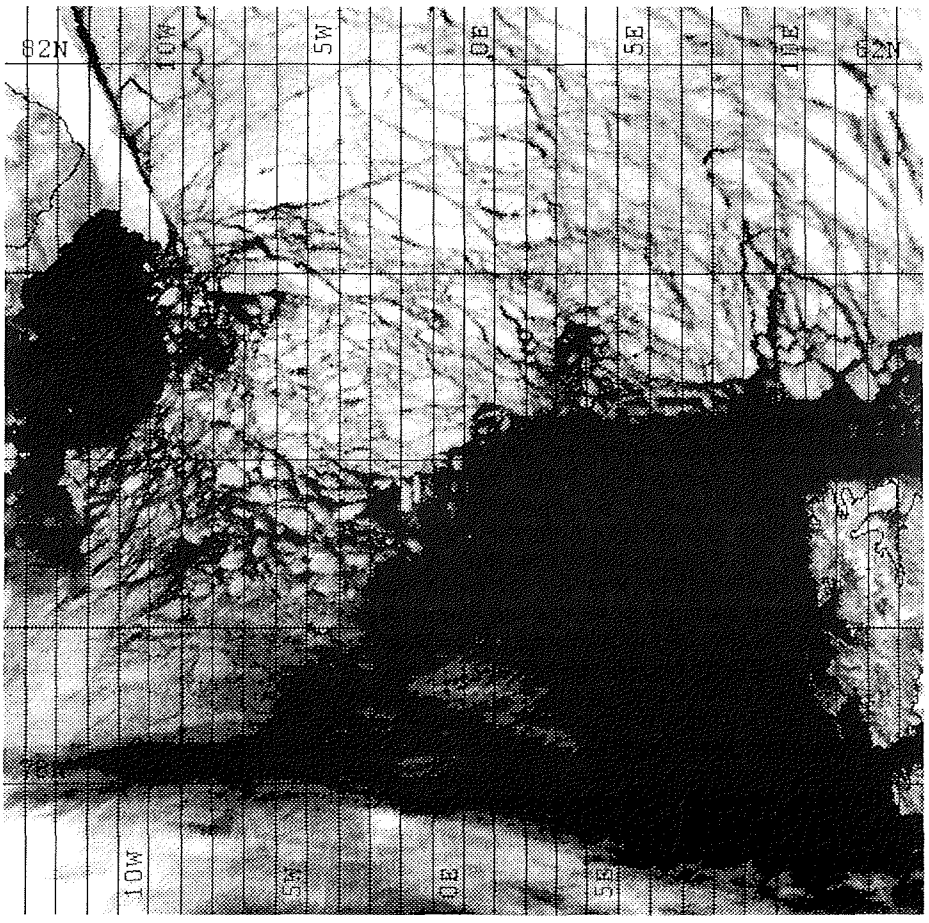

Figure 3.12: Satellite picture NOAA-9, Channel 4 (March 7, 1993).

One interesting phenomenon which was observed is shown on the satellite picture in Figure 3.12 (NOAA-9, Channel 4, March 7, 1993). There are many leads. After zooming on the original data, it was observed by the satellite that the lead where the RV *POLARSTERN* was heading north had a cross section of around seven kilometers (the interesting area was near the nadir and around six pixels form the lead's cross-section). Observations on board of the ship showed that the real cross-section was about 500 meters. It may be possible to get information on this from the micro-meteorological measurements in combination with several air-borne boundary-layer observations. This phenomenon must be dependent on the temperature difference between the open water and sea ice. Some turbulent mixing processes may be involved, but this must be shown in the data. The observations we have, give us the possibility to look for this.

4. Air chemistry: determination of atmospheric mercury and aerosol black carbon (K. Timoschenko, R. Ebinghaus)

4.1. Introduction

During the *POLARSTERN* cruise in the Nordic Seas and at the ice-camp, simultaneous measurements of atmospheric mercury and aerosol black carbon were performed by the GKSS group. The work was aimed at two subjects :

1. Although mercury usually occurs in trace concentrations, it is widely dispersed and occurs in its "background concentration" on a global scale. For the determination of the natural backgrounds, measurements of mercury in remote areas were required to exclude anthropogenic influences. To our knowledge, atmospheric mercury concentrations in polar regions were still unknown.
   At the same time as the *POLARSTERN* cruise, Canadian scientists carried out similar measurements in Alert, close to the Canadian polar circle.
   Therefore, first reliable results for the concentration of atmospheric mercury in polar regions were to be expected.
2. Aerosol black carbon and potential oxidants for gaseous mercury such as ozone are the decisive factors for the transport and deposition properties of atmospheric mercury. For the validation and improvement of a European long range transport model as used by GKSS Research Centre, simultaneous measurements of atmospheric mercury and aerosol black carbon (soot) concentrations were required.

4.2. Materials and methods

4.2.1. Determination of mercury in air

The analytical methods for determining total gaseous mercury (TGM) including elemental, organic and inorganic mercury are based on the amalgamation of mercury on gold surfaces.
For sampling, TGM was collected on gold coated glass balls which accumulate TGM quantitatively. A quartz tube, 0.4 cm in diameter, was filled with approximately 1.5 cm glass balls. A second tube filled with a gold-platinum gauze was placed between the adsorber tube and the pump to prevent contamination caused by back-diffusion of mercury from the pumping system.
Ambient air was sucked through a 0.5 cm quartz wool plug to retain particles before passing the adsorber tube. Approximately 400 l of air were collected. During the passage to the ice station and back to Bremerhaven the sample flow rate was about 5 l min^{-1} to enable short sampling periods for measuring one sample on each degree of latitude. At the ice-camp, the air was collected with flow rates of approximately 0.5 l min^{-1} because of the stationary position of the ship. At these sample volumes and flow rates a breakthrough of mercury can be excluded.
After sampling was finished, the pump was turned off, the analytical tube was disconnected from the system, closed with plastic caps and stored in a firmly closed glass container. To prevent contamination during storage, 10 g of silver wool were kept in the container to bind gaseous mercury diffusing into it. In addition, control tests were performed using adsorber tubes that were normally handled but not exposed to air. The analysis showed average values

of 35 pg mercury (number of values = 6). Consequently, contamination during storage is of minor importance.
During the *POLARSTERN* expedition 40 samples of TGM were collected. The first five samples were taken at the bow of the ship. To eliminate the influence of rough sea and heavy sea spray the following samples were taken on the uppermost deck in front of the ship. Table 1 summarizes the geographical location, date and time for all mercury measurements during the cruise. The analysis was carried out at GKSS Research Centre. Measurements were performed with cold vapour atomic fluorescence spectroscopy (CVAFS) using the two step amalgation technique. Calibration was achieved by injecting mercury saturated air into the analytical column. The statistical error in the determinations is estimated to be <10 %.

4.2.2. Determination of aerosol black carbon (soot) in air

The analytical method for measuring aerosol black carbon in the ambient atmosphere is based on its strongly optically absorbing property. These measurements were performed by a so-called aethalometer which consists of the aethalometer sampling / optical unit and an externally-supplied vacuum pump. The aethalometer was operated automatically by a laptop.

The principle of the aethalometer is to measure the attenuation of a beam of light transmitted through a quartz fiber filter, while the filter is continuously collecting an aerosol sample. The measured attenuation is found to be proportional to the mass of aerosol black carbon collected from the air stream. This measurement is made at successive regular intervals of a timebase period. The black carbon content of the aerosol deposit can be determined at each measurement time and be interpreted as the black carbon concentration in the air stream expressed in nanograms per cubic meter.

The aerosol was collected with a flow rate of approximately 17 l min^{-1}. A timebase period of 30 minutes was chosen. The samples of aerosol black carbon were taken at the same times and locations as the samples of TGM which are enumerated in Table 1.

4.3. Results

Table 4.2 shows the analytical results of the determinations of TGM and aerosol black carbon during the *POLARSTERN* cruise. The background concentrations of TGM are represented by the samples 6 - 17 measured during the ice-camp period. The samples 1 - 5 and 18 - 40 represent the latitudinal distribution of TGM measured during the sea-passages.
Figure 4.1 shows the frequency distribution of TGM concentrations determined at the ice station and during the passages. The lowest TGM concentration found is 0.25 ng/cbm. The frequency distribution shows a logarithmic distribution for the ice station values, determining the background concentration of TGM in the range of 0.2 - 0.7 ng/cbm.The frequency distribution for the passage values shows a more normal distribution, having a maximum at 1.2 - 1.7 ng/cbm, comparable to our values found on the North Sea 1991 for uncontaminated air masses.

Table 4.1: Geographical location, date and time for TGM and soot measurements

Sample	Date	Start	End	Latitude*	Longitude*
1	28.02.1993	17:45 h	19.55 h	60°22 N	4°18 E
2	01.03.1993	09:32 h	11:14 h	63°30 N	4°15 E
3	01.03.1993	14:19 h	15:49 h	64°30 N	4°14 E
4	01.03.1993	19:44 h	21:11 h	65°39 N	4°16 E
5	02.03.1993	09:10 h	11:12 h	68°22 N	4°22 E
6	10.03.1993	23:56 h	12:38 h	81°15 N	6°31 E
7	11.03.1993	13:16 h	02:06 h	81°13 N	6°29 E
8	12.03.1993	02:08 h	13:45 h	81°10 N	6°35 E
9	15.03.1993	00:30 h	11:45 h	81°02 N	5°28 E
10“	15.03.1993	12:00 h	22:55 h	80°59 N	5°30 E
10“	16.03.1993	09:15 h	13:25 h	80°52 N	4°59 E
11	16.03.1993	14:00 h	10:45 h	80°50 N	5°04 E
12	17.03.1993	11:10 h	01:15 h	80°47 N	5°16 E
13	18.03.1993	01:24 h	14:10 h	80°41 N	5°06 E
14	18.03.1993	14:21 h	01:12 h	80°36 N	4°54 E
15	19.03.1993	10:30 h	00:12 h	80°32 N	4°04 E
16	20.03.1993	00:18 h	16:03 h	80°27 N	3°27 E
17	20.03.1993	17:25 h	11:15 h	80°26 N	2°37 E
18	22.03.1993	14:23 h	15:56 h	80°09 N	0°34 E
19	22.03.1993	20:26 h	21:53 h	79°47 N	3°38 E
20	23.03.1993	08:52 h	10:08 h	78°19 N	9°20 E
21	31.03.1993	16:40 h	18:00 h	78°58 N	4°53 E
22	01.04.1993	06:11 h	07:25 h	77°00 N	0°27 E
23	02.04.1993	05:15 h	07:02 h	75°35 N	2°00 W
24	02.04.1993	16:04 h	17:33 h	74°07 N	3°00 W
25	03.04.1993	12:24 h	14:07 h	73°03 N	1°24 W
26	04.04.1993	16:01 h	17:12 h	71°44 N	5°00 W
27	13.04.1993	06:18 h	07:41 h	71°00 N	3°53 E
28	13.04.1993	11:21 h	12:48 h	70°03 N	3°54 E
29	13.04.1993	15:52 h	17:19 h	69°08 N	3°54 E
30	13.04.1993	20:31 h	22:06 h	68°11 N	4°06 E
31	14.04.1993	03:26 h	04:45 h	66°45 N	4°00 E
32	14.04.1993	06:50 h	08:15 h	66°02 N	4°01 E
33	14.04.1993	11:12 h	13:05 h	65°09 N	4°03 E
34	14.04.1993	16:00 h	17:33 h	64°89 N	4°05 E
35	14.04.1993	20:40 h	22:12 h	63°10 N	4°06 E
36	15.04.1993	02:30 h	04:20 h	61°59 N	4°08 E
37	15.04.1993	10:28 h	11:53 h	60°35 N	4°15 E
38	15.04.1993	17:50 h	19:28 h	59°11 N	4°39 E
39	16.04.1993	02:51 h	04:20 h	57°31 N	5°37 E
40	16.04.1993	13:10 h	14:45 h	56°09 N	6°30 E

* ship position when sampling started;
“ the sampling had to be interrupted because of bad weather conditions;

Table 4.2: Measured concentrations of TGM and soot and average data of weather conditions obtained by the meteorological station of the *POLARSTERN*

Sample	Air temp. [°C]	Air humidity [%]	Air press [hPa]	TGM [ng/cbm]	Soot [ng/cbm]
1	2.5	52	1029	1.40	---
2	3.3	75	1034	1.88	7.4
3	4.1	73	1032	1.56	35
4	4.5	90	1029	1.40	46
5	4.7	98	1019	1.67	33
6*	-38.1	66	1020	0.67	83
7*	-39.2	66	1020	0.33	79
8*	-39.9	66	1019	0.25	84
9*	-33.8	74	1002	0.33	95
10*	-29.6	77	992	0.50	108
11*	-26.0	80	987	0.46	108
12*	-28.9	79	996	0.40	107
13*	-29.1	78	1000	1.26	86
14*	-31.2	78	1002	1.00	127
15*	-31.5	78	1002	1.01	146
16*	-32.2	78	1011	0.68	139
17*	-28.5	80	1010	0.94	173
18	-21.6	82	1012	0.78	64
19	-10.4	95	1010	1.06	198
20	-9.0	45	1005	1.73	67
21	-10.4	85	1034	0.62	---
22	-0.4	88	1031	0.57	---
23	-1.3	99	1031	0.93	---
24	-2.5	99	1028	1.34	---
25	-1.8	99	1022	1.28	---
26	1.4	70	1021	0.71	---
27	2.2	87	1019	1.04	---
28	4.0	56	1019	0.74	---
29	4.1	54	1018	0.64	---
30	3.5	66	1017	1.07	---
31	4.7	50	1016	1.11	---
32	5.2	44	1016	1.34	---
33	5.1	57	1016	1.25	---
34	6.0	64	1015	1.39	---
35	5.5	65	1017	0.93	---
36	5.0	75	1017	1.30	---
37	5.4	71	1018	1.26	---
38	5.4	82	1017	1.08	---
39	5.7	86	1017	0.75	---
40	6.1	96	1016	1.34	---

* samples measured at the ice-camp;

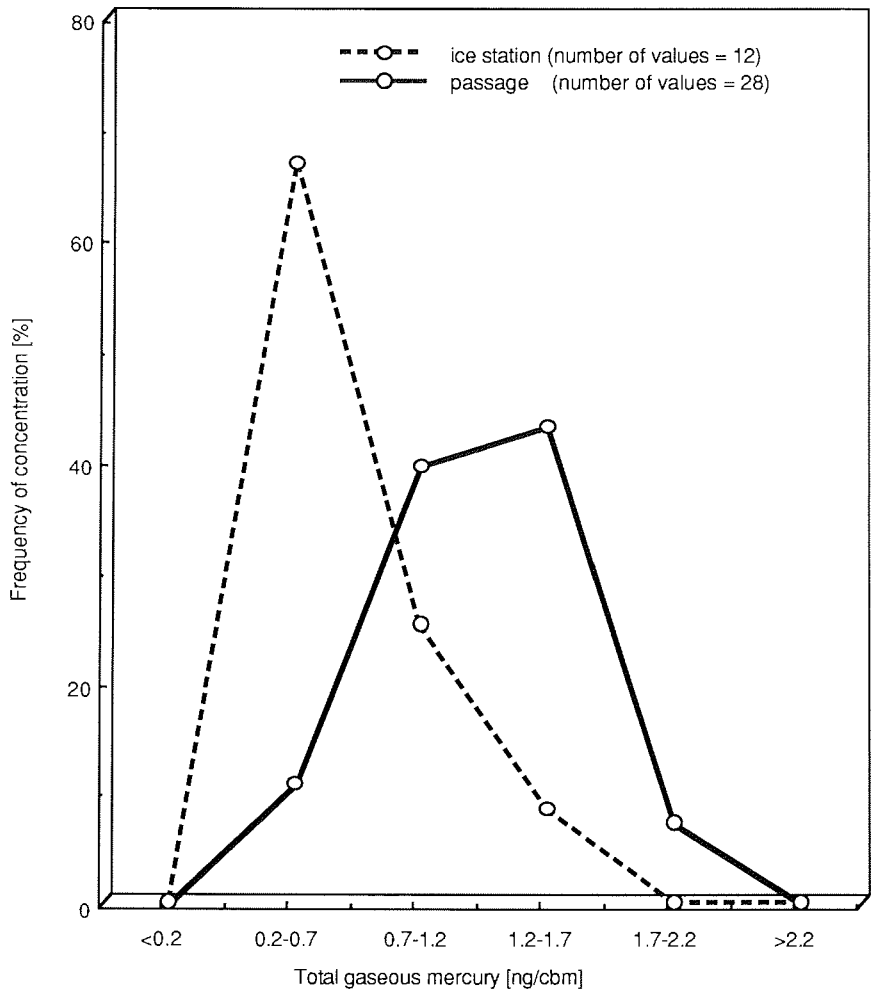

Figure 4.1: Frequency distribution of the total gaseous mercury concentration determined at the ice station and during the passage.

The measurements of soot concentrations by the aethalometer during the passage to the ice station were influenced by bad weather conditions. The optical stability of the system was disturbed because of rough sea. Also the optical property of the quartz filter changed because the filter became wet by sea-spray. Therefore the average soot concentrations of samples 2 - 5 should be treated carefully.
Final results will be discussed after statistical analysis of the data. Further evaluation with meteorological data will follow.

5. Physical oceanography (J. Meincke, N. Verch, W. Purschel, S. Baering, M. Dengler, C. Senet, G. Budeus, C. Darnall, J. Johnson, J.-C. Gascard, C. Rouault)

5.1. Aims

The physical oceanography programme is part of the international Greenland Sea Project (GSP). The measurements are aimed at convective processes in the central Greenland Sea and their dependence on the climatological status of the Arctic Ocean/Nordic Seas system. An intensive field campaign comprising small scale convection experiments and seasonal surveys of the basic state of the Greenland Sea has taken place in 1987-1989. Convective conditions during this period only showed water mass renewal to mid-depth. The planned experimental work is based on experiences from the earlier investigations and merely is a repeat under different climatological conditions. The activities on Polarstern will be focused on the larger-scale description of stratification and currents in the Fram Strait and in the Greenland Sea.

5.2. Methods

The methods employed were modern standard and are listed as follows:
(1) CTD/Rosette
The CTD was a NBIS-MK III system, temperature and pressure calibrated prior and after the cruise.
A rosette with 24 10l-bottles was mounted with the CTD, the drawing of the

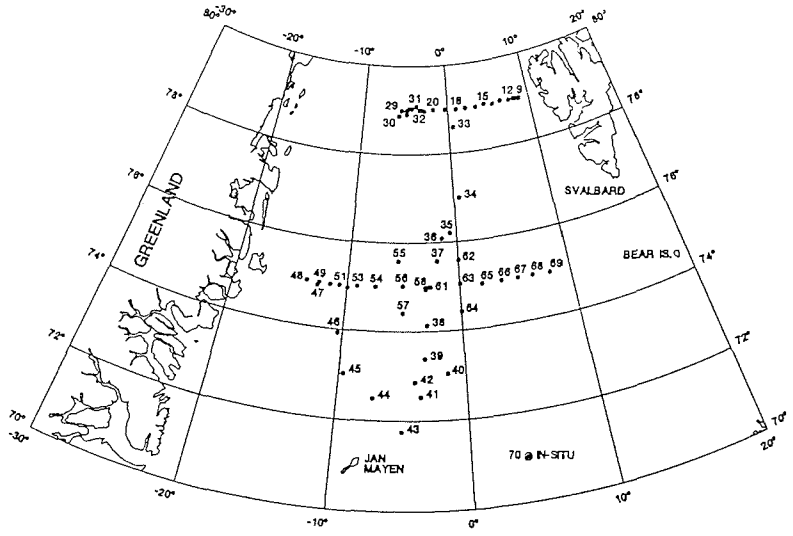

Figure 5.1: Station grid in the Greenland Sea during ARK IX/1 b.

samples was done according to the WOCE-scheme. Salinity samples for in situ calibration of the CTD were drawn from each bottle and analysed at sea. Double- and multi-trips of bottles at the same depth-level were performed regularly. Salinities are within the WOCE-standard. Electronic and mercury reversing thermometers (protected and unprotected) were used on 3 to 5 bottles throughout the cruise. The field evaluation can only be done after the post-cruise calibration.
The instrument package was used routinely from 10 to 15 m depth down to 5 to 10 m within the bottom as indicated by an altimeter.
The spacing of the hydrographic stations was according to prior experience, i.e. resolving the flows of Fram Strait water masses and resolving the features of the Greenland Sea cyclonic gyre (see Figure 5.1).
(2) Acoustic Doppler Current Profiler (ADCP)
While steaming in ice-free areas a hull-mounted ADCP (150 kHz) has been operated which measures water velocities relative to the ship. At most places a vertical range of 400 m has been achieved. An exception is the eastern part of Fram Strait where the range was reduced due to heavy weather. The measurements are intended to further the knowledge of the flow system in Greenland Sea and Fram Strait and to investigate the flow of distinct water bodies like e.g. the Jan Mayen Polar Water in the relicts of the Isodden.
(3) Moored Current Meters / ADCP's / Upward Looking Sonars
Two types of moored arrays are in long-term use within the Greenland Sea Project. In the central Greenland Basin current meters, ADCP and temperature salinity recorders (SEACAT) are used to monitor horizontal and vertical currents related to advection and convection. A triangular array, deployed in summer 92, was recovered by Polarstern and will be redeployed by Valdivia two months later. The second type of moorings consisted of current meters, temperature-salinity recorders and upward looking sonars deployed over the continental slope of East Greenland at 75°N and 79°N aimed at measuring horizontal currents and ice-thickness for estimates of fresh water outflow from the Arctic Ocean. Four such arrays have been recovered, replacements will be deployed in June/July 1993.
(4) Floats
To obtain Lagrangian measurements of horizontal currents as well as vertical velocities at preselected depth levels a set of 6 neutrally buoyant floats (3 at appr. 300 m depth, 3 at appr. 1000 m depth) have been released in the Greenland Sea gyre. Whereas the horizontal currents are measured by the displacement of the float, the vertical currents are measured by the rotation of the float, which is initiated when vertical currents pass the instrument and a rotor attached to it. The portioning is achieved by recording the arrival time of acoustic pulses emitted from 3 moored zonal sources. The data are transmitted to store via satellite after the float has released a weight and returned to the surface. The surfacing for this experiment is set to occur during early June, i.e. after two months of free drift.

5.3. First results

First results must only be seen as qualitative information, since the post-cruise calibration of the CTD-measurements have to be waited for. Therefore no estimates of water mass distributions or geostrophic circulation have been done. In addition there was no onboard-evaluation of measurements from the long-term moored instruments. However, on the basis of the experience with the hydrography of the Fram Strait (since 1983) and the Greenland Sea (since

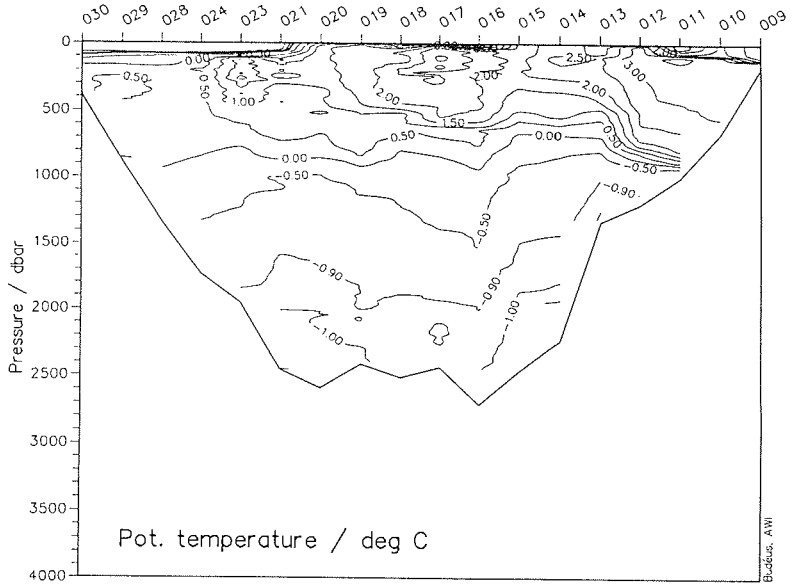

Figure 5.2: Temperature distribution along 79°N across Fram Strait (prel. data).

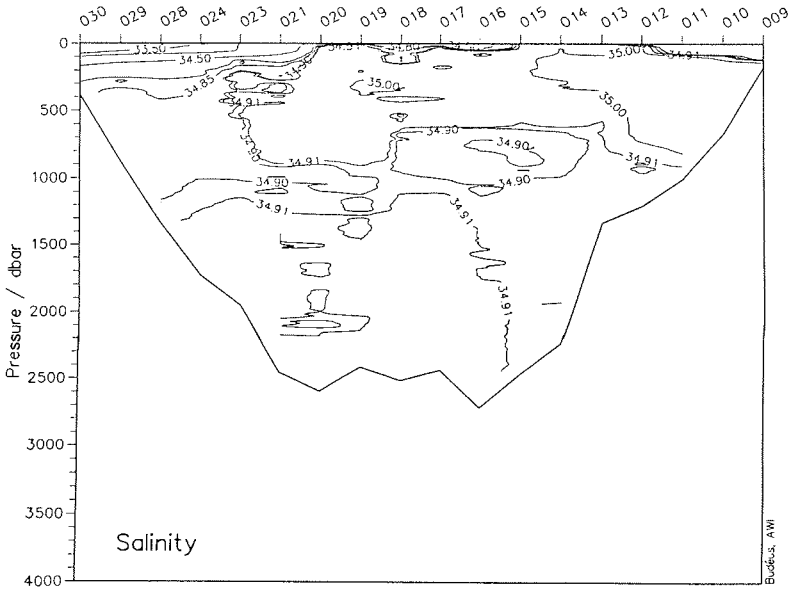

Figure 5.3: Salinity distribution along 79°N across Fram Strait (prel. data).

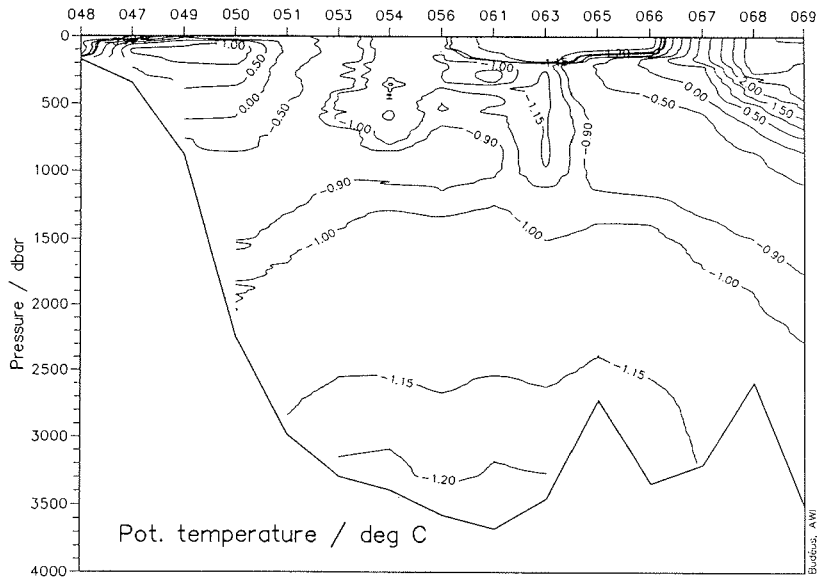

Figure 5.4: Temperature section along 75°N across the Greenland Sea basin (prel. data).

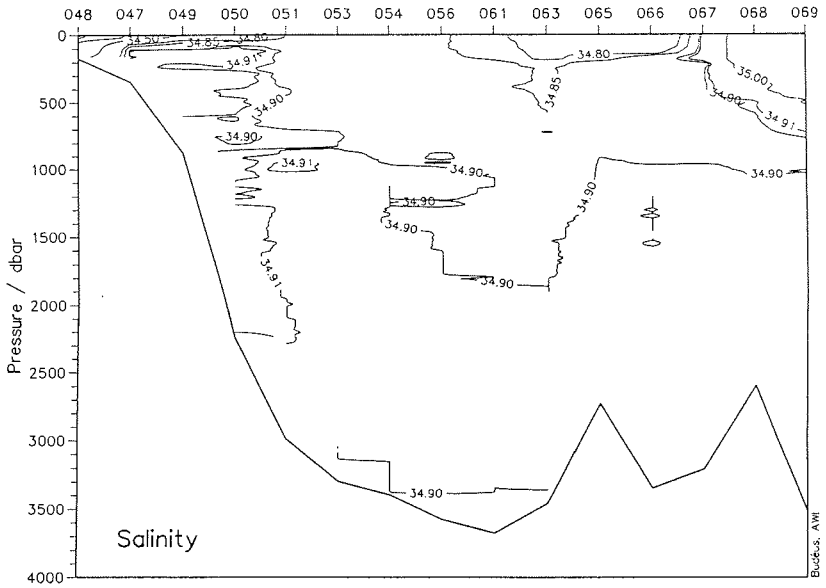

Figure 5.5: Salinity section along 75°N across the Greenland Sea basin (prel. data).

1986) and because of the high primary quality of the CTD-measurements the following statements can be made.

(1) Fram Strait (Figures 5.2, 5.3)

The section across Fram Strait along 79°N was carried out for the first time during winter. The upper 1000 m show no special features within the bandwidth of our observations up to now. The only 'winter' signature consists of a relatively thin surface layer of polar water, which spreads all over the length of the section. Below 1200 m depth there are only two water masses: The deep outflow from the Arctic Ocean with distinct cores over the Greenland slope and in the central Fram Strait and the water with characteristics of Norwegian Sea deep water, that is found over the Svalbard slope and in the deep western Fram Strait. There was no deep water from the Greenland Sea present, which is unusual for the latitude of 79°N.

(2) Greenland Sea (Figure 5.4, 5.5)

The two cross sections (N-S and W-E) spanning the Greenland Sea gyre and the additional data in the deepest part of the Greenland Basin gave a good coverage of the winter 1992/93 success in deep convection. This success was found to be rather meager: A maximum of approximately 1000 m for convective activity was clearly seen in the western part of the deep basin. Signs of freshly convected water at depths between 300 m and 800 m were also found as far east as to the Arctic front (3°E), however, there were blanketed by a thick (150 m) layer of relatively fresh water near the freezing point.

The temperature and salinity of the deep waters below 2000 m in the central basin were found warmer and saltier than all reliable measurements of deep water properties since the 1950's. This indicates, that no convective renewal of the Greenland Sea deep water has taken place since the early 70's, the last phase of deep convection.

With respect to TS-properties the deep water of the Greenland Sea is changing its characteristics toward the Arctic deep water, which were also found as a strong signal over the Greenland slope at 75°N. However, tracer measurements (see Tracer oceanography) suggest that a complex mixing pattern with waters of rather recent convective transformation must be involved. A more detailed evaluation of the trend in Greenland Sea deep water has to include the horizontal gradients in the deep basin related to the cyclonic spreading paths of the water masses and also the mixing processes in the Fram Strait.

6. Tracer oceanography (M. Rhein, R. Bayer, M. Elbrächter, J. Waniek)

6.1. Aims

The main purpose of the tracer measurements (Freons, Helium, Tritium, Radiocarbon) during ARK IX/1 was to study the deep water renewal in the Greenland Sea, the water mass exchange between the Arctic and the Nordic Sea through Fram Strait, and the circulation of deep water between the Greenland Basin and the Norwegian Sea.

6.2. Methods

Freon can be measured directly on board by degassing ca. 30 ml of water in a purge and trap device. The Freon components (F11 and F12) are then separated on a gaschromatographic column and detected by an electron capture detector. As these instruments show a serious drift in their efficiency, a gas standard containing a known amount of Freons has to be analysed with the water measurements. On ARK IX/1 ca. 2000 analyses have been made with ca. 1000 water samples distributed over 42 stations and 24 analyses of air samples. These samples have been taken partly in a rubber boat outside the ship and partly with the helicopter. Because of problems with the carrier gas, F11 measurements are only available for the Fram Strait section and some stations in the Greenland Sea. Besides F11 and F12 we tried to analyze Carbontetrachloride (CCl_4), another useful tracer to estimate deep water renewal times. But despite the good results of the CCl_4 standard measurements, the CCl_4 signal of the water samples were too small and too erratic to be analysed, and the problem could not be solved during the cruise. The other tracer samples taken on this cruise have to be analysed in the home laboratory as their measurement techniques are too complex and elaborated to be done at sea. About 300 tritium and helium samples from 35 stations have been collected together with a few radiocarbon samples. The Helium and Tritium concentrations will be determined using a dedicated mass spectrometer and the water sampled for the Tritium determination will also be used to measure the oxygen isotopes $^{18}O/^{16}O$ with a mass spectrometer. Radiocarbon is measured by Accelerator Mass Spectrometry (AMS) in cooperation with the University of Zürich. At one station in the central Greenland Sea a profile with 12 samples of Sulphurhexafluoride (SF_6) was obtained. To avoid contamination during transport, the samples are stored in a box filled with seawater. The analysis will be done with a Gaschromatograph.

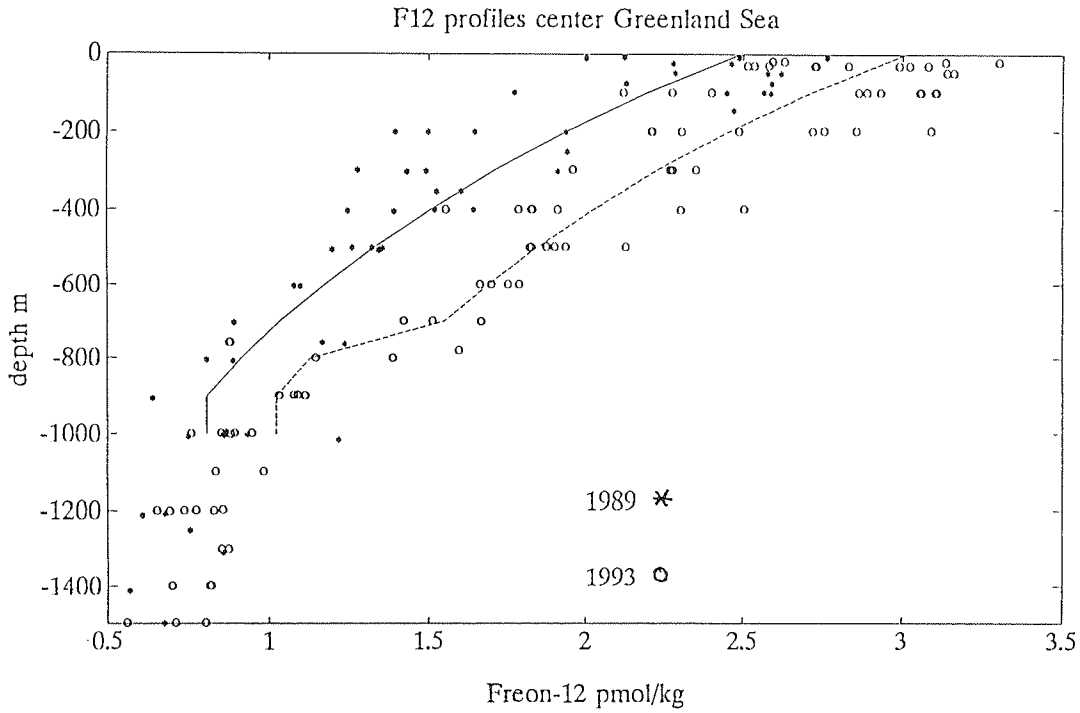

Figure 6.1: F12 profiles in the central Greenland Sea taken in March 1989 (+) and in April 1993 (o).

6.3. First results

Similar to the temperature and salinity data, the Freon distributions in the Greenland Sea show that since 1982 no deep convection has occured. The concentrations below 2000 m have only slightly increased since 1989 and a vertical gradient in the formerly homogeneous deep water has developed. Both features show the influence of turbulent vertical diffusion. It could not be advective, as the Freon concentrations of Greenland Sea Deep Water are higher than the values of all deep water masses (AODW or NSDW) around. The Freon profile at the calibration station in the Lofoten Basin shows a slight increase of the Freon concentrations in Norvegian Sea Deep water (NSDW) since 1989. The values are however smaller than in the Greenland Sea reflecting the fact, that NSDW is formed by about 50 % GSDW and 50 % Arctic Ocean Deep Water. AODW exhibits a smaller Freon signal than GSDW. Convection down to about 800-1000 m has been observed in some stations in the western Greenland Sea. As expected, convection leads also to a homogenized Freon distribution in the water column down to 800 m. Compared to March 1989, the mean concentrations in the upper 1200 m of the water column have increased (Figure 6.1), most likely caused by convective events. Similar to our results in 1989 the short duration of the convection event prevented the gas exchange between atmosphere and ocean to augment the amount of Freons in the water column: in 1989 and in 1993 the mean Freon concentration in the convected water above 1000 m cannot be distinguished from the mean concentrations in regions in the Greenland Sea, where no convection was observed.

7. Marine chemistry

7.1. Measurements of the CO_2 partial pressure (B. Schneider, U. Karbach)

The partial pressure of CO_2 (pCO_2) was measured continuously between the northern edge of the North Sea and Spitzbergen. Water from a depth of about 10 m was pumped into the measuring system consisting of an equilibrator and an IR detection system. The CO_2 content in the atmosphere was also determined sporadically, especially during periods when the pCO_2 seawater system could not be used because ice prevented operation of the seawater pump. To support the interpretation of the pCO_2 data, samples for nutrient and chlorophyll analysis were taken at intervals of about 30 nautical miles.
Although the final evaluation of the data has not yet been finished, some of the most important findings may be reported. In February, during the transect between 55°N and the polar front at 73°N, pCO_2 of surface water was rather uniform with a mean value of about 340 µatm. Hence, also during wintertime this part of the North Altlantic has a negative partial pressure difference with respect to the atmosphere (Δ pCO2 $\approx$ -20 µatm) and acts as a source for atmospheric CO_2. Beyond the polar front, the pCO_2 is even lower with a level of about 310 µatm. These findings will add an important piece of information for a global mapping of the pCO_2 distribution as these were the first continuous wintertime measurements in this area of the North Atlantic.
In April, when steaming back from Spitsbergen to the North Sea, the situation was quite similar in the first part of the transect. But at about 64°N a sudden decrease of pCO_2 to values of about 210 µatm was observed. Such low pCO_2 levels in the North Atlantic have not been reported before and may be explained only by a strong plankton bloom. However, this has to be confirmed by chlorophyll data which are not yet available, and also changes in temperature and salinity have to be taken into account.
For the CO_2 content in the atmosphere a mean value of 363 ppm (dry air) was found which is consistent with previous measurements.
In addition to the underway measurements, pCO_2 for discrete samples were analyzed by an equilibrator/GC system. Samples from about 20 stations in the Greenland Sea and the Fram Strait were used to determine the depth profiles of pCO_2, but the data have not yet been evaluated.

7.2. Determination of nutrients (G. Kattner, A. Michel)

Nutrients were measured to determine the concentrations in winter in the Greenland Sea. Due to the absence of phytoplankton initial values available for phytoplankton growth in spring/summer could be determined. Until now nothing has been known on the nutrient situation in winter in this area. The investigation of nutrients is also closely connected with the physical investigations. For the determination of water masses nutrients, especially silicate in combination with nitrate, are good tracers. For example, high silicate concentrations are typical for the outflow of the Arctic upper halocline water flowing southward along the East Greenland slope.
The nutrients - nitrate, nitrite, phosphate and silicate - were measured from all water samples, taken with the CTD sampler system. Measurements were performed immediately onboard with a Technicon Autoanalyser system

according to standard methods. The accuracy was set by running 4 standards at the beginning and 2 standards at the end of each run. A preliminary view on the results show that the nutrients values in the surface layer were well mixed and increase with depth. The final evaluation and interpretation of the data is still in progress.

8. Biology

8.1. Plankton ecology

8.1.1. Primary production and the microbial loop (P. Henriksen, A. Claudius Nielsen)

Aims. The carbon flux through the marine food web is influenced by the sizes, species compositions and productivity of the populations of phytoplankton, zooplankton, and the microbial loop (bacteria, heterotrophic flagellates, ciliates). The present research project was carried out as part of a seasonal study of the carbon flux through the biological processes in the Greenland Sea.

Methods. During ARK IX/1b, samples for primary production, bacterial production, bacterial abundance and biomass, flagellate abundance and biomass, and ciliate abundance, biomass and growth, were taken on the following stations: 14, 17, 20, 21, 24, 29, 37, 38, 40, 43, 45, 46, 47, 53, 55, 56, 61, 63, 66, 69 and 70. Samples for determining phytoplankton growth rates were taken at stations 14, 17, 20, 24, 40, 43, 45, 47, 56, and 66. Water samples were taken from depth of 20, 40, 75, 100, and 200 m.

Phytoplankton primary production was measured by cellular ^{14}C incorporation in 25 ml watersamples from 20 m depth during incubation in an artificial light incubator at 8 different light intensities. Particulate and total primary production will be calculated from liquid scintillation counting of the activity retained on filters after filtration and in the unfiltered watersamples, respectively.

Phytoplankton growth rates were measured by ^{14}C incorporation into chlorophyll-a during incubation in an artificial light incubator. Chlorophyll-a was extracted with 96% ethanol for subsequent purification by HPLC and assaying of the activity by liquid scintillation counting.

Bacterial production in the watersamples was calculated by ^{3}H-thymidine and ^{3}H-leucine incorporation into bacterial DNA and bacterial protein, respectively. Three plus two samples with pre-killed bacteria from each depth were incubated with each ^{3}H-labelled amino acid. After 4 h incubations, the samples were filtered and the incorporation of ^{3}H was calculated by liquid scintillation counting of the filters. Bacterial numbers were quantified by epifluorescence microscopy of filtered and acridine-orange-stained 20 ml water samples.

Flagellate abundance, biomass and trophic status (autotrophic or heterotrophic) were determined by epifluorescence microscopy of filtered proflavin stained 20 and 100 ml water samples. Ciliate numbers were quantified from Lugol-preserved 1 l water samples. Prior to enumeration in an inverted microscope, the ciliates were concentrated by filtration. Other samples were filtered to remove larger zooplankton and left for 48 h at 0 °C before preservation with Lugol. Ciliate growth was determined by comparison of the number of organisms in the samples immediately preserved and in the samples left for 48 h before preservation.

Results. Our preliminary results only indicate relative primary and bacterial production on the examined stations. Generally, the primary production as well as the bacterial production was very low, indicating winter conditions. Very low production was found on the stations in Fram Strait and on the stations closest to the ice edge in the western part of the Greenland Sea. The highest primary and bacterial production was found on the station at Isodden (st. 40) and on the eastern stations 66 and 69 on the West-East transect in the Greenland Sea.

Microscopy revealed very few phytoplankton and bacterial cells in samples from stations with low production. The phytoplankton was mainly *Phaeocystis* sp. and few diatoms. A more diverse planktonic community was found on the stations with higher production. These stations were dominated by *Phaeocystis* sp., dinoflagellates (autotrophic and heterotrophic) and other nanoflagellates (autotrophic and heterotrophic).

8.1.2. Ciliate ecology (H. auf dem Venne)

Aims. Planktonic ciliates are thought to play an important role within the microbial food web as consumers of smaller organisms, mainly flagellates and bacteria. Some auto- or mixotrophic species may also act as primary producers with the help of symbionts or chloroplast retention. In order to complete former work the abundances of planktonic ciliate populations and their degree of auto- and mixotrophy was to be determined for the first time in late winter both in ice-covered and ice-free surface waters. Furthermore, live ciliates were isolated from water samples in order to establish cultures from different species for later growth and feeding experiments. Ciliate growth rates were also determined from incubation experiments of surface populations.

Methods. During leg 1a, when the ship was totally frozen within the ice, on each day 30 l of water were taken with a bucket from an ice hole and immediately transported to the ship. For the quantification of ciliates and determination of auto-, mixo- and heterotrophy among them 250 ml subsamples were fixed with formalin (2% final concentration), filtered onto 0.6 µm Nuclepore filters and stained with DAPI. Whole filters were then inspected for ciliates using epifluorescence microscopy. This method allows detection of chlorophyll within individual cells and thus differentiation between auto-, mixo- and heterotrophy. For isolation of ciliates these had to be concentrated due to the low abundances in the water. The remaining water from the ice hole was either gently filtered with a modified reverse filtration device based on a large glass fiber filter or simply with a net gauze of 10 µm mesh size. Live ciliates were inspected under the stereo microscope, picked out with a drawn pipette and individually transferred into cell culture wells. Several algae from cultures grown at room temperature were added as food and the ciliates then incubated in the laboratory container at 0 °C with a 12-h-light/12-h-dark cycle. During leg 1b surface water samples were also taken with a bucket from the ship. In addition to further isolations, growth experiments were carried out with surface water samples from 10 stations. 5 l of water were incubated at 0 °C for 48 h. At the beginning and the end of the incubation subsamples were fixed for epifluorescence microscopy onboard the ship. Particle-size spectra were determined with a particle counter. In the lab in Kiel, transmitted light microscopy will be used to determine population and species growth rates.

Results. During leg 1a ciliate populations within the pack ice were found only in very low abundances of generally up to 200 cells/l, mixotrophic ciliates were nearly absent. However, considerable variability occured from day to day and the autotrophic *Mesodinium rubrum* sometimes dominated the populations. One day this species reached densities of more than 500 cells/l. Except for the general occurrence of *Mesodinium rubrum*, the populations were similar to those found on an earlier cruise in late autumn to the Greenland Sea. In contrast, the populations found on leg 1b seemed to approach the typical summer situation with sometimes very high degrees of up to 90 % of auto- and mixotrophic cells. However, the total abundances ranged between 100 and 900 cells/l and were thus considerably lower than typically found during summer.

Enrichment techniques clearly favour larger, more robust, but rare species. From concentrated samples especially the tintinnids, but also *Laboea strobila*, *Condylostoma* sp. *Didinium* sp. and *Tontonia* sp. could be isolated.The more abundant naked and smaller ones obviously pass the filter or disappear due to damage. Tintinnids (apparently *Coxliella* sp.), which were isolated during leg 1a, were observed to divide and kept alive in low numbers until the end of the cruise. Several others eventually died under laboratory conditions. During leg 1b, a *Strombidium* species could be isolated and successfully cultured in higher numbers.

8.1.3. The life strategy of *Calanus hyperboreus* in the Greenland Sea Gyre and its influence on the spring bloom (S. Duesterloh)

Aims. There has been some research on distribution and life strategies of calanoid copepods in the Greenland Sea. As the dominant species of the Greenland Sea Gyre (GSG) *Calanus hyperboreus* plays a key role in the timing of vertical migration, spawning and feeding of copepods in this area. The hydrographical situation of the GSG provides little export of organisms into the Atlantic Water. Thus, the population of *C. hyperboreus* may be considered to be homogeneous.

The copepods show a seasonal vertical migration as they spend the winter in deep water layers between 1000 and 1500 m and ascend to the surface euphotic zone in spring. Herbivorous zooplankton calanoids depend on the highly seasonal primary production in order to reproduce and survive the winter without feeding. Former expeditions have always been too early or too late to observe their vertical ascent. The influence of grazers on the spring bloom is among other factors a matter of timing. Since algal growth describes an exponential curve, a hypothetical model suggests that early grazing will inhibit an extensive spring bloom. Since extensive spring blooms (with nutrient depletion in surface waters typical of boreal seas) have not been observed in the Greenland Sea as yet, this model is applied to this region. Another factor influencing the impact of grazers on the spring bloom is the size of the overwintering population.

Methods. We used a Multinet for vertical hauls, sampling depths were 1500 - 1000, 500 - 200, 200 -100 and 100 - 0 m. Eleven Multinet samples were taken during the cruise which were widely distributed over the Greenland Sea and Fram Strait area. Later sorting of the samples will show the vertical distribution of copepods and the timing of the ascent. In addition, we took 18 Bongo net hauls (200 µm mesh size) which were split into two subsamples. One will be used for biomass calculations, whereas the other was preserved in formalin. Later sorting will provide data on species and stage distributions.

Parallel to the net samples water samples from different depths in the upper 200 m were taken (200, 100, 75, 50, 40, 30, 20, 11 m) to obtain information on the spring bloom development within the euphotic zone.

Results. A rough inspection of the Multinet samples indicates the ascent of copepods from depths below 1000 m in the Fram Strait to more intermediate depths on the 75°N transect about a week later. During the first week of the cruise, the Bongo net samples from 100 - 0 m also showed almost no biomass but biomass increased as we crossed the GSG.

Data from this winter/spring cruise will be compared to summer data which will be taken in May/June 1993. Feeding rates of different stages of *C. hyperboreus* will be obtained experimentally for the assessment of their grazing impact on the spring bloom.

8.1.4. Gonad development of calanoid copepods (B. Niehoff)

Aims. One important point in investigating life cycles of copepods is to determine the developmental stage of the gonads which directly corresponds with reproductive activity. This staging is often based on width and length of the ovary/oviducts and the number and color of the eggs. Knowledge of these structures was achieved by staining and microscopy of the copepods. On the other hand, little is known about the internal morphology and cytology of the gonads and the formation of yolk. To get more information about the internal organization histological methods are used in addition to ecophysiological experiments.

Methods. Three of the dominant copepod species of the northern oceans, *Calanus finmarchicus, C. glacialis* and *C. hyperboreus*, were collected by vertical Bongo net hauls (300 µm mesh size) down to 100 or 200 m depth. For histological investigations females and the copedite stages V (CV) were fixed with 2.5% glutaraldehyde buffered with sodiumcacodylate. Furthermore, the boreal species *C. finmarchicus* was sampled at the Atlantic water stations (ST. 9, 10, 69 and 70) in the Westspitsbergen current. Females and CV stages were sorted for determination of dry weight, carbon content and gonad maturity. In addition, females were kept in beakers and daily egg production was determined. Fifty females were fed with diatoms (*Thalassiosira antarctica*), another fifty were starved. After 12 days 10 females of each experiment were fixed for electron microscopy. Another 40 were used for dry weight and carbon analysis. The experiment has not yet been finished. Histological and biochemical investigations will be carried out at the AWI.

8.1.5. The lifecycle of *Metridia longa* in the Greenland Sea (T. Scherzinger)

Aims. One objective was to complete our data set on the horizontal and vertical distribution of *Metridia longa* for a better understanding of the general migration pattern of the different ontogenetic stages. Trophic investigations aimed at detecting the different food sources during late winter, whether starvation occurs and how this lack of food might influence metabolic conditions.

Methods. The following vertical net hauls have been carried out:

9 Multinets	(150 µm; sampling depth 1500/1000/500/200/100 m)
2 Multinets	(150 µm; sampling depth 500/400/300/200/100 m)
1 Multinets	(150 µm; sampling depth 3000/2000/1500/1000/500 m)
8 Bongo nets	(200/300 µm; sampling depth 1000-0 m)

In addition, experiments have been carried out on starvation effects (mortality,carbon and lipid depletion) and samples collected and preserved in 4% formalin or 70% ethanol for faecal pellet analyses by electron microscopy.

Results. Preliminary results indicate higher abundances of young stages (CII - CIV) in the deeper water layers (1500 - 1000 m depth) of ice-covered areas, while adults were found in the entire area investigated . Ovaries with eggs were detected in females, but no spawning occured as yet.

8.1.6. Lipid biochemistry of meso- and macrozooplankton (W. Hagen)

Aims. Investigations of the lipid biochemistry of Arctic zooplankton continued previous studies of the IPÖ in the Fram Strait and the Greenland Sea. Our major objective during ARK IX/1b was to characterize the energetic status of plankton in late winter and to compare this situation with the one encountered during spring (ARK VIII/1) and summer (ARK VII/2). The results of this cruise will be important to understand the seasonal processes of lipid accumulation and depletion in the northern North Atlantic.

Methods. Mesozooplankton for lipid analyses was mainly sampled along the transects on 79°N and 75°N by vertical Bongo hauls (200 µm/335 µm). Maximum hauling depth was usually 1000 m. Macrozooplankton was collected at four stations using oblique RMT 1+8 tows (320 and 4500 µm) down to 1000 m depth . The organisms were identified to species level (if possible), sexed and sorted according to developmental stage, gonad maturity and body size. The samples were immediately frozen at -80 °C. A total of almost 500 samples were collected, including hydromedusae, ctenophores, pteropods, ostracods, copepods, euphausiids, decapods, amphipods and chaetognaths. The determination of total lipid content, lipid classes and fatty acid/alcohol composition will be carried out in close cooperation with the AWI (Dr. Kattner) in the laboratories in Kiel and Bremerhaven.

8.1.7. Heavy metals in zooplankton (G.-P. Zauke, J. Ritterhoff, J. Frerichs)

Aims. Recent studies on polar crustaceans showed that metal concentrations in these organisms are not generally at background levels, especially cadmium being high in some species. This high ability for accumulation of potentially toxic metals requires efficient mechanisms of storage and detoxification, well known for crustaceans from temperate waters. In this context, metal-binding proteins (e.g. metallothioneins) play an important role. We aim at investigating these problems using different Arctic crustaceans and some other taxa, combining field studies and toxicokinetic experiments on board.

Methods. Mesozooplankton for determination of metals was mainly sampled along transects on 79°N (8 stations) and 75°N (10 stations) by vertical Bongo hauls (mainly 1000 - 0 m). Macrozooplankton was collected at 4 stations using oblique RMT 1+8 tows (0 - 1000 - 0 m), as pointed out in the previous section. Organisms were identified to species level (if possible), sorted and immediately frozen at -80 °C. Special care was taken to avoid contamination, e.g. by maintaining animals always in water or closed containers. Occurrence of paint particles or other materials was excluded by close inspection of each specimen collected using a binocular microscope.

Sampled material included 7 copepod species, 4 amphipod, 1 decapod, 1 ostracod, 4 euphausiid, and 2 chaetognath species. Additionally, 13 samples were taken for determination of metal-binding proteins under natural conditions, including the copepods *Calanus hyperboreus*, *C. finmarchicus*, and *Euchaeta norvegica*, the amphipods *Themisto libellula* and *T. abyssorum*, and the euphausiid *Meganyctiphanes norvegica*. Furthermore, laboratory experiments on induction of metallothioneins were performed with *C. hyperboreus, T. libellula*, and *T. abyssorum*, exposing the animals to concentrations of 12 - 15 µg Cd l^{-1}.

Further experiments were done as a tool for calibration of monitor organisms to follow the time course of uptake (7 d) and depuration (5-7 d) of cadmium, lead, copper and zinc in 4 copepod species and the amphipod *T. abyssorum*. Nominal exposures were (i) 0.6 µg Cd l^{-1}; 1.2 µg Pb l^{-1} 8 µg Cu l^{-1} 40 µg Zn l^{-1} and (ii) 3 µg Cd l^{-1}; 6 µg Pb l^{-1} 40 µg Cu l^{-1}; 200 µg Zn l^{-1}. Finally, uptake experiments were performed using a wider range of 10 exposure levels to investigate accumulation strategies of *C. hyperboreus, T. libellula* and *T. abyssorum* in more detail. During these experiments mortality rates were noted.

Results. Preliminary data on toxicity indicate 50 % lethal concentrations after 24 and 40 h for a metal mix of 18 µg Cd l^{-1}; 36 µg Pb l^{-1}; 240 µg Cu l^{-1} and 600 µg Zn l^{-1}, regarding *T. abyssorum*, whereas Cd alone did not seriously affect

these organisms up to 75 µg Cd l^{-1}. For *C. hyperboreus*, toxicity of the metal mix was within the same range. Our results found for *T. abyssorum* support the hypothesis that the observed toxic effects of the metal mix are due to a failure in regulating the essential metals Cu and/or Zn, since Pb is rather immobile in aquatic systems.

8.2. Sea-ice biology (D. Thomas)

The original plan for this expedition had been to measure the biological activity and chemical composition of sea-ice algal communities, and to relate these observations with the prevailing physico-chemical conditions. However, due to the very low brine volumes in the ice cores obtained (see Section 9.2), it was not possible to carry out this programme. To obtain enough brine it would have been necessary to take large numbers of ice cores (logistically impossible), or to drill "sack-holes" from which brine could be collected directly. The latter was not feasable since brine percolating into the sack-hole froze immediately on contact with the air.
However, sections of seven ice-cores were melted at 4 °C, including cores from the main ice floe, and also from ice forming over the lead around *POLARSTERN*. Under-ice water samples were taken as well as water from a single CTD cast (surface, 40, 120, and 1500 m). After salinity determination samples were filtered on precombusted GFC filters, and the filters and filtrates stored (-30 °C) for later chemical analyses in conjunction with R. Lara, U, Hubberten, A. Skoog (AWI). These include measurement of chlorophyll*a* (Chl*a*) and phaeopigment contents, dissolved organic carbon and nitrogen (DOC/DON) and major nutrients. Fractionation of DOC into "humic" and "non-humic" components will be carried out, and fractionated and unfractionated samples will be analysed for free/combined amino acids and total carbohydrates. Fluorescence spectral analysis will be conducted to search for traces of terrestrial humic material. Such information will be highly informative in appraising the availability of organic matter in Arctic multi-year sea-ice, and will serve as a basis for further studies into the transport processes of material from the Siberian Shelf into the Atlantic through the Arctic outflow.
Figure 8.1 shows the distribution of salinity, DOC, Chl*a* and phaeopigments in two complete cores along with the textural stratigraphy (for details and legend see Section 9.2 and Figure 9.16). The concentrations of Chl*a* measured are low compared to those commonly recorded in Arctic ice cores at different times of the year. In both cores there is a concentration of Chl*a* on the bottom which is expected, however, in both cores there are clear internal bands of chlorophyll: in AR9107402 between 100-150 cm and in AR9106902 between 50 and 120 cm. Such internal bands of algal material as of yet have not been frequently observed in Arctic sea ice. In this case these layers correspond to microstructural traces of the termination of ice growth during the summer season. The ratio of chlorophyll *a* to phaeopigments is generally low, especially towards the bottom of the two cores. This is a good indication that a high degree of degredation and/or grazing has taken place within these algal communities. The higher Chl*a* to phaeopigment ratios in the internal layers does not necessarily reflect a better physiological status, but is probably due to this ice being at much lower temperatures at which algal degradation cannot proceed so quickly.
There is little variation in the DOC content in the core AR9106902, the values being consistantly low. In AR9107402, however, there is large peak in DOC levels just above the bottom layer Chl*a* maximum. Presumably this results

from the breakdown of the previous years' bottom algal community. Very few measurements of DOC levels in sea ice have been recorded in the past, and those reported here indicate that it is possible for very high concentrations to accumulate, and be subsequently released into the water column on ice break-up and melting.

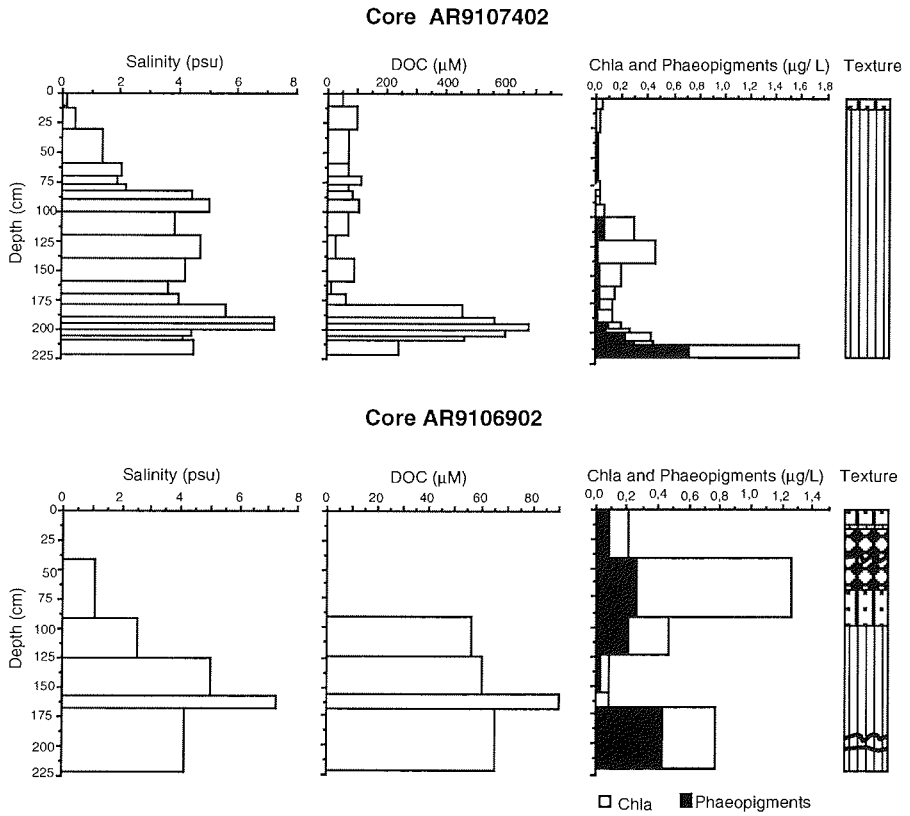

Figure 8.1: Distribution of salinity, dissolved organic carbon (DOC), Chlorophyll *a* (Chl*a*) and phaeopigments along with the textural stratigraphy (striated is columnar ice; for detailed explanation of textural signatures refer to Section 9.2 and Figure 9.16) in the two cores AR9107402 and AR9106902.

8.3. Cryopelagic fauna (M. Poltermann)

During the ice camp a qualitative registration of the cryopelagic macrofauna was to be subject of the zoological studies. Furthermore living animals had to be provided for future laboratory work in Bremerhaven. It was also planned to employ the underwater-video-system "ELSE" to get a picture of the macrofauna living at the lower side of the ice. The results shall deepen our knowledge of cryopelagic coupling, especially regarding questions on the feeding biology of the macrofauna living under the ice.

As planned, samples were taken by means of different tackles at the underside of the ice and in the watercolumn directly below. Invertebrates were caught with baited traps. Catching fish was more difficult as there was no open water in the vicinity of the ship due to the low air temperatures and holes dug into the ice froze within a short time. Nevertheless several fish traps and a fyke-net with wings could be deployed at the lower edge of the ice. Moreover, it was tried to angle for fish, but without success. The daily control of the tackles was problematic because a layer of new ice 20 cm thick had to be removed each time.

Putting the underwater-video-system "ELSE" into service was less difficult. Already existing holes in the ice could be used to employ this endoscope camera protected by a steel construction. Yet, the system could not be deployed during the phase of minimum air temperatures due to the sensitive electronics.

The live catches were stored in a container and kept at a water temperature -1.5 to +2.0 °C in aquaria and ventilated tanks.

During the drift-station phases 14 fish individuals and large numbers of amphipods could be caught. Moreover, several species of Ctenophora were obtained from the water layers directly below the ice, since these were swept into the fish traps by the current.

After a first examination, the fish were identified as Polar Cod (*Boreogadus saida*). Only younger specimens (1-2 years old) were represented. Despite problems in feeding them, some of the animals could be kept alive on board. Because of the low temperatures it was rather difficult to convey the fish alive from the traps to the transport box. For only a few seconds in the open air (-35 to -40 °C) were enough for the animals to freeze to death.

Two species of amphipods could be identified: *Gammarus wilkitzkii* and a species of the genus Onisimus. Both species displayed positive phototaxis and visited the baited traps which were lighted by underwater lamps in a larger number during the night. Some of the animals were conveyed into aquaria and keeping them proved to be unproblematic. The animals were fed with pieces of fish and meat. Many females of *Gammarus wilkitzkii* carried eggs or almost completely developed juvenile animals on their body.

It was possible to film the activities of *Gammarus wilkitzkii* at the underside of the ice by means of the underwater-video-system "ELSE". It turned out that these animals live less directly on the lower side of the ice but rather in the porous lowest layer of the ice where they move about in passages and caverns. Life in this layer does not only protect them from grazers but also prevents them from being carried away involuntarily by currents. Astonishing is also the high activity and speed of these animals as the water temperatures are just between -1.6 and -1.8 °C.

The formalinized material will be analyzed and interpreted in particular with regard to feeding ecology of these ice-associated animals. Observations and more extensive experiments with 20 cm thick animals in aquaria will increase our understanding of the feeding strategy of Polar Cod and amphipods.

9. Sea-ice research

9.1. Sea-ice physics (P. Wadhams, E. Aldworth, M. Brandon, D. Crane, E. Prussen, M. Reisemann, P. Struckman, S. Wells)

9.1.1. Purpose of programme

The sea ice physics programme was designed to study five major aspects of the properties and behaviour of sea ice:

1. Its response to the passage of flexural-gravity waves generated by internal waves in the pycnocline, penetrating ocean swell, local wind forcing and forcing due to nearby mechanical processes in the ice;
2. The effect of rapid refreezing of leads, either in the form of frazil ice or as nilas, upon the local stability in the lead, in particular the stimulation of convection through the salt flux;
3. The properties of the overlying snow and upper part of the ice cover that determine the response to active microwave, in particular ERS-1 SAR. The chief properties are snow wetness, conductivity and dielectric constant; small-scale roughness of the snow-ice interface; and brine volume and bubble density in the upper part of the ice sheet;
4. Acoustic properties of the ice, particularly generating mechanisms for ambient noise and the attenuation of acoustic waves by crystal grain boundaries;
5. The nature and properties of the ice cover in the fast-changing Odden ice tongue, a very variable feature of the Greenland Sea in winter which in some models is associated with triggering of the convection process.

9.1.2. Background to experiments

Waves. We used a heave-tilt-strain array to measure the directional spectrum of the oscillations of the sea ice. This comprises a vertical and two horizontal accelerometers, two tiltmeters and three strainmeters. The accelerometers act as the equivalent to a directional wave buoy, while the strainmeters measure flexure directly and the tiltmeters indirectly via the inclination of the ice surface. The total instrument package therefore involves some redundancy and not all sensors were used in every experiment. Measurements were made for periods of from one to several hours and at a sampling rate of 3 Hz. The resulting spectra can therefore cover the relevant frequencies for the ice response to the following stimuli:

a) Internal waves of typical period 10-20 min. The ice surface moves with the sea surface in its response to high amplitude waves in the pycnocline.

b) Swell, of typical period 12-20 s. This penetrates from the open sea, suffering attenuation by scattering from ice floes along the way, the relative energy loss being greater at higher frequencies. The surviving energy represents the long-period tail of the wave spectrum of the ocean.

c) Local wind waves, of typical period 8-12 s, depending on ice thickness. Pressure fluctuations on the ice surface due to wind can generate freely propagating flexural-gravity waves (waves which cause ice to flex) so long as wind speed exceeds the minimum group velocity for these waves (which depends on ice thickness). It was therefore necessary to know wind speed and ice thickness at each measuring site.

d) Short period oscillations, of typical period 1-3 s. These have been observed in several earlier experiments in the Arctic and Antarctic, but their nature and origin remain to be explained. They cannot propagate more than a few hundred metres without heavy attenuation, and so must represent a response to very local mechanical forcing. We believe that they are due to a local

pressure ridge bobbing or tilting whilst embedded in an elastic ice sheet, in response to the addition of ice blocks or some other force, and thus sending out flexural-gravity waves at the resonant frequency for such a bobbing or tilting response. The waves may, however, be due to shear between neighbouring floes and would thus be a stick-slip effect.

To support these measurements we carried out aerial photographic flights by helicopter to the ice edge (to define ice floe sizes) and drilled and cored at and around the wave measuring sites. During ARK IX/1b we also deployed a Datawell Waverider Argos-transmitting directional wave buoy outside the ice edge while wave measurements were being made inside the ice, so that the incoming wave spectrum from the open sea would be known at all times.

*Water structure under ice...*In midwinter, when air temperatures in the Arctic are very low (the lowest experienced on ARK IX/1a was -46°C), a newly opened lead loses heat to the atmosphere at an enormous rate and rapidly refreezes. If a strong wind is blowing, the refreezing initially occurs in the form of frazil ice which piles up against the downwind side of the lead. The high growth rate of frazil ice results in a high salt flux into the lead, causing a local convection process under the lead, for which the dynamics and thermodynamics are not well understood. If refreezing occurs in calm conditions so that a continuous sheet of nilas forms immediately, there is still a significant salt flux in the early stages and convection may still occur, albeit for a shorter period.

During both legs, local convection and frazil production in leads were measured using a portable CTD (either an instrument developed at SPRI or a Seacat) lowered by hand winch, and a calorimetric sensor (developed by Eric D'Asaro and Paulette Struckman, University of Washington) to measure frazil ice concentration as a function of depth (a "frazilometer"). The instruments were operated down to 105 m and 60 m respectively. In addition, when frazil was present an underwater video camera was lowered in stages to measure the depth of the frazil layer and to examine the nature of its underside.

During the latter part of ARK IX/1a and most of ARK IX/1b the ice stations were carried out on floes in the marginal ice zone (MIZ). This permitted CTD casts to be done over the floe edge into the brash ice between floes, thus sampling the near-surface water structure under pack ice in a place where it is not disturbed by the ship. In addition, during our two excursions into the Odden ice feature, the CTD and frazilometer could be taken off in a rubber dinghy into a regime of frazil-pancake ice and used to measure frazil concentration and near-surface water structure far away from the ship in a totally undisturbed environment.

Snow and ice properties . The best imagery of ice in relation to resolution is obtained from SAR. However, the image brightness depends both on the electrical properties of the snow and near-surface ice (conductance, dielectric constant) and also on the physical roughness of the snow and ice surfaces, on small and large scales. Snow electrical properties and small scale roughness were studied during this experiment. Electrical properties were measured using a "snowfork", an instrument designed at the Finnish Institute of Technology, Espoo, which consists of two parallel prongs inserted into the snowpack. A resonant frequency (in the vicinity of 600-700 MHz) is measured by the instrument, together with bandwidth and attenuation of the resonant peak. From these values the instrument computes relative permittivity, snow density and snow wetness. Roughness was measured using a mechanical profilometer over 1-m lengths of ice surface from which the snow had been cleared. To examine properties of the upper part of the ice surface, 1 m cores were taken which were analysed for salinity and ice crystal fabric.

Acoustics. It is very difficult to sound through ice by electromagnetic means, because of scattering by brine cells and air bubbles. Ice thickness surveys up to now have depended upon the use of submarines or moored upward sonar. Acoustic techniques hold some promise, but depend on a knowledge of sound velocity and attenuation in relation to ice characteristics. During ARK IX/1a the opportunity of a long drift station was used to carry out small scale experiments to measure the in-ice attenuation across short lengths of ice cover.

Ambient noise is very low under ice in the interior of the pack, and is mainly due to tiny cracks produced by stresses induced by air-sea temperature differences. At the ice edge ambient noise levels are very high, due to waves breaking against floes, and collisions between floes. Hence there is a need to measure noise near the edge and in the interior. However, it is necessary to move several km from the ship, to avoid ship-induced noise, and this limited the number of ambient noise measurements that could be made to a few helicopter-borne operations.

The Odden ice tongue. In the central Greenland Sea, just south of the main gyre centre, an ice tongue usually develops during winter. It grows eastwards from the main East Greenland ice edge in the vicinity of 72-74°N latitude and often curves round to the northeast until it reaches east of the prime meridian. It is called Odden, and in its curvature it embraces a bay of open water, centred on the gyre centre, which is known as Nordbukta. It is believed to form mainly by local ice production, since the tongue-shaped region corresponds to the region of influence of the Jan Mayen Polar Current (the southern part of the Greenland Sea Gyre) which maintains cold surface water. There is currently great interest in Odden, for two reasons. Firstly, the contribution of local ice production as opposed to advection of older ice from the East Greenland Current is not know for certain. Secondly, and related to this, the local ice production is believed to occur largely in the form of frazil and pancake, since the intense wave field in the winter Greenland Sea inhibits ice sheet formation, while remote sensing imagery shows rapid changes in the size, shape and position of Odden, such as would not occur if it were composed of large floes. Again, frazil and pancake production implies high growth rates and high salt fluxes, possibly on a cyclic basis related to cold air outbreaks from Greenland. In recent models of winter convection in the central Greenland Sea, this periodic salt flux is believed to play an important role in triggering narrow convective plumes. One of the objectives of the Winter Greenland Sea Project, and of the associated EC-supported ESOP (European Subpolar Ocean Programme) is to understand winter convection and the role of sea ice-ocean interactions in it.

During winter 1993 an experiment in early February using the vessels *Valdivia* and *Northern Horizon* and a BAC 1-11 research aircraft of the Royal Aerospace Establishment, Farnborough, established that Odden had developed this year as a tongue of dense pancake ice, with little or no older ice present. During her voyage north on ARK IX/1a, *POLARSTERN* skirted the eastern edge of Odden at 73-75°N, 3°E on March 3, encountering scattered pancake and frazil ice whilst in the polar surface water regime. The Odden may well have been broken up by the intense northerly winds experienced during the transit, which also caused severe superstructure icing. Meanwhile passive microwave and SAR images showed that the Odden ice tongue had completely separated from its root and become a long island of ice oriented N-S centred on the prime meridian. This island later broke into separate north and south islands, and (on passive microwave) the north

island appeared to dissolve and reform late in March while the south island steadily shrank.
The ship was able to visit both islands of Odden during ARK IX/1b, on April 3 (south island) and April 10 (north island). The opportunity was taken to carry out an ice physics programme to try to establish the nature and origin of the ice cover and the mechanism underlying its rapid variability. On each occasion the ice cover was found to consist overwhelmingly of pancake ice, with a very sparse admixture of older floes in the case of the south island only. The region was overflown with the helicopter and aerial camera to yield pancake sizes; the CTD and frazilometer were deployed from a Zodiac dinghy in the pancake ice distant from the ship; the Waverider buoy was launched to determine the wave field present in the region; frazil samples and underwater photography were carried out from the dinghy; and ice was lifted onto the deck to recover and analyse pancakes and frazil. Several whole pancakes were recovered, and analysed to examine three-dimensional salinity distributions and ice fabrics, as a test of the hypothesis that the thicker pancakes are actually quite old and can remain in the Odden without evolving into other ice types, on account of the wave energy present.

9.1.3. Conduct of experiments

The ice physics station work fell into five phases:-
1. ARK IX/1a: the long drifting ice station, March 7-20
2. ARK IX/1a: individual ice stations, March 20-22
3. ARK IX/1b: individual ice stations in Fram Strait, March 28-31
4. ARK IX/1b: transects of Odden, April 3, 10
5. ARK IX/lb: ice stations at 75°N April 6

Whenever the ship was moving in ice, an ice watch was kept from the bridge, the work being shared with several other groups on board. Every hour (every two hours during the night), ice conditions were assessed and logged using a standard format used on many previous cruises, and photographs taken from the bridge to port and starboard. The purpose is to produce an illustrated ice report for the cruise which will be of value to all participants. During daylight hours, while the ship was in motion in ice, a video was kept running on the bridge, looking forward, to record ice conditions.
Table 9.1 is a summary of the experiments of each type that were carried out during the five phases of the cruise.
During phase 1 all work was done on the vast multi-year floe alongside the ship, except for four helicopter operations where a group was put on a floe several km from the ship to carry out acoustic studies and CTD measurements. Two helicopter visits were also made to remote sites for snow studies and validation of SAR imagery. Two wave sites were established 100 m apart on the floe, and almost continuous data received from one by telemetry; the other functioned for periods of 1-3 hours using a data logger, giving concurrent wave data from two sites separated by a pressure ridge system. A network of snow sampling sites was set up, many of them studied in relation to concurrent snow radiometry measurements by the University of Bern group. The CTD and frazilometer were mostly operated at the edge of the wide refrozen lead which the ship had used to penetrate to this high latitude. Three 2 m thermistor chains were installed in the floe, giving temperatures at 10 cm intervals. The ice thickness was profiled along a line joining the wave sites, and three surface cores taken.
During phase 2 a standard procedure was employed for short experiments on single ice floes. The heave-tilt array was deployed at the centre of the floe; ice thickness was measured at the centre; a 1 m core taken; snow sampling

carried out; and as many CTD casts as possible carried out manually over the edge of the floe. The frazilometer was deployed when frazil was present between floes, and where possible an aerial photographic transect carried out between the floe and the ice edge.
During phase 3, in ARK IX/1b, this single-floe procedure was further refined for work in Fram Strait. Before the ship entered the ice a Waverider directional wave buoy was deployed in the open sea, giving a continuous reference level for incoming wave energy. It was recovered on our exit from the ice on March 31. The number of snow sites and drill holes per floe was increased.
Phase 4 comprised two visits to the southern and northern parts of the Odden ice tongue, at this time comprising two islands. The work done is described above.
Phase 5 comprised an entry into the main East Greenland ice cover at 75°N, where the ice had retreated westward of the shelf break. Again the Waverider buoy was deployed outside the ice edge and recovered at the end of the experiments. Two single-floe experiments were carried out, together with an aerial photographic transect of the region between the experimental sites and the ice edge.

9.1.4. Work accomplished and preliminary results

Wave Experiments. The equipment used to detect the waves present in the ice cover consisted of two horizontal (at right angles) and one vertical accelerometer alongside two tiltmeters also orientated at 90 degrees to each other. The outputs from these sensors were fed into an amplifier unit, through an anti-aliasing filter with a cut off frequency of 1.4 Hz and then either into a 12-bit digitising unit connected to a telemetry system or into a 12-bit data logger. Both digitised the signal at 3 Hz.
On ARK IX/1a the ice station experiments were positioned at two sites, 100 metres apart and separated by two distinct ridges. For the first half of the station the equipment was located at site 1 and then moved to site 2 for the second half. During the second five days some simultaneous measurements of vertical acceleration and three-directional strain (from a rosette of three strainmeters at 120° to one another) were made at site 1 for comparison. An ice thickness profile was obtained along a line between the two sites and a survey of the surrounding ridges was made. After the ice station was finished six further short experiments were carried out on floes of opportunity with the data being recorded on the data logger. Around 8 days of wave data were collected from the ice station and a further 12 hours from separate floes after the station.

Figure 9.1 shows an hour-long record of the output from the two tiltmeters from an experiment conducted near the beginning of the ice station on March 8. The swell period can be clearly seen superimposed on lower frequency oscillations which could be the surface effect of internal waves propagating along the pycnocline. Comparison with simultaneous shallow CTD casts will help to confirm the nature of these waves. The phase difference between the two tiltmeters, for these waves, varies throughout the record, indicating that these oscillations have different sources.

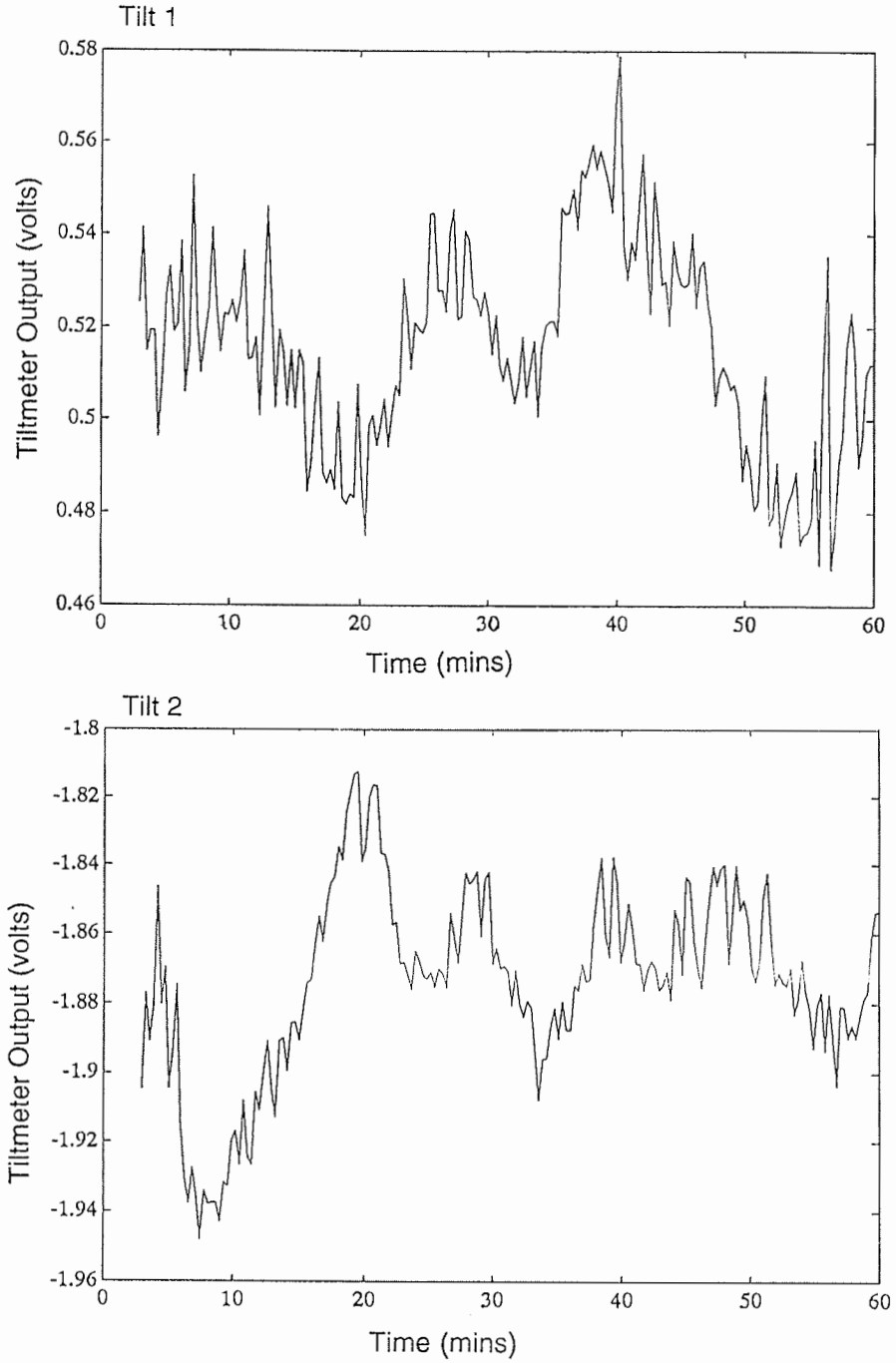

Figure 9.1: Output from two orthogonally oriented tiltmeters, from drifting ice station on March 8. At this station, far inside the ice edge, energy of presumed swell origin is of unusually long period - about 60 s - while it is also modulated by much longer waves of some 20 min period which are likely to be internal waves.

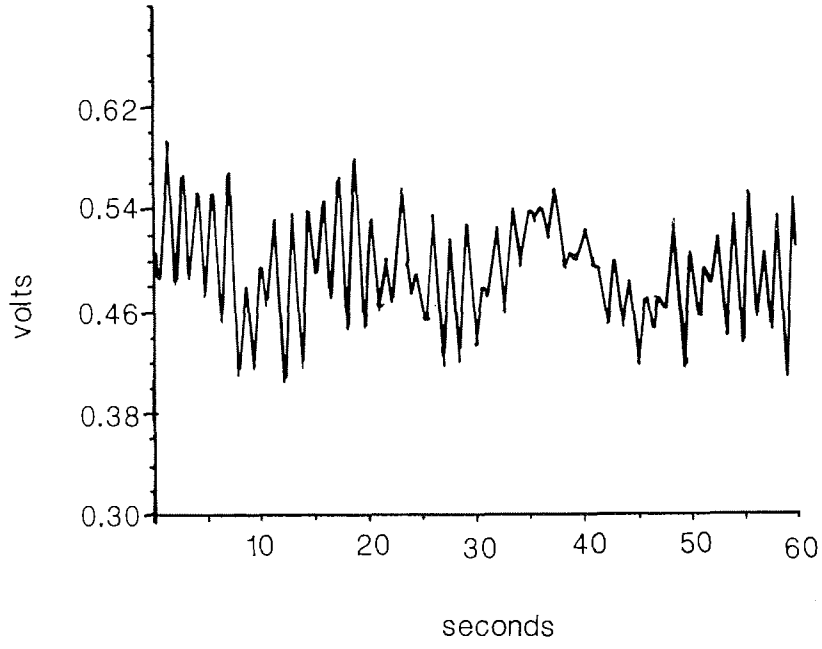

Figure 9.2: A 60 s segment of output from a tiltmeter on the drifting ice station. Here a 17 s swell modulates high frequency waves, of about 2 s period, which are probably associated with ice deformation.

Figure 9.2 shows a 60 second portion of one tiltmeter output for the same experiment. Higher frequency waves with a period of around 2 s are clearly seen on top of the 17 second swell. Further analysis of the directionality of these waves and the variation in power throughout the period of the experiment will provide further insight into their source.
For the attenuation experiments in Fram Strait and at 75°N on ARK IX/1b a Datawell Waverider buoy was deployed in open water before entering the ice. The buoy obtained the directional wave spectra and transmitted the data via satellite. The Waverider spectra can then be compared with the spectra obtained from the wave equipment deployed at stations within the pack. Figure 9.3 shows the superimposed spectra from the five ice stations in Fram Strait. The energy at the swell frequency (around 0.075 Hz) decreases to a minimum on the morning of March 30 and then increases again. Plotting this against the distance from the ice edge (Figure 9.4) shows a negative exponential relationship. This agrees well with the theory of energy attenuation within pack ice and differences will be examined in conjunction with the variation in swell energy present outside the ice edge obtained from the Waverider. At the second station on March 30 there is more energy from the local wind waves (0.15 Hz) than from the swell, the only occasion that this is seen. The cause of this is twofold: higher wind speed and thinner ice than at the other stations, permitting the wind to generate freely propagating flexural-gravity waves.

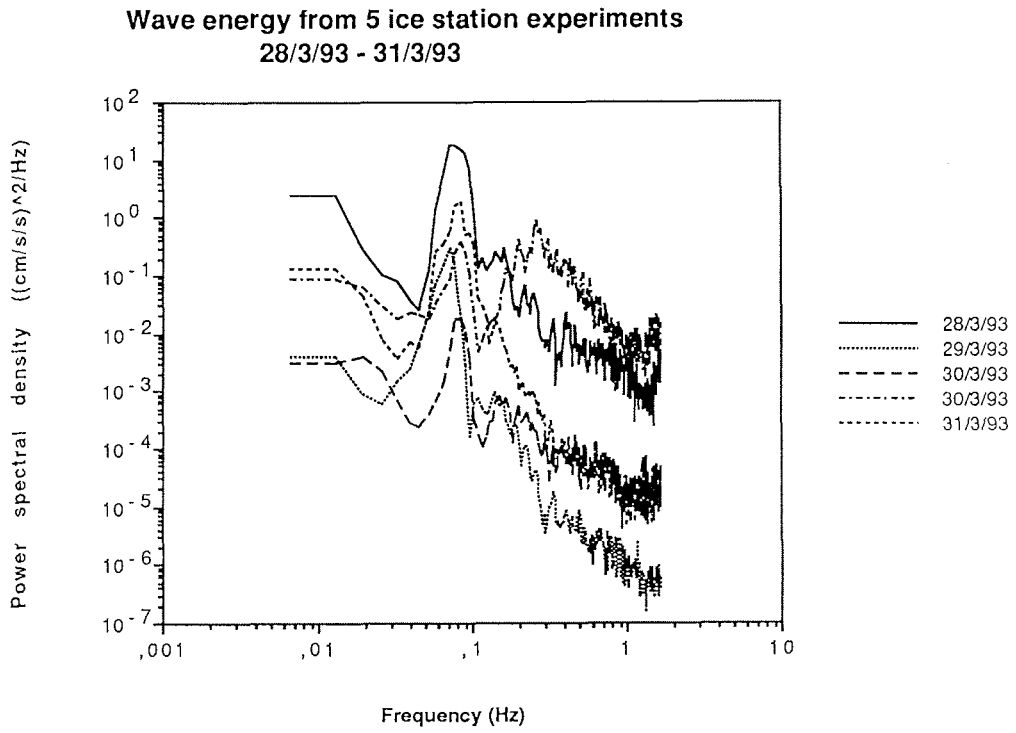

Figure 9.3: Wave energy spectra from five ice stations in Fram Strait. The shapes of the spectra are similar, with the energy levels decreasing with increasing distance into the pack. The exception is the second ice station on March 30, where there is enhanced energy in the 0.2 - 1 Hz range. This station was done on thin ice, over which the wind was capable of generating local flexural-gravity waves.

Water structure under ice. Oceanographic measurements taken by SPRI and APL fell into two distinct sections. On the drift phase of ARK IX/1a the experiments were based around lead convection which causes frazil ice production and a resulting salt flux. On the individual ice stations the experiments were based on oceanographic processes beneath a growing or decaying ice cover.

During ARK IX/1a three sensor packages were deployed. The first was the APL frazilometer, a Seabird Electronics Seacat (SBE19) modified to measure frazil ice concentration at depth calorimetrically, as well as the standard conductivity, temperature and depth. Seawater is pumped through a heating chamber, where any ice present will melt. The temperature of the heated water is measured; melting of the ice results in both a decrease in the heated temperature and a decrease in conductivity. Thus a true frazil ice signal shows up as an increase in the calculated ice concentration with a decrease in the salinity. The other two instruments deployed were the SPRI CTD and a Seabird Seacat CTD.

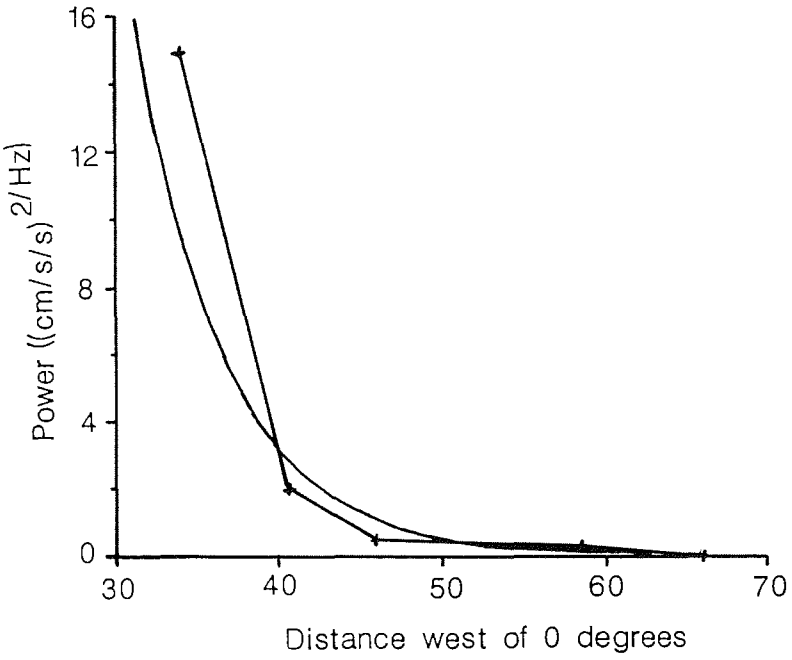

Figure 9.4: Energy at the swell peak plotted against distance from ice edge (0°W) for Fram Strait ice stations, showing reasonable fit to negative exponential.

Temperature is a sensitive indicator of water masses in the vicinity of the Yermak Plateau. A temperature of greater than 0 °C can be taken as water with an Atlantic origin, while below 0 °C the water has a Polar origin. Measurements during the drift of *POLARSTERN* , when there was no open water present, revealed a mixed layer with a temperature at the freezing point at -1.8 °C, and a salinity of 34.1. The thickness of the mixed layer showed high variability, revealing the presence of internal waves, possibly caused by diurnal tides over the Yermak Plateau. Beneath the mixed layer were varying mixtures of Atlantic Water and Polar Water. In Figure 9.5 we show a typical potential temperature, salinity and density profile taken at 81°05'N 5°30'E in which the Atlantic Intermediate Water had a temperature of 1.6 °C and a salinity of 34.65.

The University of Washington frazilometer was deployed on nine occasions. Four deployments were from the working deck of *POLARSTERN* . One deployment was from the vast floe next to the ship. Because of the rapid refreezing of any open water the ship's helicopters were used to deploy at remote leads which were open. There were four deployments to remote leads. By far the most promising experiments were the helicopter deployments, but even on these occasions the frazilometer could not be deployed into open water. First a suitably sized hole had to be made through up to 7 cm of nilas ice. We were unable to detect any frazil ice at depth even when there were visible frazil ice slicks on the surface. The preliminary conclusion is that the lack of wave energy present in leads precludes the advection of frazil ice into the water column.

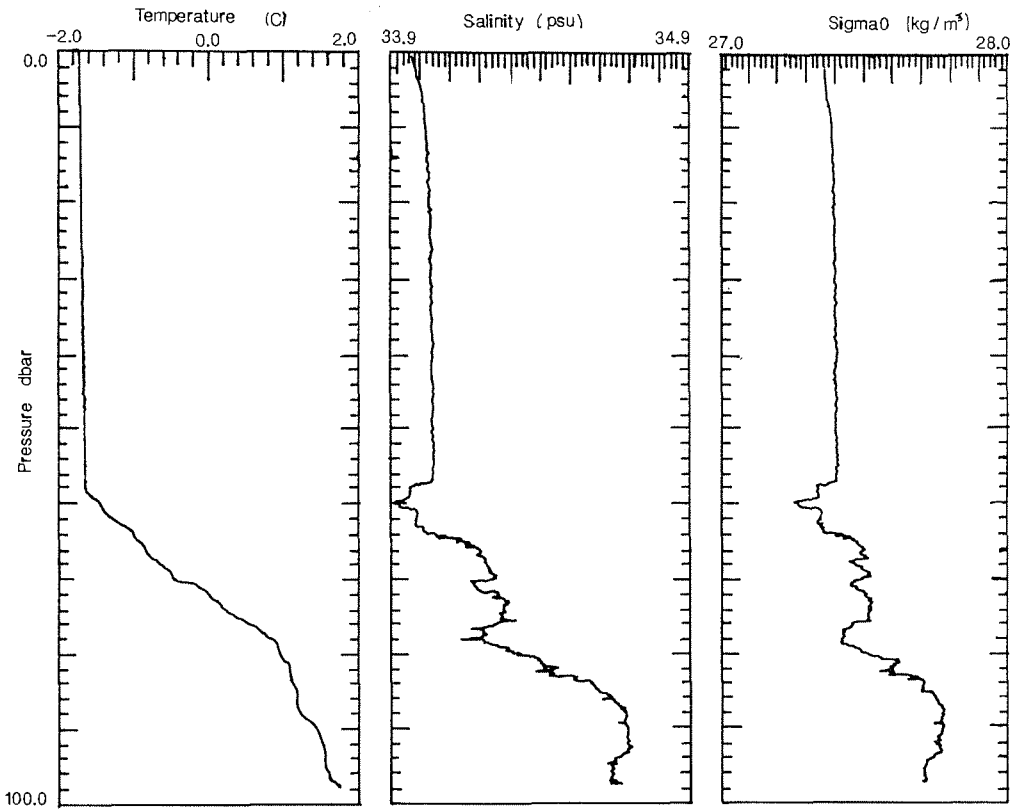

Figure 9.5: Temperature-salinity structure of the uppermost 100 m of ocean at 81°05'N, 5°30'E, under the drifting ice station

The work on the individual ice stations involved lowering the SPRI CTD and Seacat CTD to between 60 m and 100 m from the edge of ice floes. Unlike the drift phase, the stations were in the marginal ice zone (MIZ) and under conditions of ice growth and melt. Typical CTD profiles from the MIZ are shown in Figure 9.6. Figure 9.6a shows a profile taken on March 29 at 78°58'N 4°52'W at the edge of a very wide lead during a remote helicopter deployment whilst *POLARSTERN* recovered a mooring. There is a strong halocline at 14 m depth with a layer of warmer water beneath. Beneath this are interleaved layers of warm and cold water with a uniform density and salinity gradient down to 55 m. Figure 9.6b shows a profile taken on April 6 at 74°55'N 13°11'W from the edge of a multiyear floe in the marginal ice zone. The structure is very different with a cold fresh mixed layer down to 30 m and then evidence of double diffusive convection down to 60 m.

The Odden provided the chance to make measurements on two occasions under ice which had been formed in the open ocean. Because our interest was the very near surface water structure CTD deployments were made from a Zodiac inflatable boat away from the influence of *POLARSTERN* . The CTD was lowered from the Zodiac repeatedly to 60 m through a layer of frazil ice. Two profiles taken from beneath the Odden are shown in Figure 9.7. Figure 9.7a was taken on April 3 and shows a layer of fresher water colder water down to 20 m and then a small jump where both the salinity and temperature increase. The initial analysis suggests that this lighter, fresher water is the result of melting of the pancake ice in the region. Figure 9.7b shows a profile taken on April 10 in the northern Odden. In this profile we see a supercooled surface layer down to 5 m and then a uniform temperature and salinity profile down to 60 m. Any ice formation under conditions such as those shown in Figure 9.7b and the resulting salt rejection will have a significant convective effect.

Snow and ice structure. During ARK IX/1a most of the data were collected from various locations on the single vast multi-year floe which was used as the base for the drifting ice station. Overnight on March 18-19 this floe broke up and it was necessary to abandon the site. On March 20 and 21 data were collected from a smaller multi-year floe in the same general area, and on March 22 a final experiment was done on a heavily hummocked floe which was deeply riven by cracks and which appeared to be composed mainly of a segment of partially consolidated pressure ridge overlain by deep snow.

The ERS-1 overflights on March 9, 12, 15, 18 and 21 covered the site of the drifting ice station, and will be used for a joint analysis of SAR brightness against snow and ice properties; in some cases *POLARSTERN* was located in the intersection of both the ascending and descending swaths.

On the drifting ice station the snow cover depth over the test area was very variable; it lay in the range 0 - 1 m on the relatively flat surfaces and up to 3 m where the snow had drifted between the blocks and near the ridges. The readings from the first day of measurements on a rectangular gridded site, showed considerable variability in snow wetness and density at 5 cm below the surface. The permittivity was less variable with the real part e' being dominant with e" either zero or very small. Because of this and for logistic reasons, it was decided to concentrate on collecting depth profiles in drifted snow for the remainder of the experiments. At each site 3-5 snow profiles were measured plus a temperature profile using a 20 cm probe. The orientation and GPS position of the snow pit were also recorded. Snow samples were collected at 8 locations for salinity and density measurement; salinities were all found to be less than 0.2 ppt.

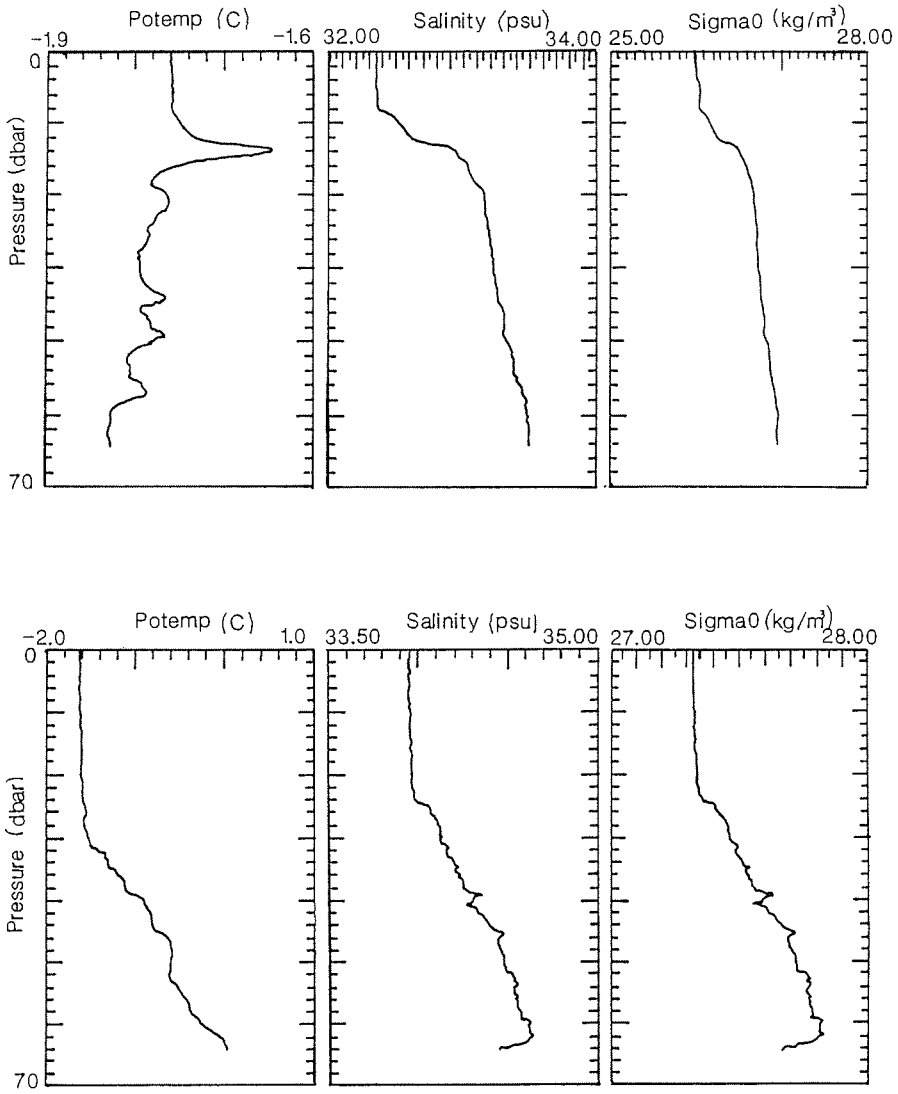

Figure 9.6: Temperature-salinity structure under the marginal ice zone. (a) 78°58'N, 4°52'W, showing strong halocline at 14 m and interleaved layers below. (b) 74°55'N, 13°11'W, with cold fresh layer down to 30 m and possible double diffusion below.

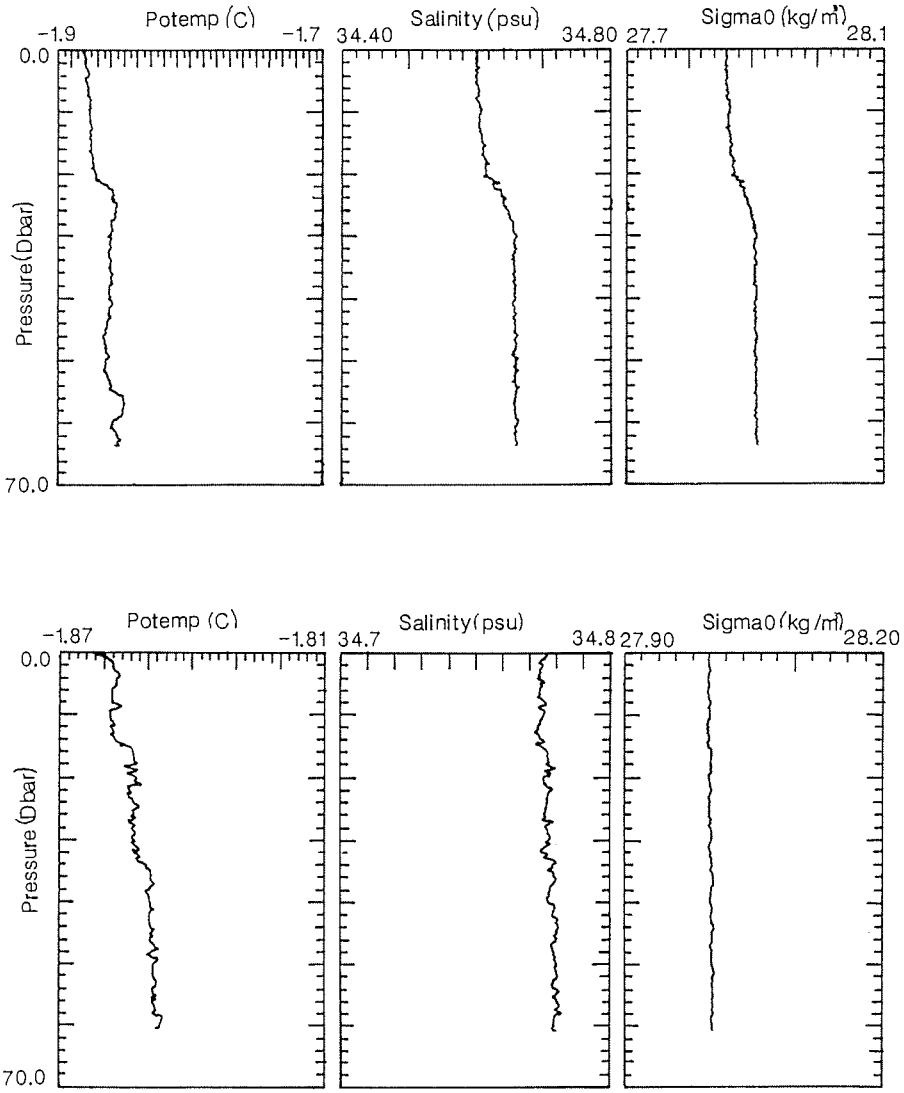

Figure 9.7: Temperature-salinity structure under the Odden ice islands. (a) Southern island, April 3, showing fresh cold water down to 20 m, possibly due to recent ice melt. (b) Northern island, April 10, showing supercooled surface layer to 5 m then uniform profile to 60 m.

The first large-scale snow sampling site, in which snow was sampled from 10 locations, was close to the wave measurement site in order that ice thickness drilling and core sample collecting could be facilitated. Four further sites were located close to undisturbed areas of the floe where the University of Bern group was making emissivity measurements, in order that comparisons of data could be made. As near as possible we tried to arrange these to coincide with the dates of the appropriate ERS-1 overflights. Further sites were sampled in a deep snow drift by a pressure ridge, and at a location where the University of Hamburg was monitoring snow temperature profiles.

In many places the lower surface of the snow had developed into depth hoar, featuring very large granular lenses of ice interleaved with air pockets. This material was strongly bonded to the top of the ice surface, which made it difficult to identify the undisturbed ice surface for levelling measurements. These were therefore confined to two sites where wind-blown snow had revealed a bare ice surface, although it is recognised that these are unrepresentative of the ice surface as a whole. Levelling measurements were done with a mechanical profilometer. These interfacial measurements were repeated at the March 20 floe, where a small-scale vertical roughness of 1-1.5 cm was found.

Temperature measurements were collected over a seven day period, from air, snow and ice through a 2.0 m depth with three thermistor chains which recorded temperatures at 10 cm intervals. On some of the days data were collected both morning and evening to check for diurnal variations.

On two days measurements were made at remote sites using helicopter flights. On one occasion, on March 17, a flight was made shortly after the ship received, by air drop from a Dornier, a SAR image of the region received at Kiruna on March 12. The ship herself was visible in the image, as were some clearly identifiable ridges and leads which were visited by helicopter. It was found that the very brightest parts of the image corresponded to ridges which included in their structure large up-ended single blocks of broken multi-year ice of thickness greater than 2 m and height 3-4 m. The normal components of a ridge (smaller blocks from refrozen leads) gave lesser brightness levels.

Because of the limited duration of the stations on ARK IX/1b, a slightly different sampling strategy was used. Snow measurements, including snowfork and temperature profiling, and collection of snow samples were done on six of the seven floe stations. Although distribution of data sites varied from floe to floe, the purpose was to establish a 10x10 metre sampling grid covering a significant portion of the floe. Snow temperature profiles included ice temperature (at 5 cm into ice),snow pack temperature, and air temperature. Snow pack temperatures were collected by inserting a temperature probe 5-10 cm into the snow along an undisturbed edge of a snow pit. Temperature were taken at 5 cm intervals, starting at the snow/ice interface and progressing upwards. Snow depths were measured at each pit. Samples of depth hoar and surface snow were collected at a number of stations and analyzed for both salinity and density. Density results were then used for calibration of measurements obtained by the snowfork. Figure 9.8 gives an example of measurements taken at the floe station on April 6 at 75°01'N, 13°38'W. The large variability in properties among snow pits on the same floe is evident.

In general, the floe stations on ARK IX 1/b showed a larger range in e'' (0-0.085) corresponding to snow wetness volumes of 0-7.8%. The extremely low temperatures on ARK IX/1a were the likely cause of the very low e'' values observed on that leg.

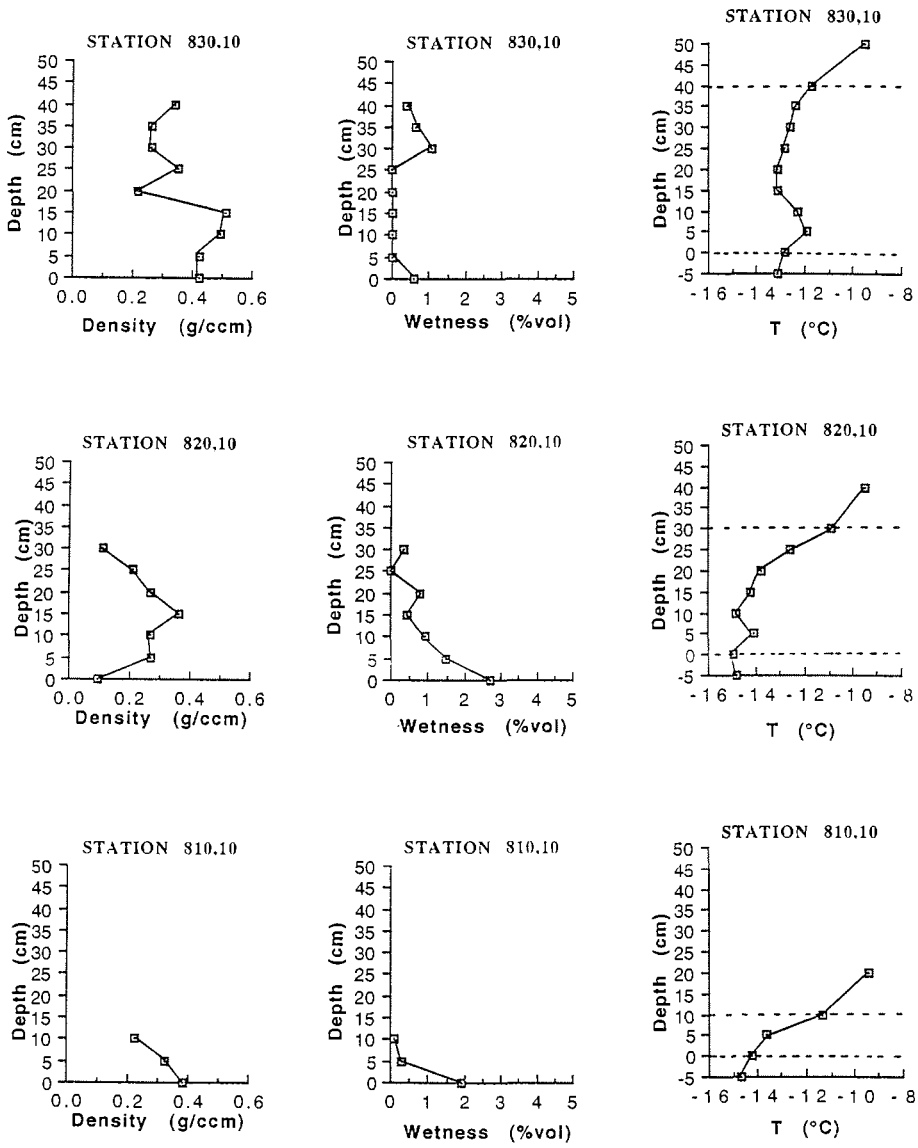

Figure 9.8: Snow density, wetness and temperature (the snow layer being between the two dashed lines) at three sites 10 m apart on the same floe, 75°01'N, 13°38'W. The spatial variability of snow properties is evident.

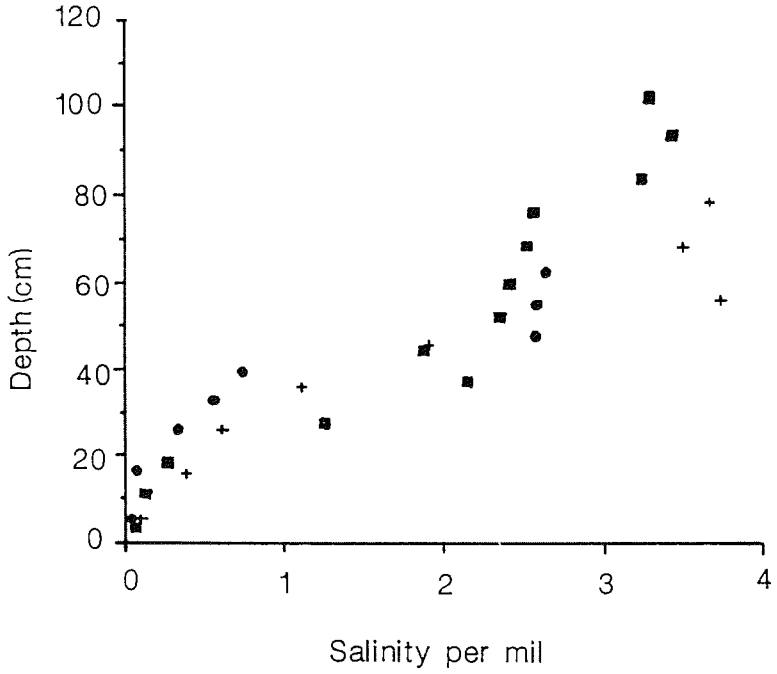

Figure 9.9: Salinities from three ice cores obtained from drifting ice station.

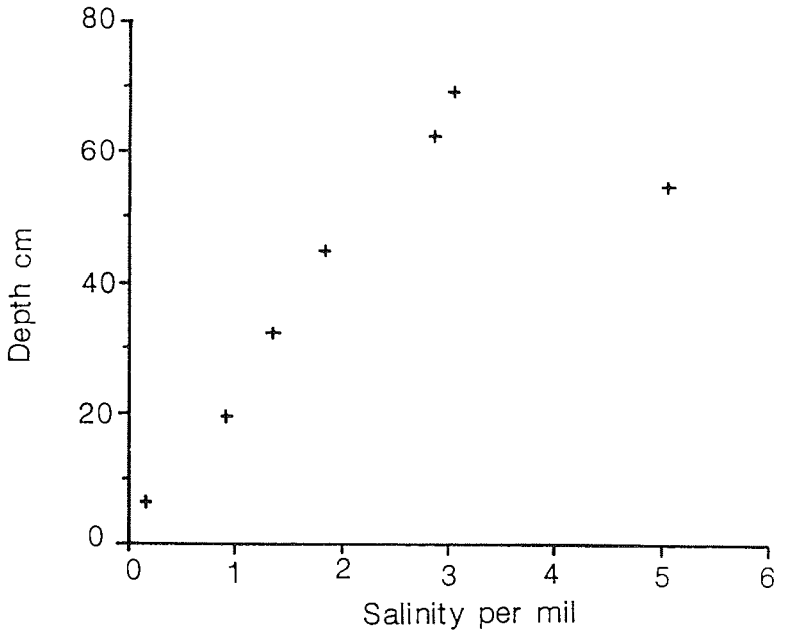

Figure 9.10: Salinity profile from uppermost part of a multiyear floe at 78°59'N, 2°50'W.

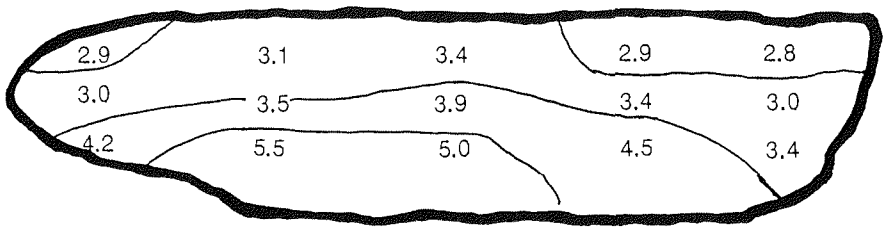

Figure 9.11: Salinity cross-section through centre of a large pancake recovered from Odden ice island, showing evidence of brine drainage.

Seven ice cores were taken on ARK IX1/a, three from the drifting ice station and four from other floes (see Table 1). In all cases only the uppermost 1 m was sampled. A further eight cores were taken from ice stations during ARK IX/1b. Cores were taken with a CRREL-type 3.5 inch corer. The samples were then stored and analysed in the -27 °C cold room. Each core was split into roughly 10 cm sections for analysis - the cores had a tendency to stick in the corer barrel and had to be broken into sections to be removed and where possible these breaks were used. The lengths were initially halved lengthwise and photographed on a light box. One half was then melted down to calculate the salinity, the other half being cut vertically and horizontally to provide "thick" (approximately 5 mm) sections. Figure 9.9 shows a composite salinity profile from the three cores taken during the drifting ice station on ARK IX/1a, while Figure 9.10 shows a profile from an ARK IX/1b ice station at 78°59'N 2°50'W. The thick section was photographed under crossed polaroid filters, cut down as far as possible on a microtome and subsequently photographed again under the polarizing filters in order to display the crystal structure. Sections taken from pancakes collected in the Odden in the latter part of the cruise were treated in the manner described above. The salinity values for such a pancake are shown in Figure 9.11.

Samples analysed showed structures typical of the ice types from which they came, whether first or multi-year ice. Thin sections taken from cores at the station at 75°01'N 13°38'W displayed crystals up to 15 mm in width in both horizontal and vertical planes. Sections from the pancakes collected in the Odden displayed no obvious vertical or horizontal variation in crystal size or type, all sections displaying small (1-2 mm) randomly oriented crystals.

Aerial photography. Seven aerial photographic missions were carried out in support of the ice physics measurements, using a Vinten 70 mm aerial survey camera mounted under the helicopter. This gives 500 frames at uniform time intervals. Depending on visibility and ice conditions, flights were made at heights of 100 m to 1500 m, with intervals designed to give overlapping imagery. The normal flight pattern was to carry out one or more transects between the experimental site and the ice edge, in order to determine the amount of ice and distribution of floe sizes, which determine the attenuation of ocean waves. In the Odden ice tongue, contextual photography from 100 m was carried out to determine the distribution of pancake sizes. Figure 9.12 shows a frame from this survey. On some occasions photography was carried out in parallel with infra-red line scan missions, in order to yield ice type distributions under the swath of satellite passes.

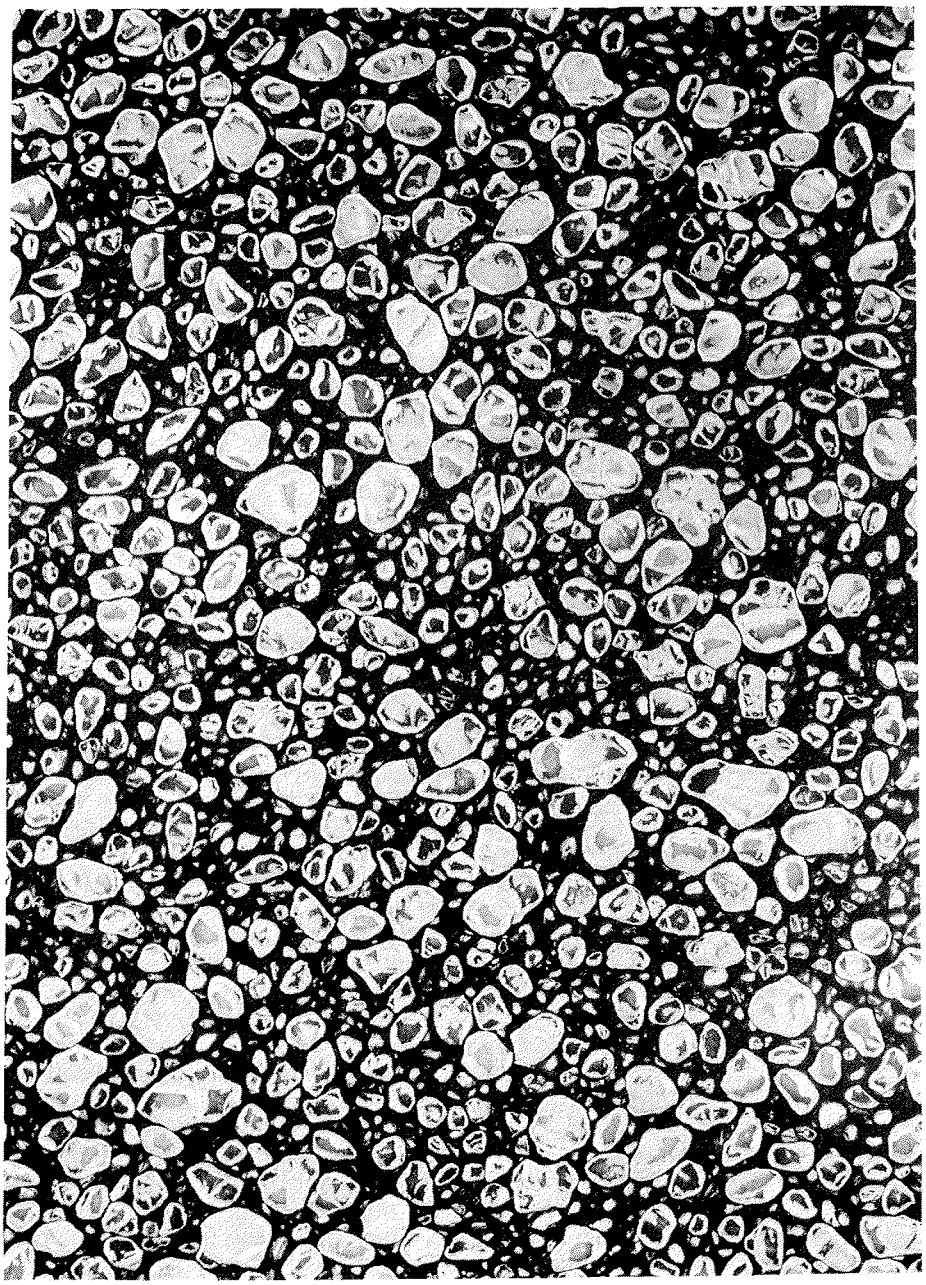

Figure 9.12: Aerial photograph of pancake ice in southern Odden ice island. Long axis of image is 120 m.

The Odden ice tongue. During the two Odden ice stations of April 3 and 10, data were collected by deploying the Zodiac and by using the AWI ice-lifter. The ice-lifter was used three times on 3 April, with four types of data obtained. Four complete pancakes, with dimensions ranging from 30 x 33 x 9 cm to 68 x 101 x 13 cm were collected. Vertical slices of width 10 cm were taken through these pancakes. These slices were then cut up into segments 10-15 cm long and 5 cm deep to measure the spatial variation of salinity within the pancake. Figure 9.11 shows a profile through one of these pancakes. The second deployment "caught" a large compound pancake which consisted of two pancakes (one approximately 70 x 150 cm) rafted onto a third basal pancake (80x100 cm). Four salinity slices were taken through this compound pancake. Additionally, this compound pancake had 8-10 cm of snow cover, and both temperature and snowfork measurements were taken. Cores measuring 10 x 10 cm were taken near the centre of each pancake for fabric analysis. Additionally, frazil samples were collected for thin section analysis of their crystal structure, and a selection of brash fragments was taken to do a size versus salinity analysis.

The ice-lifter was used an additional three times on 10 April. Two pancakes, with dimensions 68 x 47 x 10 cm and 58 x 61 x 10 cm were retrieved. Samples from the centres and edges of these were taken for further salinity measurements. The pancakes were considerably more brine-filled than on 3 April and a third pancake fell apart while being removed from the ice-lifter. An additional eleven small pancakes were taken for salinity versus size analysis.

In addition to the CTD and frazilometer work that was done from the zodiac, frazil samples and samples of meltwater from the tops of pancakes were taken. For the frazil samples, a 50 cm long piece of tubing covered with a 300 μm mesh screen was lowered into the water so that the top was approximately 50 cm below the surface, and then raised to the surface to collect a frazil sample. Frazil concentration and salinities were calculated from these samples. Frazil concentrations were calculated for the surface diameter of the sampler, and ranged between 4.2 and 20.3 g cm^{-2}. Salinities of the frazil samples ranged between 6.7 and 14.4 ppt. Underwater video footage was taken on two of the Zodiac runs during the April 3 Odden station. This footage shows several interesting features included the rafting of several pancakes and distinct algal growths on the undersides of pancakes.

During both stations, several types of other photographic data were collected. Video footage was taken from the bridge during daylight hours. These were run from the first encounter with the ice until the ship stopped in the centre of the frazil/pancake patch. During the 3 April station, 500 aerial photo frames were taken from the helicopter in the region of the station. Video footage and still photos were also taken. Weather conditions during the 10 April station prevented the use of the helicopter. Pancakes in the vicinity of the ship were photographed from the working deck with a scale lowered over the side. This work will be used to determine the distribution of pancake sizes during the two stations.

Sea Ice Acoustics. The objective of these experiments was to investigate the acoustic transmission properties of sea ice in the frequency range of 1.0 - 100.0 kHz. The apparatus used consisted of a control and amplification unit, piezo-electric transducers and hydrophones for transmission and reception of the signal. The transducers used had different natural frequencies and the hydrophones had a level frequency response over the frequency range mentioned above. Only one experiment was carried out due to difficulties with the instrumentation. This experiment is described in the following text.

Transducers and hydrophones were frozen into the ice floe at 0.5 m depth with distances of 1.0, 2.0, 3.0 and 4.0 m between transmitter and receivers. The multi year ice floe showed recrystallized and virtually salt free, bubbly ice along the horizontal transmission path. Figure 9.13 shows a typical signal of 1.8 milliseconds length and a frequency of 11.7 kHz.

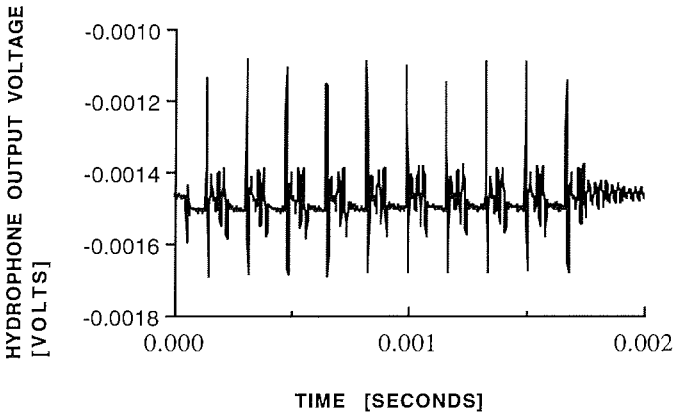

Figure 9.13: Typical hydrophone output signal from acoustic transmission experiment.

The attenuation of the signal is expected to increase (the received signal energy to decrease) with longer transmission paths as well as higher signal frequency. Figure 9.14 shows the hydrophone output voltage in volts versus the time in seconds for three different hydrophones and travel path lengths. The received signals are digitized at a sampling frequency of 500.0 kHz. The plots show the first 1500 samples which corresponds to 3.0 ms. The y-axis is uniformly scaled for all three plots, to enable comparison of the output for the different hydrophones at 2.0, 3.0 and 4.0 m distance from the source. One has to keep in mind that the plots are not corrected for the beam width - the spreading of the energy over a larger sphere with increasing distance to the source.
An attenuation of the signal is noticeable as a trend in the decreasing signal energy with longer travel paths. Correction for the transducer beam width will certainly emphasise this trend.
Experiments using different signal frequencies over the same travel path have not yet been corrected for the frequency response of the transducer. Plots of the raw data do, however, suggest a decrease with higher frequencies, as would be expected.
The anticipated study of the acoustic transmission properties for different textures of sea ice has not been carried out in the form planned. The results collected on this cruise show that the method works and will provide valuable data. Alterations to the instrument will be carried out to make it more stable and reliable for future use.

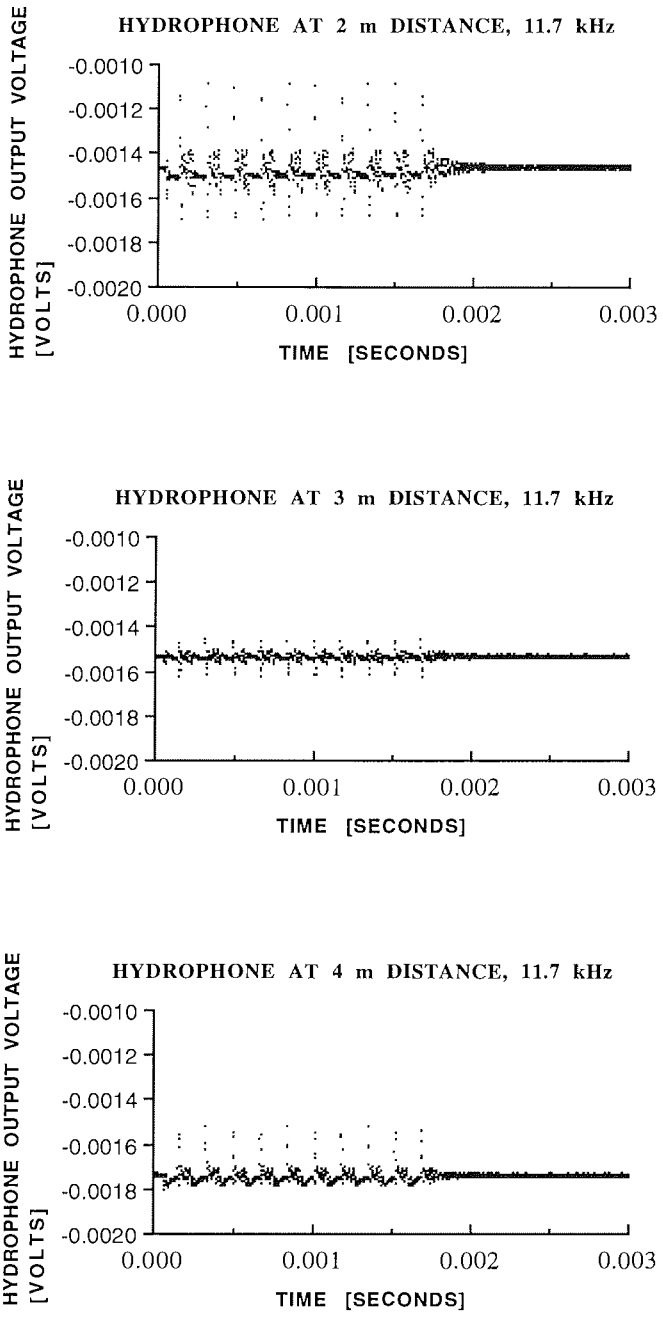

Figure 9.14: Received signal strength at three different distances.

Table 9.1: Summary of ice physics experiments and sites

Date	Time GMT	Position	Ice Type	Number of experiments Wave	CTD	Frazil	Core	Holes	Snow sites	Aerial photo
Phase 1: ARK IX/1a drifting ice station, March 7-20										
Mar 7-20		81°29'N 7°42'E	MY	2*	45	8	3	19	21	1
	drifting to	80°27'N 3°10'E								
Phase 2: ARK IX/1a ice stations, March 20-22										
Mar 20	0930-1630	80°26'N 2°58'E	MY	2	0	0	2	1	1	0
Mar 21	1030-1700	80°24'N 1°28'E	MY	2	25	1	1	0	1	1
Mar 22	1000-1300	80°12'N 0°19'E	MY	1	0	0	1	0	1	1
Phase 3: ARK IX/1b Fram Strait ice stations, March 28-31										
Mar 28	0945-1045	79°00'N 2°04'W	MY	1	0	0	0	0	0	0
Mar 28	1300-1600	78°59'N 2°50'W	MY	1	0	0	2	2	5	1
Mar 29	1030-1230	78°58'N 4°52'W	FY	1	6	0	0	0	2	0
Mar 30	0830-1030	78°51'N 5°50'W	FY	1	0	0	0	13	8	0
Mar 30	1900-2100	79°03'N 3°50'W	FY	1	0	0	1	31	0	0
Mar 31	0600-1015	78°59'N 3°24'W	MY	1	12	0	1	1	6	1
Phase 4: ARK IX/1b Odden ice stations, April 3, 10										
April 3	0630-1645	73°02'N 1°30'W	Pan-cake	1	31	1	0	0	0	1
April 10	0830-1230	75°01'N 0°04'E	Pan-cake	1	12	0	0	0	0	0
Phase 5: ARK IX/1b ice stations at 75°N, April 6										
April 6	0830-1030	74°55'N 13°11'W	MY	1	4	0	2	1	6	1
April 6	1200-1430	75°01'N 13°38'W	MY	1	14	0	2	1	6	0

*Multiple wave experiments at two sites concurrently, including almost continuous monitoring at one site by telemetry.

9.2. Structure and physical properties of sea ice and application of geophysical methods for ice thickness measurements (H. Eicken, S. Gerland, C. Haas, S. Hannke, F. Valero Delgado)

9.2.1. Introduction

The sea-ice thickness distribution depends critically on the effects of climate change in the polar regions. Furthermore, in conjunction with the structure and physical properties of the ice cover, it affects the local exchange of heat and momentum between ocean and atmosphere. At present, reliable measurements of ice thickness depend on the use of submarine sonar, laser altimeter or drill-hole techniques. Geophysical methods have been employed sporadically to obtain information on ice thickness (e.g., Hunkins, 1960, Thyssen et al., 1974, Kovacs and Morey, 1991). The ARK IX/1a cruise afforded the possibility of validating a number of techniques in drifting Arctic first- and multi-year ice, for which little data exist up to date. During the drift phase, seismic and electromagnetic measurements were carried out jointly with ice-thickness drilling and coring along a 200-m profile through level and deformed multi-year ice at up to 4 m spacing (Figure 9.15). In addition, several sites in new, first-year and multi-year ice were probed. The ice-core measurements are also of use because they provide essential information on the growth and decay of sea ice in Fram Strait and the Greenland Sea, the major study areas of the ARK IX/1 expedition. These ground-based data help in interpretating remote-sensing data gathered by ERS-1 SAR, SSM/I and AVHRR.

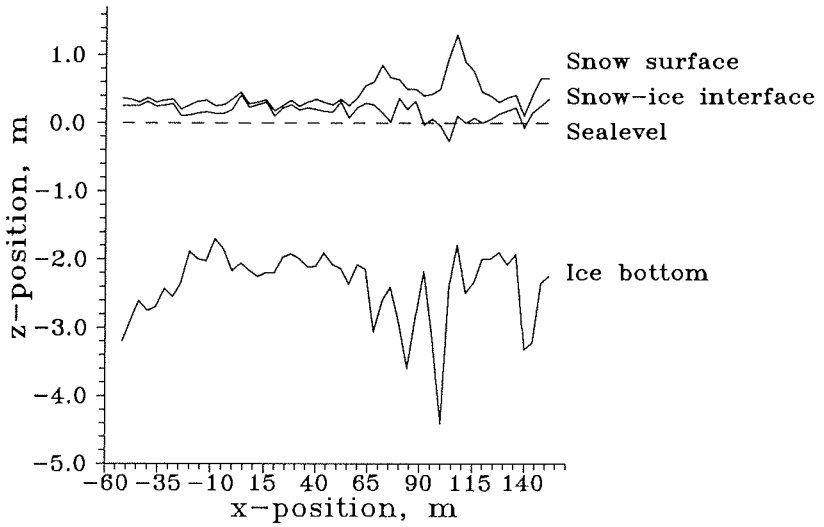

Figure 9.15: Ice thickness, ice draft and snow depth along the main profile through multi-year ice, located roughly 500 m away from the ship.

9.2.2. Ice thickness and ice core measurements

The main profile was selected such that it encompassed stretches of both level and deformed ice (left and right half of Figure 9.15, respectively). Measurements of ice thickness, snow depth and draft were taken at 4 m

spacing (compatible with the footprint of the electromagnetic instrument). Mean snow depth along the profile amounted to 0.25 ± 0.27 m, mean ice thickness was 2.56 ± 0.53 m with a mean draft of 2.39 ± 0.53 m.
Ice cores of 100 mm diameter were obtained at positions -40 m (07611), 0 m (07301), 5 m (07402), 20 m (06901), 50 m (06902) and 110 m (07621) along the profile. In addition, cores were drilled at 9 other measurement sites. After taking temperature readings from within the core (contained in an insulated tube), samples were transferred to the cold laboratory aboard the ship. Thick sections were cut over the entire length of cores for the determination of textural ice stratigraphy in ordinary and polarized light. Cores were then cut according to texture in 5 to 15 cm segments. After weighing for a determination of density, samples were melted for electrolytical conductivity (salinity) measurements. Part of the samples and additional cores were taken to Bremerhaven for further laboratory studies.

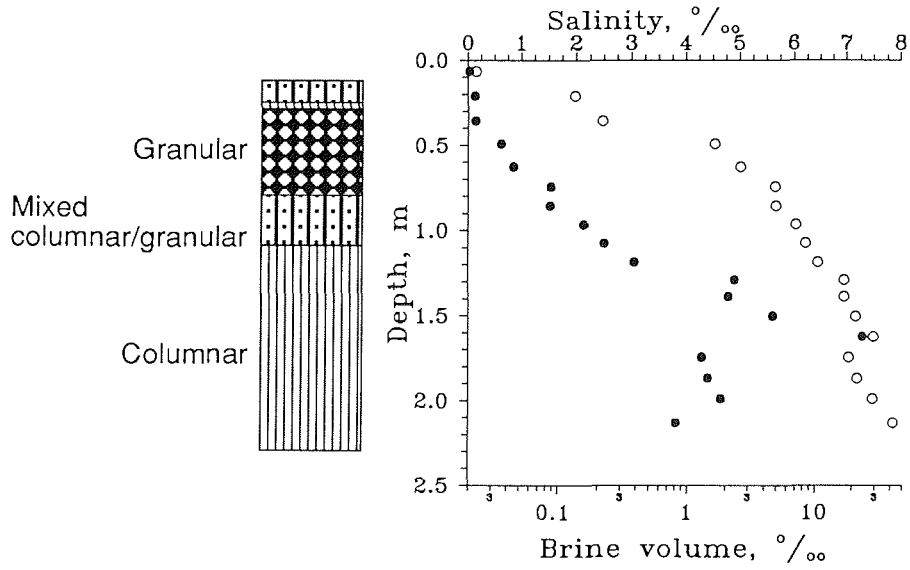

Figure 9.16: Stratigraphy (left) and salinity (closed circles) and brine volume (open circles) profile for an ice core obtained at position 50 m along the profile shown in the previous Figure. Stratigraphic signatures explained at left.

A typical multi-year ice core taken at position 50 m along the profile is shown in Figure 9.16. The core stratigraphy shown at left indicates that the upper half of the ice column originates from dynamic ice growth processes, whereas the lower 1.23 m of ice are columnar ice, formed through undisturbed congelation of seawater at the ice bottom. At the right, salinity and brine volumes computed from salinity, density and temperature measurements are shown. Due to the low temperatures (-36 °C at the surface, -16 °C at 1.4 m depth) and low salinities, brine volumes are extremely low. Consequently, the electrical

conductivity of the ice is rather low. As shown below this has favourable consequences for the electromagnetic method, while geoelectric measurements were hampered by high contact resistivities. As a result of low brine volumes and low permeabilities, brine seepage into sack holes was observed only in few cases when coming to within 0.5 m or less to the ice bottom. Thus, the sea-ice thermal conductivity, for instance, was essentially the same as that of freshwater ice down to depths of 1.5 to 2 m.

9.2.3. Electromagnetic measurements

Introduction. For some decades electromagnetic methods have been widely used as a tool for detecting shallow conductivity distribution and anomalies. Especially for ground water research, waste deposit detection and archaeological prospection the worth of electromagnetic methods has been documented in many cases. For measurement of first-year sea-ice thickness these methods have been applied as well (Kovacs and Morey, 1991). The aim of performing electromagnetic measurements during leg ARK-IX/1a was to determine the possibilities, resolution and limits of this method especially under Arctic winter conditions and different types of sea-ice. An important point and a big advantage was the fact that these measurements were done within a program of several ice-properties investigations as seismics, thickness drillings and coring. This provided an integrated data set which enabled calibration calculations and direct comparison of the methods used.

The Method. For the electromagnetic measurements a commercially available portable instrument (Geonics EM-31) was used. It consists of two coplanar oriented coils, one for transmitting and one for receiving the signals. The intercoil spacing is 3.66 m, the operating frequency 9.8 kHz. The basic principle can be described as follows: The transmitter coil located at one end of the instrument induces circular eddy current loops in the underground (earth, soil, ice or sea-water). The magnitude of any one of these current loops is directly proportional to the terrain conductivity in the vicinity of that loop. Each one of the current loops generates a magnetic field which is proportional to the value of the current flowing within that loop. A part of the magnetic field from each loop is intercepted by the receiver coil and results in an output voltage which is therefore also linearly related to the terrain conductivity. The conductivity reading is shown on a liquid crystal display (LCD), which was not without problems under low-temperature conditions. Measurements are possible with different coil orientations in relation to the surface (vertical or horizontal loop axis) and on freely selectable heights above the ground.

Measurements and examples. The EM-31 was used for several kinds of measurements on the sea-ice: Time series at fixed locations for the consideration of instrument drift effects due to temperature, measurements along profiles at two heights above the surface and two coil orientations and measurements at different heights from zero to 4 m above the ground, using a ladder.

The time series are important to obtain quantitative information on the the instrument's behaviour at extremely low temperatures. After carrying the instrument from the ship (T = +20 °C) outside (during the first week on the ice, temperatures between -35 and -41 °C) the EM-31 needed about 90 minutes to come to equilibrium as shown in Figure 9.17. Another experiment demonstrated that instrument drift is largely due to cooling of the coils. Thus, the coils were taken outside before the measurements to attain thermal equilibrium. The temperature drift due to the console which was taken out immediately before measuring is inverse to and not as significant as that due to the coils (Figure 9.17). To exclude any further drift effects, we made repeat

measurements at base locations, as usually done in gravity and magnetic field work.

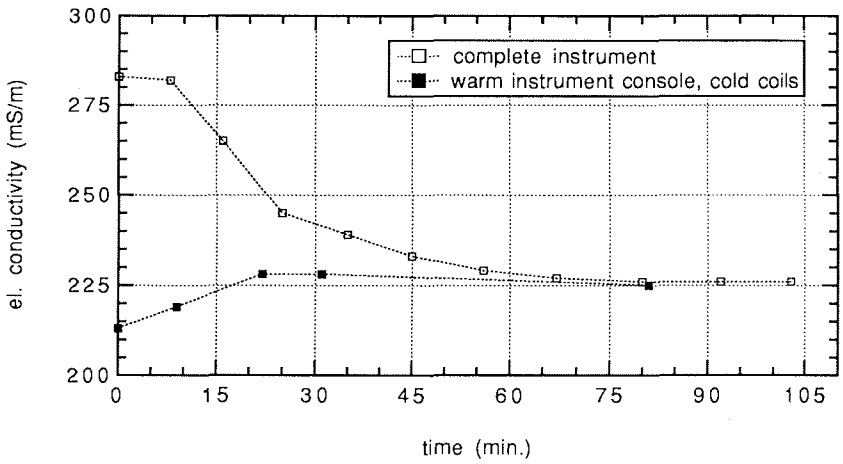

Figure 9.17: Temperature drift effects of the EM-31 instrument. Shown is the transfer from +20 °C (time = 0) to -38 °C (time >0). Two cases are shown: the drift due to the entire instrument adjusting to ambient temperatures and the drift due to cooling only the instrument console.

Altogether measurements were performed at four meter spacing along six profiles of total length 382 m. Additional surveys were performed on a small grid (8 m x 8 m) at 2 m spacing, along four profiles with conductivity determination at different heights of up to 4 m above the surface and on several sites, where also loudspeaker-seismic surveys were performed. As an example, a section of the 200-m-profile discussed above is shown in Figure 9.18 together with drilling results. The measurements shown are raw data and were obtained on the snow surface (about 0.10 m height) with vertical coil axis orientation. The data show a very good reproduction of total thickness. However, the limits of spatial resolution are obvious regarding the ridge between 70 and 115 m. In the near future further data processing and modelling is planned to assess the power and limitations of the method.

9.2.4. Seismic measurements

Introduction. Two approaches were taken to perform seismic measurements: hammer blows with a 6 kg sledge hammer generated waves relatively long in wavelength which provide integral values of ice thickness and ice properties over longer distances. In a second attempt, high frequency signals (frequency range 1 to 5 kHz) were generated by a loudspeaker source. The idea was to apply standard reflection seismic methods to get a continuous image of the ice underside. For registration, standard 30 Hz vertical and 4 Hz horizontal geophones, with spikes fixed in the ice, and a 24-channel Geometrics ES2401 seismograph (maximum sampling frequency 0.05 ms) were used.
Hammer-source seismics. Geophones were spaced roughly 10 m and in line shotpoints roughly 40 m apart along the profile. The maximum source-to-geophone offset was about 230 m. Additionally, for polarization analysis and wave identification, several 2- or 3-component registrations were made.

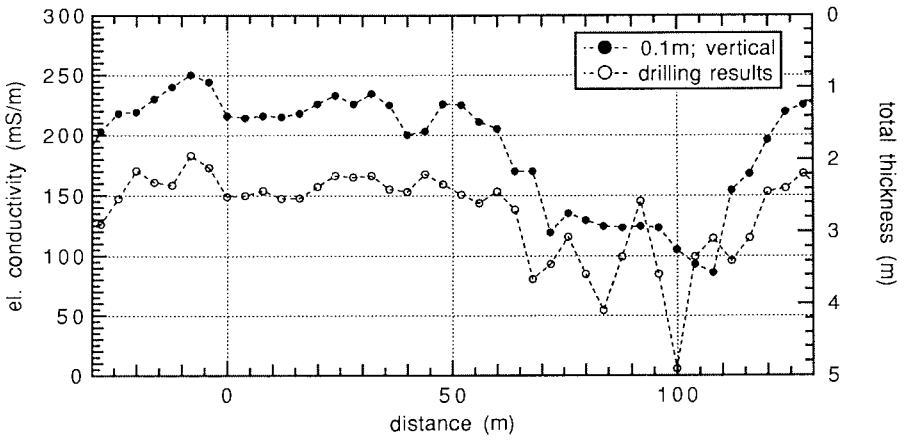

Figure 9.18: Section of the 200-m-profile. The data from the conductivity measurements (left axis) are plotted together with the results from thickness drilling (right axis) versus horizontal distance. The conductivity measurements were performed at a height of 0.1 m above the surface with vertical coil orientation.

Compressional and flexural waves were generated by hammer blows onto a metal plate lying on the bare ice, while horizontally polarized shear waves were produced by striking a bar fixed horizontally to the ice surface.

Compressional and flexural waves. Direct compressional waves (longitudinal plate waves) were observed with a relatively high velocity of 3000 to 3300 m/s. This was due to the low ice temperatures and the corresponding virtual absence of brine and pores in combination with the age of the ice (see above). The most prominent feature in all seismograms is a dispersive flexural wave travelling with a mean velocity of 1500-1600 m/s. Maximum frequencies ranged around 200 Hz and could be observed down to 20 Hz. These waves can be identified by their retrograde elliptical polarization in the z-x-plane. From the dispersional behaviour, phase velocities can be calculated and lead to integral estimates of ice thickness between source and geophone by means of forward modelling. Figure 9.19 shows such an exemplary dispersion curve. Of interest is the fact that the flexural waves are not significantly damped by ridged zones and occur even though the floe geometry is far from the ideal case of a uniform flat ice sheet. The seismic data will be studied further with particular attention on individual channels and on wavefield variability with changing ice thickness.

Horizontally polarized shear waves. Direct horizontally polarized shear waves (first mode Love waves) were observed at velocities of about 1800 m/s. Polarization is linear horizontal, vertical to the direction of propagation. These waves interfere with higher Love wave modes which results in a dispersive wave containing information about ice thickness. However, these waves did not develop as clearly as the flexural waves. Shear and compressional wave velocities enable us to calculate bulk elastic moduli of the ice, which will then be related to the thickness distribution along the profile and compared with values derived from the processed ice cores.

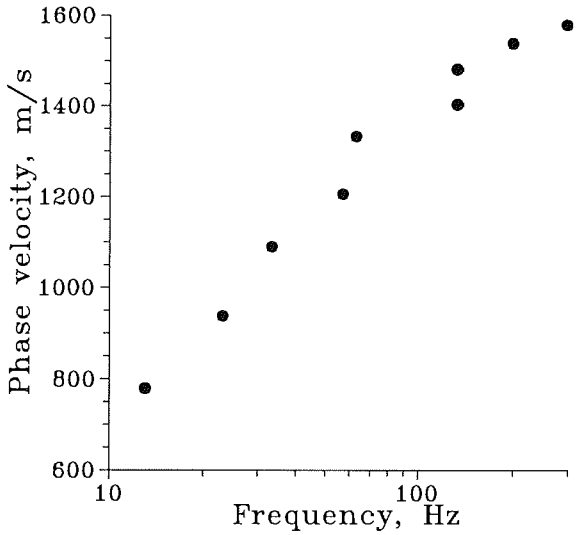

Figure 9.19: Exemplary dispersion curve of a flexural wave excited by hammer blow. Source-geophone offset 100 m. Through comparison with theoretical curves, ice thickness can be estimated.

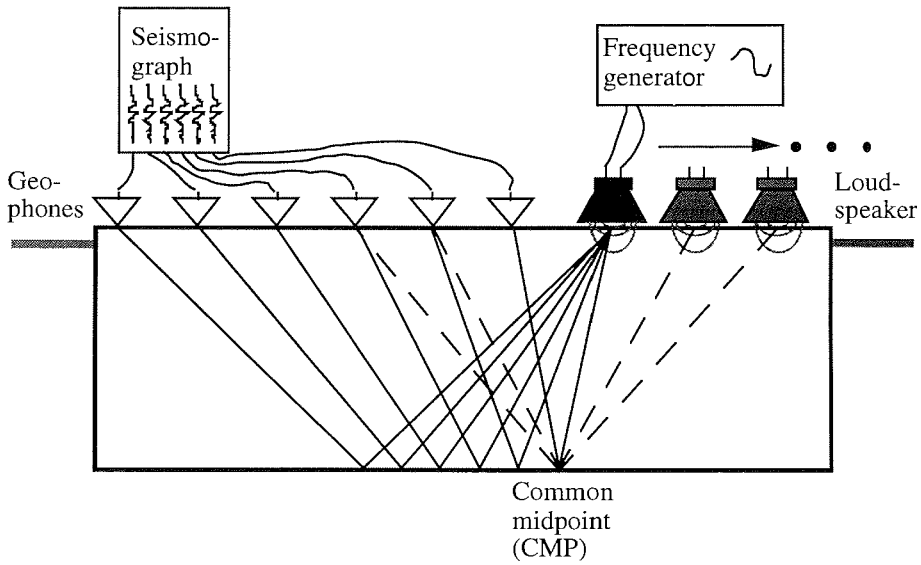

Figure 9.20: Sketch depicting principal set-up for loudspeaker reflection seismics.

Loudspeaker seismics. Loudspeaker seismics being a technique still under development (cf. Weniger, in press), experiments were carried out to obtain a sound base for further developments. A number of high-resolution reflection seismic measurements were performed with an acoustic signal of 1 to 5 kHz generated by a hifi piezo loudspeaker source and stacked up to 250 times. Within the snowcover the signal was transformed into an elastic wave, then travelling through the ice. Geophone spacing was 0.15 to 0.2 m, enabling correlation between distinct phases. The source was moved away from the geophone spread such that 3-fold CMP (common midpoint) data were obtained (Figure 9.20). Due to the stacking, the wave energy was big enough to be traced for more than 15 m, although the low-frequency noise level was often rather high. However, the generated signal was too long to resolve incoming reflections expected to arrive within a few milliseconds. By means of a reference geophone which was placed directly under the loudspeaker it is possible to improve the quality of the data through crosscorrelation and deconvolutional processing techniques.

10. Gravity measurements (S. Gerland, K. Hoops)

Shipboard gravity measurements were carried out during both legs ARK-IX/1a and ARK-IX/1b. In particular during the drift phase over the Yermak plateau northwest of Svalbard, an area for which little to no gravity data exist as of yet, excellent measuring conditions resulted in a data set of high quality. Normally, gravity data obtained in ice-covered regions are affected by strong noise due to ice-breaking activities of the ship; in this case the drift phase provided for calm, equable measuring conditions.
The gravity values were obtained with a KSS 31 Marine Gravity Meter (Bodenseewerke) installed fixed on board, all data were stored in analogue and digital form every 20 seconds. Except for two time intervals of some hours (due to power-supply failure and hard-disk crash), a continuous data series could be obtained.
For the determination of absolute gravity data, measurements were carried out with a land gravity meter (Lacoste-Romberg G-877) alongside the ship at the beginning and the end of the cruise at points for which absolute gravity is known. The results of these measurements are shown in the table below. In the near future the data will be processed to an absolute level based on the results of these measurements.

Date	Location	Instrum.	Reading (scale val.)
26-FEB-93	Lloydwerft, Bremerhaven	G-877	4879.64
26-FEB-93	onboard FS Polarstern	KSS 31	1092.19
17-APR-93	onboard FS Polarstern	KSS 31	1092.13
17-APR-93	Lloydwerft, Bremerhaven	G-877	4879.82
17-APR-93	AWI building D, Bremerhaven (point of known absolute gravity)	G-877	4879.81

11. References

Hunkins, K. (1960): Seismic studies of ice. J. Geophys. Res., 65, 3159-3472

Kovacs, A. and R. M. Morey (1991): Sounding sea ice thickness using a portable electromagnetic induction instrument. Geophysics, 56 (12), 1992-1998

Thyssen, F., H. Kohnen, M. V. Cowan and G. W. Timco (1974): DC resistivity measurements on the sea ice near Pond Inlet, N. W. T. (Baffin Island). Polarforsch., 44, 117-126

Weniger, W. (in press): Luftschall-Reflexionsseismik auf Meereisschollen. *In* H. Miller (ed.): Die Expedition ARKTIS VII/3. Ber. Polarforsch.

12. Appendix

12.1. List of stations

12.1.1. List of stations ARK IX/1a

Station	Date	Time	Lat. (N)	Long. (E)	Depth (m)	Activity
	5.3.93	14:00	80°24.8´	01°06.1´		Argos buoy from helicopter
	7.3.93	10:30	81°29.5´	10°55.3´		Argos buoy from helicopter
	7.3.93	14:00	81°29.7´	03°53.9´		Argos buoy from helicopter
24/001	7.3.93	20:31	81°28.1´	07°37.3´	582	CTD-calorimeter
		-20:48	81°28.0´	07°37.3´	569	
		21:02	81°27.9´	07°37.2´	546	CTD
		-21.33	81°26.1´	07°36.8´	529	
24/002	8.3.93	08:20	81°27.3´	07°22.2´	472	Ice work, assembly 15-m mast
		-17:30	81°27.3´	07°22.2´	480	
24/003	8.3.93	19:35	81°25.5´	06°59.7´	521	CTD-calorimeter
		-20:25	81°25.2´	06°58.5´	642	
		20:31	81°24.9´	06°57.3´	762	CTD
		-20:45	81°24.7´	06°56.5´	818	
24/004	9.3.93	09:08	81°21.7´	06°33.2´	765	Ice work
		-11:00	81°21.1´	06°30.7´	754	
	10.3.93	08:30	81°17.7´	06°28.4´	726	Ice work, assembly met station
		-18:00	81°16.7´	06°32.1´	736	
	11.3.93	08:30	81°14.4´	06°33.4´	751	Ice work
		-18:00	81°12.6´	06°38.5´	747	
	12.3.93	08:30	81°10.1´	06°33.7´	763	Ice work
		-18:00	81°08.5´	06°22.4´	751	
	13.3.93	08:30	81°07.0´	05°33.5´	763	Ice work
		-15:00	81°07.7´	05°08.3´	751	
	14.3.93	08:30	81°08.1´	05°30.4´	641	Ice work
		-18:00	81°04.5´	05°29.5´	651	
	15.3.93	08:30	81°01.4´	05°30.3´	686	Ice work
		-18:00	80°57.3´	05°19.4´	698	
		20:55	80°56.4´	05°14.8´	705	Ice work
		-21.25	80°56.3´	05°14.2´	706	
	16.3.93	09:00	80°52.9´	04°59.2´	694	Ice work
		-18:00	80°48.9´	05°05.3´	700	
	17.3.93	09:00	80°47.6´	05°14.7´	707	Ice work
		-18:00	80°43.6´	05°17.4´	690	
	18.3.93	09:00	80°39.5´	04°57.8´	665	Ice work
		-18:00	80°33.8´	04°42.6´	650	
	19.3.93	06:00	80°32.5´	04°10.0´	887	Ice work, salvaging met station
		-16:30	80°30.3´	03°51.5´	980	
24/005	20.3.93	08:35	80°26.7´	03°06.5´	1405	CTD
		-09:20	80°26.7´	03°05.0´	1421	
		10:15	80°26.8´	03°02.3´	1443	Ice work
		-11:40	80°26.7´	03°05.0´	1421	
		13:50	80°26.8´	02°54.0´	1565	Ice work
		-15:45	80°26.7´	02°46.4´	1659	
		14:00	80°26.8´	02°53.4´	1565	CTD
		-15:25	80°26.7´	02°47.9´	1622	

Station	Date	Time	Lat. (N)	Long. (E)	Depth (m)	Activity
24/006	21.3.93	08:40	80°24.2´	01°37.0´	2784	CTD
		-09:35	80°24.0´	01°34.5´	2800	
		10:55	80°23.7´	01°29.7´	2812	Ice work
		-12:15	80°23.6´	01°26.5´	2823	
		13:55	80°23.2´	01°22.1´	2825	Ice work
		-17:30	80°22.2´	01°14.9´	2784	
24/007	22.3.93	08:40	80°12.9´	00°22.3´	3058	CTD
		-11:05	80°11.3´	00°13.8´	3114	
		10:25	80°11.7´	00°16.1´	3094	Ice work
		-11:16	80°11.1´	00°12.9´	3121	
		11:35	80°10.8´	00°11.5´	3127	CTD-calorimeter
		-12:10	80°11.1´	00°12.9´	3121	
24/008	23.3.93	09:10	78°19.6´	09°28.4´	428	CTD
		-09:55	78°23.2´	09°28.4´	463	

12.1.2. List of stations ARK IX/1b

Stat. No.	Date	Time (UTC) Start	End	Position		Depth (m)	Gear
09	25.03	13.12	19.47	79°00.4'N	08°48.4'E	216	CTD (2x), HN
				78°59.5'N	08°46.5'E	217	BO (3x)
10	25.03	20.47	22.35	78°59.7'N	08°23.9'E	677	MN, CTD
				79°00.8'N	08°23.2'E	730	
11	26.03	00.05	01.30	79°00.3'N	08°04.9'E	1036	CTD
				79°00.9'N	08°06.1'E	1026	
12	26.03	03.00	04.40	79°00.0'N	07°29.3'E	1240	CTD
				79°00.2'N	07°37.3'E	1221	
13	26.03	06.32	10.53	79°00.1'N	06°30.1'E	1450	BO (3x),CTD
				79°01.4'N	06°24.3'E	1394	
14	26.03	13.23	15.39	78°59.6'N	05°28.9'E	2308	MN, CTD
				78°59.1'N	05°25.8'E	2374	
15	26.03	17.48	00.50	79°00.0'N	04 °29.0'E	2540	BO (2x), CTD
				79°00.6'N	04° 23.5'E	2571	MN
16	27.03	03.07	06.17	78°59.7'N	03°18.0'E	2915	CTD, WR depl
				78°59.5'N	03°50.9'E	2802	
17	27.03	09.02	17.26	78°59.8'N	02°09.5'E	2480	BO (3x), CTD
				78°59.8'N	02°10.9'E	2484	MN (2x)
18	27.03	19.19	22.25	78°59.6'N	00°59.5'E	2557	CTD, BO
				78°57.8'N	00°57.9'E	2549	
19	28.03	00.47	02.45	78°59.9'N	00°21.0'W	2463	CTD
				78°59.6'N	00°24.3'W	2441	

Stat. No.	Date	Time (UTC) Start	End	Position		Depth (m)	Gear
20	28.03	05.17-	10.04	79°00.2'N	01°43.0'W	2647	CTD, BO (3x)
				78°59.5'N	02°02.3'W	2628	
21	28.03	13.07-	15.20	78°59.3'N	02°50.6'W	2497	ICEWORK (2x)
				78°57.3'N	02°55.0'W	2501	CTD
22	28.03	17.15		79°00.3'N	03°11.8'W		A1 rec
23	28.03	19.14-	02.24	79°00.0'N	03°25.7'W	2279	CTD, BO, MN
				78°56.7'N	03°26.1'W	2319	
24	29.03	05.38-	07.03	79°01.9'N	04 °20.7'W	1775	CTD
				79°01.3'N	04 °18.5'W	1788	
25	29.03	08.50-	14.12	78°59.8'N	04°50.1'W	1428	A3 rec
				78°59.7'N	04°52.1'W	1422	
26	29.03	14.49-	16.05	79°01.5'N	04°41.8'W	1537	A2 not rec
				79°01.2'N	04°38.9'W		
27	29.03	17.35-	18.43	78°54.2'N	04°55.2'W	1262	V2 rec
				78°53.8'N	04°54.5'W	1248	
28	29.03	20.32-	00.01	78°59.8'N	04°55.2'W	1369	CTD, BO, MN
				78°58.2'N	04°50.9'W	1400	
29	30.03	01.42-	05.43	78°59.6'N	05°32.2'W	926	CTD, BO (2x)
				78°59.4'N	05°32.7'W	910	
30	30.03	08.08-	10.14	78°52.1'N	05°49.4'W	404	CTD, ICEWORK
				78°51.7'N	05°49.3'W	367	
31	30.03	14.30-	20.45	79°05.0'N	03°46.8'W		V1 rec
				79°02.6'N	03°49.9'W		ICEWORK
32	31.03	06.15-	08.35	79°00.1'N	03°16.0'W		ICEWORK
				78°59.3'N	03°23.6'W		
33	31.03	19.55		78°35.4'N	00°27.5'E		WR rec
34	01.04	06.18-	12.14	77°00.4'N	00°27.1'E	3246	RMT, MN (3x)
				76°57.9'N	00°44.9'E	3245	
35	01.04	17.13-	17.57	76°13.5'N	00°44.2'W	2244	G1 depl
				76°12.2'N	00°39.8'W	2225	
36	01.04	20.03-	00.58	76°05.2'N	01°29.1'W	3765	CTD, BO (2x)
				76°09.0'N	01°27.9'W	3763	
37	02.04	04.52-	07.09	75°35.1'N	01°59.2'W	3727	CTD, SD
				75°34.6'N	01°57.7'W	3727	
38	02.04	15.32-	17.20	74°07.9'N	03°00.0'W	3645	CTD, HN, SD
				74°08.8'N	03°00.1'W	3644	

Stat. No.	Date	Time (UTC) Start	End	Position		Depth (m)	Gear
39	02.04	22.24	02.45	73°23.0'N	03°15.0'W	3055	CTD, BO (2x)
				73°22.4'N	03°14.9'W	3050	
40	03.04	06.30	16.30	73°01.8'N	01°35.6W	3147	ICEWORK
				73°04.3'N	01°19.5'W	3211	CTD (2x), SD PLA (2x)
41	03.04	21.41	01.47	72°32.0'N	03°34.9'W	3021	
				72°30.6'N	03°30.7'W	2983	CTD, MN
42	04.04	07.27	08.05	72°53.2'N	03°58.4'W	2420	G2 depl
				72°51.9'N	04°01.4'W	2168	
43	04.04	14.58	18.37	71°54.0'N	05°00.0'W	2372	CTD, SD
				71°44.1'N	05°01.2'W	2453	BO (2x)
44	04.04	23.55	01.47	72°30.0'N	07°15.2'W	2753	CTD
				72°30.4'N	07°16.5'W	2163	
45	05.04	06.46	08.41	73°02.1'N	09°40.4'W	2938	CTD, SD
				73°02.4'N	09°40.7'W	2944	
46	05.04	13.19	20.07	73°51.4'N	10°26.0'W	3065	RMT, CTD
				73°54.4'N	10°31.3'W	3063	SD, BO, MN
47	06.04	05.00	09.51	74°56.4'N	12°39.3'W	1012	AWI 411 rec
				74°55.3'N	13°10.9'W	370	ICEWORK, CTD BO
48	06.04	12.24	13.29	75°00.8'N	13°36.6'W	204	ICEWORK
				75°01.2'N	13°37.9'W	196	CTD, SD
49	06.04	18.57	21.01	75°00.6'N	12°32.9'W	913	CTD, BO
				74°59.6'N	12°37.9'W	844	
50	06.04	23.20	01.45	75°00.0'N	11°32.2'W	2261	CTD
				74°58.3'N	11°30.7'W	2351	
51	07.04	03.38	07.50	75°00.0'N	10°44.1'W	3002	CTD, BO (2x)
				74°59.4'N	10°43.9'W	3029	
52	07.04	09.06	10.11	74°59.8'N	10°00.7'W	3203	G3 depl
				74°57.5'N	10°00.1'W	3266	
53	07.04	12.30	16.54	74°59.9'N	09°09.6'W	3312	CTD, SD, MN
				75°00.0'N	09°08.6'W	3312	PLA (2x)
54	07.04	19.35	00.22	75°00.1'N	07°29.5'W	3422	CTD, BO (2x)
				74°59.6'N	07°25.3'W	3417	
55	08.04	04.17	06.52	75°35.0'N	05°30.6'W	3477	CTD, SD
				75°35.3'N	05°32.3'W	3477	2x FLOAT depl
56	08.04	10.16	16.59	74°58.3'N	04°56.5'W	3599	RMT, CTD, HN
				75°00.2'N	05°07.5'W	3582	2x FLOAT depl BO (2x)

Stat. No.	Date	Time (UTC) Start	End	Position		Depth (m)	Gear
57	08.04	20.03	22.43	74°24.8'N	05°00.8'W	3534	CTD
				74°24.6'N	05°03.6'W	3535	2x FLOAT depl
58	09.04	05.17	06.48	74°56.5'N	03°04.0'W	3675	No.1 rec
				74°56.3'N	03°01.8'W	3675	
59	09.04	07.35	10.50	74°58.6'N	03°05.5'W	3576	No.3 rec
				74°58.7'N	03°00.1'W	3677	
60	09.04	11.24	12.18	74°59.6'N	02°53.4'W	3683	No.2 rec
				74°59.1'N	02°51.2'W	3684	
61	09.04	12.49	22.06	74°59.7'N	02°37.9'W	3688	CTD, SD,PLA
				74°57.2'N	02°36.1'W	3691	(2x), BO (2x) MN (3x)
62	10.04	02.46	05.24	75°35.0'N	00°00.2'E	3755	CTD
				75°35.6'N	00°02.0'W	3754	
63	10.04	08.25	12.50	75°02.5'N	00°00.4'E	3759	WR depl, CTD
				75°04.7'N	00°05.1'E	3760	SD, WR rec ICESAMP.
64	10.04	16.21	18.49	74°24.9'N	00°00.2'E	3752	CTD
				74°25.4'N	00°00.5'E	3760	
65	10.04	22.55	03.01	75°00.0'N	02°00.0'E	2780	CTD, BO (2x)
				75°01.4'N	01°57.2'E	2689	
66	11.04	05.51	08.47	75°00.0'N	03°54.0'E	3387	CTD, MN, SD
				75°00.2'N	03°45.3'E	3380	
67	11.04	12.51	17.41	74°56.6'N	04°58.6'E	3273	RMT, CTD
				75°00.6'N	05°12.2'E	3265	BO
68	11.04	20.05	22.21	75°00.1'N	06°35.6'E	2659	CTD
				75°00.7'N	06°34.9'E	2626	
69	12.04	01.05	04.55	75°00.0'N	08°09.7'E	3528	BO (2x), PLA
				74°58.5'N	08°07.8'E	3519	CTD, SD
70	13.04	01.58	06.41	70°59.9'N	03°59.6'E	3179	CTD (2x), HN
				71°00.2'N	03°53.8'E	3184	BO (3x)

12.2. Participating institutions

	Address	No. of participants	Cruise leg
Canada			
AES	Atmospheric Environmental Service AES/CRESS Microwave Group Petrie 214 - York University 4700 Keele Street North-York, Ontario, Canada M3J 1P3	2	1b
Denmark			
MBLH	Marine Biological Laboratory Helsingør 3000 Helsingør	2	1b
France			
LODYC	Laboratoire d'Oceanographie Dynamique et de Climatologie Université de Paris 6 75252 Paris Cedex 05	2	1b
Germany			
AWI	Alfred-Wegener-Institut für Polar- und Meeresforschung Columbusstraße 27515 Bremerhaven	7 9	1a 1b
GKSS	Forschungszentrum Geesthacht GmbH Max-Planck-Str. 21494 Geesthacht	4	1a
HSW	Helicopter Service Wasserthal GmbH Kätnerweg 43 22393 Hamburg 54	4 4	1a 1b
ICBM	Institut für Chemie und Biologie des Meeres Postfach 26111 Oldenburg	3	1b

IMH	Institut für Meereskunde Universität Hamburg Troplowitzstr. 7 22529 Hamburg	1 6	1a 1b
IMK	Institut für Meereskunde Universität Kiel Düsternbrooker Weg 20 24105 Kiel	3 5	1a 1b
IPÖ	Institut für Polarökologie der Universität Kiel Wischhofstraße 1-3 24148 Kiel	1	1b
IUP	Institut für Umweltphysik Universität Heidelberg Im Neuenheimer Feld 366 69120 Heidelberg	1	1b
MIH	Meteorologisches Institut der Universität Bundesstr. 55 20146 Hamburg 13	18	1a
MPI	Max-Planck-Institut für Meteorologie Bundesstr. 55 20146 Hamburg 13	3	1a
SWA	Seewetteramt Hamburg Deutscher Wetterdienst Bernhard-Nochte-Str. 76 20305 Hamburg	3 3	1a 1b
(SFB 318	Sonderforschungsbereich 318) Klimarelevante Prozesse Universität Hamburg	(s. MIH, MPI und IMH)	

Russia

AARI	Arctic and Antarctic Research Institute 38, Bering Street St. Petersburg Russia, 199 226	1	1b

Sweden

UUG	Universität Uppsala Geophysics Box 560 S-751 22 Uppsala	1	1a

Switzerland

UBP	Universität Bern Institut für angewandte Physik Sahligstr. 6 3012 Bern	2 2	1a 1b

United Kingdom

SPRI	Scott Polar Research Institute Lensfield Road Cambridge, CB 3 9 EW	5 5	1a 1b
AMTP	University of Cambridge Dept. of Applied Mathematics and Theoretical Physics Silver Street Cambridge, CB 3 9 EW	1	1a

United States of America

APL	Applied Physics Laboratory University of Washington, HN -10 Seattle, WA 98195	2	1b

12.3. Cruise participants

12.3.1. Scientists

ARK IX / 1a

Aldworth, E.	SPRI
Andersson, S.	MIH
Auf dem Venne, H.	IMK
Bauer, M.	MIH
Brandon, M.	SPRI
Brey, H.	HSW
Castagne, T.	MIH
Claußen, M.	MPI
Crane, D.	SPRI
Eicken, H.	AWI
Erdmann, H.	SWA
Ewald, H.	HSW
Fischer, B.	MIH
Flückiger, K.	UBP
Frisius, T.	MIH
Gerland, S.	AWI
Gmünder, H.	UBP
Grelle, A.	UUG
Haas, C.	AWI
Hannke, S.	AWI
Hölscher, E.	MIH
Huppertz, W.	(MIH)
Jeske, H.	MIH
Kähler, C.	IMK
Kapp, R.	MIH
Karbach, U.	IMK
Klaepp, C.	MIH
Köhler, H.	SWA
Kornblueh, L.	GKSS
Lambert, H.-P.	SWA
Lohse, H.	GKSS
Loth, B.	MPI
Mai, S.	MIH
Münster, H.	MPI
Pakendorf, M.	MIH
Paul, F.	MIH
Peters, G.	MIH
Poltermann, M.	AWI
Rattay, W.	GKSS
Reisemann, M.	AMTP
Riewesell, C.	HSW
Schäfer, B.	MIH
Schneider, H.	MIH
Schreiber, D.	HSW
Soltau, T.	IMH
Steiger, M.	MIH
Struckmann, P.	SPRI
Thomas, D.N.	AWI
Timoschenko, K.	GKSS
Valero Delgado, F.E.	AWI
Wadhams, P.	SPRI
Walz, U.	MIH

ARK IX / 1b

Auf dem Venne, H.	IMK
Baering, S.	IMH
Bayer, R.	IUP
Besnainou, E.	IMH
Brandon, M.A.	SPRI
Brey, H.	HSW
Budeus, G.	AWI
Crane, D.	SPRI
Darnall, C.	APL
Dengler, M.	IMH
Düsterloh,S.	AWI
Elbrächter, M.	IMK
Erdmann, H.	SWA
Ewald, H.	HSW
Flückiger, K.	UBP
Frerichs, J.	ICBM
Gascard, J.C.	CODYC
Gmünder, H.	UBP
Hagen, W.	IPÖ
Henriksen, P.	MBLH
Johnson, J.	APL
Kähler, C.	IMK
Karbach, U.	IMK
Klaepp, C.	MIH
Köhler, H.	SWA
Korablev, A.	AARI
Lambert, H.-P.	SWA
Meincke, J.	IMH
Michel, A.	AWI
Niehoff, B.	AWI
Nielsen, A.	MBLH
Oelke, C.	AWI
Ortlam, J.	AWI
Paul, F.	MIH
Prussen, E.	SPRI
Pürschel, W.	IMH
Ramplee-Smith, C.	AES
Ramseier, R.	AES
Rhein, M.	IMK
Riewesell, C.	HSW
Ritterhoff, J.	ICBM
Rouault, C.	LODYC
Scherzinger, T.	AWI
Schreiber, D.	HSW
Senet, C.M.	IMH
Stuart, C.	AES
Verch, N.	IMH
Viehoff, T.	AWI
Wadhams, P.	SPRI
Waniek, J.	IMK
Wells, S.	SPRI
Zauke, G.-P.	ICBM
Zintz, K.	IMH

12.3.2. Ship's crew

Master	E.-P. Greve
Chief Mate	I. Varding
2nd Officer	M. Bürger
2nd Officer	S. Schwarze
2nd Officer (1b only)	M. Block
Physician	V. Wiemann
Radio Officer	K.-H. Wanger
Radio Officer	J. Butz
Chief Engineer	D. Knoop
1st Engineer	W. Delff
2nd Engineer	W. Simon
2nd Engineer	H. Folta
Electronician	K.-J. Hoops
Electronician	A. Piskorzynski
Electronician	M. Fröb
Electrician	G. Schuster (1a), R. Erdmann (1b)
Electronician	R. Rabenhorst
Boatswain	W. Hopp
Carpenter	P. Kassubeck
A. B.	A. Suarez-Paisal
A. B.	K. Bindernagel
A. B.	U. Burghardt (1b)
A. B.	S. Moser (1b)
A. B.	M. Meis-Torres
A. B.	B. Pereira-Portela
A. B.	A. Prol-Otero
A. B.	L. Gil-Iglesias
Storekeeper	B. Barth
Mechanic	A. Padur
Motorman	G. Jordan
Motorman	F. Buchas
Motorman	S. Reimann
Motorman	G. Fritz
Cook	W. Köwing
Cook Mate	F. Roggatz
Cook Mate	M. Kästner
1st Steward	D. Peschke
Stewardess	B. Hildebrandt (1a), H. Wübber (1b)
Stewardess	V. Daute
Stewardess	A. Hopp
2nd Steward	A. Neves
2nd Steward	J.-M. Tu
2nd Steward	K.-Y. Yu
Laundryman	C. C. Chang

Folgende Hefte der Reihe „Berichte zur Polarforschung" sind bisher erschienen:

Verkaufspreis/DM

* **Sonderheft Nr. 1/1981** – „Die Antarktis und ihr Lebensraum"
Eine Einführung für Besucher – Herausgegeben im Auftrag von SCAR

Heft Nr. 1/1982 – „Die Filchner-Schelfeis-Expedition 1980/81" 11,50
zusammengestellt von Heinz Kohnen

Heft Nr. 2/1982 – „Deutsche Antarktis-Expedition 1980/81 mit FS ‚Meteor'" 10,—
First International BIOMASS Experiment (FIBEX) – Liste der Zooplankton- und Mikronektonnetzfänge
zusammengestellt von Norbert Klages

Heft Nr. 3/1982 – „Digitale und analoge Krill-Echolot-Rohdatenerfassung an Bord des Forschungsschiffes ‚Meteor'" (im Rahmen von FIBEX 1980/81, Fahrtabschnitt ANT III), von Bodo Morgenstern 19,50

Heft Nr. 4/1982 – „Filchner-Schelfeis-Expedition 1980/81" 12,50
Liste der Planktonfänge und Lichtstärkemessungen
zusammengestellt von Gerd Hubold und H. Eberhard Drescher

* **Heft Nr. 5/1982** – "Joint Biological Expedition on RRS 'John Biscoe', February 1982"
by G. Hempel and R. B. Heywood

* **Heft Nr. 6/1982** – „Antarktis-Expedition 1981/82 (Unternehmen ‚Eiswarte')"
zusammengestellt von Gode Gravenhorst

Heft Nr. 7/1982 – „Marin-Biologisches Begleitprogramm zur Standorterkundung 1979/80 mit MS ‚Polarsirkel' (Pre-Site Survey)" – Stationslisten der Mikronekton- und Zooplanktonfänge sowie der Bodenfischerei 13,—
zusammengestellt von R. Schneppenheim

Heft Nr. 8/1983 – "The Post-Fibex Data Interpretation Workshop" 10,—
by D. L. Cram and J.-C. Freytag with the collaboration of J. W. Schmidt, M. Mall, R. Kresse, T. Schwinghammer

Heft Nr. 9/1983 – "Distribution of some groups of zooplankton in the inner Weddell Sea in summer 1979/80" 15,—
by I. Hempel, G. Hubold, B. Kaczmaruk, R. Keller, R. Weigmann-Haass

Heft Nr. 10/1983 – „Fluor im antarktischen Ökosystem" – DFG-Symposium November 1982 23,—
zusammengestellt von Dieter Adelung

Heft Nr. 11/1983 – "Joint Biological Expedition on RRS 'John Biscoe', February 1982 (II)" 16,—
Data of micronecton and zooplankton hauls, by Uwe Piatkowski

Heft Nr. 12/1983 – „Das biologische Programm der ANTARKTIS-I-Expedition 1983 mit FS ‚Polarstern'" 14,—
Stationslisten der Plankton-, Benthos- und Grundschleppnetzfänge und Liste der Probennahme an Robben und Vögeln, von H. E. Drescher, G. Hubold, U. Piatkowski, J. Plötz und J. Voß

* **Heft Nr. 13/1983** – „Die Antarktis-Expedition von MS ‚Polarbjörn' 1982/83" (Sommerkampagne zur Atka-Bucht und zu den Kraul-Bergen), zusammengestellt von Heinz Kohnen

* **Sonderheft Nr. 2/1983** – „Die erste Antarktis-Expedition von FS ‚Polarstern' (Kapstadt, 20. Januar 1983 – Rio de Janeiro, 25. März 1983)", Bericht des Fahrtleiters Prof. Dr. Gotthilf Hempel

Sonderheft Nr. 3/1983 – „Sicherheit und Überleben bei Polarexpeditionen"
zusammengestellt von Heinz Kohnen

Heft Nr. 14/1983 – „Die erste Antarktis-Expedition (ANTARKTIS I) von FS ‚Polarstern' 1982/83" 40,—
herausgegeben von Gotthilf Hempel

Sonderheft Nr. 4/1983 – "On the Biology of Krill *Euphausia superba*" – Proceedings of the Seminar and Report of the Krill Ecology Group, Bremerhaven 12.–16. May 1983, edited by S. B. Schnack 75,—

Heft Nr. 15/1983 – "German Antarctic Expedition 1980/81 with FRV 'Walther Herwig' and RV 'Meteor'" – First International BIOMASS Experiment (FIBEX) – Data of micronekton and zooplankton hauls 22,50
by Uwe Piatkowski and Norbert Klages

Sonderheft Nr. 5/1984 – "The observatories of the Georg von Neumayer Station", by Ernst Augstein 8,—

Heft Nr. 16/1984 – "FIBEX cruise zooplankton data" 19,—
by U. Piatkowski, I. Hempel and S. Rakusa-Suszczewski

Heft Nr. 17/1984 – „Fahrtbericht (cruise report) der ‚Polarstern'-Reise ARKTIS I, 1983" 29,—
von E. Augstein, G. Hempel und J. Thiede

Heft Nr. 18/1984 – „Die Expedition ANTARKTIS II mit FS ‚Polarstern' 1983/84", 25,—
Bericht von den Fahrtabschnitten 1, 2 und 3, herausgegeben von D. Fütterer

Heft Nr. 19/1984 – „Die Expedition ANTARKTIS II mit FS ‚Polarstern' 1983/84", 41,—
Bericht vom Fahrtabschnitt 4, Punta Arenas–Kapstadt (Ant-II/4), herausgegeben von H. Kohnen

Heft Nr. 20/1984 – „Die Expedition ARKTIS II des FS ‚Polarstern' 1984, mit Beiträgen des FS ‚Valdivia' und des Forschungsflugzeuges ‚Falcon 20' zum Marginal Ice Zone Experiment 1984 (MIZEX)" 42,—
von E. Augstein, G. Hempel, J. Schwarz, J. Thiede und W. Weigel